MAGNETOHYDRODYNAMIC CONJUGATE FREE CONVECTION FLOW FROM AN ISOTHERMAL HORIZONTAL CIRCULAR CYLINDER

NUR HOSAIN MD. ARIFUL AZIM

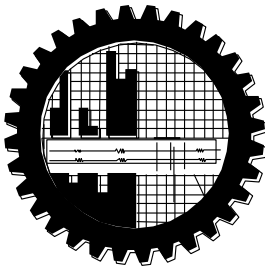

DEPARTMENT OF MATHEMATICS

BANGLADESH UNIVERSITY OF ENGINEERING AND TECHNOLOGY

DHAKA-1000, BANGLADESH

FEBRUARY, 2014

MAGNETOHYDRODYNAMIC CONJUGATE FREE CONVECTION FLOW FROM AN ISOTHERMAL HORIZONTAL CIRCULAR CYLINDER

A thesis submitted in fulfillment of the requirement for the award of the degree

of

DOCTOR OF PHILOSOPHY

in

MATHEMATICS

By

NUR HOSAIN MD. ARIFUL AZIM

Student No.: P10060902P, Session: October/2006

Registration No.: 0402403

Under the supervision of

Professor Dr. Md. Mustafa Kamal Chowdhury

DEPARTMENT OF MATHEMATICS

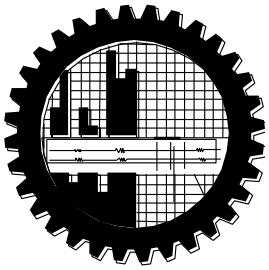

BANGLADESH UNIVERSITY OF ENGINEERING AND TECHNOLOGY

DHAKA-1000

FEBRUARY, 2014

The thesis entitled "**Magnetohydrodynamic Conjugate Free Convection Flow from an Isothermal Horizontal Circular Cylinder**" Submitted by N**ur Hosain Md. Ariful Azim,** Roll No.: P10060902P, Registration No.: 0402403, Session: October-2006 has been accepted as satisfactory in partial fulfillment of the requirement for the degree of **Doctor of Philosophy in Mathematics** on February 08, 2014.

Board of Examiners

1.

Dr. Md. Mustafa Kamal Chowdhury — Chairman (Supervisor)
Professor
Department of Mathematics
BUET, Dhaka-1000

2.

Head — Member (Ex-Officio)
Department of Mathematics
BUET, Dhaka-1000

3.

Dr. Md. Abdul Maleque — Member
Professor
Department of Mathematics
BUET, Dhaka-1000

4.

Dr. Md. Manirul Alam Sarker — Member
Professor
Department of Mathematics
BUET, Dhaka-1000

5. _____

Dr. Md. Abdul Alim Member
Professor
Department of Mathematics, BUET
BUET, Dhaka-1000

6. _____

Dr. Md. Shahjada Tarafder Member
Professor
Department of Naval Architecture and Marine Engineering
BUET, Dhaka-1000

7. _____

Dr. Mohammad Arif Hasan Mamun Member
Professor
Department of Mechanical Engineering
BUET, Dhaka-1000

8. _____

Dr. Md. Shamsul Alam Sarker Member
Professor (External)
Department of Mathematics
University of Rajshahi

4

Dedication

This work is dedicated to
My parents
and
My beloved wife

Certificate

This is to certify that the thesis entitled "**Magnetohydrodynamic Conjugate Free Convection Flow from an Isothermal Horizontal Circular Cylinder**" submitted by Nur Hosain Md. Ariful Azim to Bangladesh University of Engineering and Technology, Dhaka, is a record of original research work carried out by him under my supervision in the Department of Mathematics, Bangladesh University of Engineering and Technology, Dhaka. Mr. Nur Hosain Md. Ariful Azim has worked sincerely for preparing his thesis and the thesis is, in my opinion, worthy of consideration for the award of degree of Doctor of Philosophy in Mathematics in accordance with the rules and regulations of this University. I believe that this research work is a unique one and has not been submitted elsewhere for the award of any degree.

_____

Professor Dr. Md. Mustafa Kamal Chowdhury
Supervisor

6

Statement of Originality

I here by declare that the work which is being presented in the thesis entitled "Magnetohydrodynamic Conjugate Free Convection Flow from an Isothermal Horizontal Circular Cylinder" is an authentic record of my own work. I also declare that the matter contained in this thesis has not been submitted for the award of any other degree or diploma at any other university or institution other than publications.

_____

Nur Hosain Md. Ariful Azim February 08, 2014

7

Acknowledgment

I would like to express my profound gratitude and sincere appreciation to my honorable supervisor Prof. Dr. Md. Mustafa Kamal Chowdhury, Department of Mathematics, Bangladesh University of Engineering and Technology, Bangladesh for his guidance and constant encouragement. He inspired me to conceptualize a problem by the underlying geometry and its physical motivation. I deeply acknowledge his overwhelming generosity with his time, suggestions and insightful comments.

My regards also due to Prof. Dr. Md. Manirul Alam Sarker, Chairman, Department of mathematics, Bangladesh University of Engineering and Technology, Bangladesh for providing me all research facilities from the department without any famine.

I wish to express my deep gratitude to Prof. Dr. Md. Abdul Maleque, Prof. Dr. Md. Abdul Hakim Khan, Prof. Dr. Md. Elias and Prof. Dr. Md. Abdul Alim, Department of mathematics, Bangladesh University of Engineering and Technology for their valuable suggestions and constructive comments on my thesis. I am also indebted to Prof. Dr. Md. Shahjada Tarafder, Department of Naval Architecture and Marine Engineering for sharing his idea on the method of solution and Prof. Dr. Mohammad Arif Hasan Mamun, Department of Mechanical Engineering for his suggestion on the subject of the organization of thesis presentation. I had to study further to answer each of the comments they made and I believe at the end it enriched my knowledge.

I am grateful to all of my respected teachers of the Department of Mathematics, Bangladesh University of Engineering and Technology, Bangladesh for their useful advice and generous help during course work and thesis. I am also grateful to the external member Prof. Dr. Md. Shamsul Alam Sarker, Department of Applied Mathematics, University of Rajshahi, for his time and cooperation.

My sincere thanks to my colleagues and the authority of Southeast University, Dhaka, Bangladesh for providing me necessary support and facilities during my research works.

It is impossible to express in words my indebtedness to my wife Mrs. Shohana Sharmin for her sacrifice, assistance and motivation during the preparation of this thesis work.

Finally, I must acknowledge my debt to my parents for whom I have been able to see the beautiful sights and sounds of the world.

8

Abstract

The problem of steady, laminar, two-dimensional conjugate heat transfer through an incompressible and electrically-conducting fluid from an isothermal horizontal circular cylinder in the presence of a uniform magnetic field acting normal to the cylinder has been studied. An extensive literature review is introduced with the endeavor of the present study at the very beginning of the thesis. The detailed derivation of the governing equations for the flow field and heat transfer from standard vector form to the case by case is presented. The developed governing equations and the associated boundary conditions for this analysis are transferred to dimensionless forms using a suitable transformation. Implicit finite difference method with Keller-box scheme has been applied to solve the problem and the method of numerical solution is also discussed completely.

Firstly, Magnetohydrodynamic (MHD) conjugate free convection flow from an isothermal horizontal circular cylinder is investigated. Numerical outcomes are found for different values of the Magnetic parameter, conjugate conduction parameter and Prandtl number for the velocity profiles and the temperature distributions within the boundary layer as well as the skin friction coefficients and the rate of heat transfer along the surface. Results are presented graphically and discussed.

Secondly, the numerical solutions are obtained for the problem of MHD-conjugate natural convection flow from a horizontal cylinder taking into account Joule heating and internal heat generation. The effects of the Magnetic parameter, conjugate conduction parameter, Prandtl number, Joule heating parameter and heat generation parameter are analysed for the skin friction coefficients and the rate of heat transfer along the surface and the velocity and the temperature within the boundary-layer. It is found that the skin friction increases, and heat transfer rate decreases for escalating value of Joule heating parameter and heat generation parameter.

Thirdly, the effects of the stress work and viscous dissipation on MHD-conjugate free convection flow from an isothermal horizontal circular cylinder is studied. Numerical results for the Prandtl number, magnetic parameter, conjugate conduction parameter, stress work parameter, temperature ratio parameter and viscous dissipation parameter are found for the velocity profiles, temperature distributions, coefficient of skin friction and heat transfer rate. Like other literature, it is found that the effects of the viscous dissipation are smaller than stress work on the flow field and heat transfer.

Finally, MHD-conjugate free convective heat transfer analysis from isothermal horizontal circular cylinder with temperature dependent viscosity is considered. The velocity profiles, temperature distributions, the skin friction coefficient and the rate of heat transfer are computed and discussed in detail for various values of viscosity variation parameter, magnetic parameter, conjugate conduction parameter and Prandtl number. It is observed that the velocity increases and the temperature decreases within the boundary layer for increasing values of the viscosity variation parameter. Comparisons are performed with available results reported by previous investigations in all cases and the results show excellent agreement.

CONTENTS

11

12

NOMENCLATURE

Symbol	Entities	Dimension
a	: Outer radius of the cylinder	[L]
b	: Thickness of the cylinder	[L]
B_0	: Applied magnetic field	$[ML^2T^{-1}Q^{-1}]$
C_{fx}	: Skin friction coefficient	[---]
c_p	: Specific heat	$[L^2\theta^{-1}T^{-2}]$
f	: Dimensionless stream function	[---]
g	: Acceleration due to gravity	$[LT^{-2}]$
M	: Magnetic parameter	[---]
N	: Viscous dissipation parameter	[---]
Nu_x	: Local Nusselt number	[---]
Pr	: Prandtl number	[---]
Q	: Heat generation parameter	[---]
T_f	: Temperature at the boundary layer region	[θ]
T_s	: Temperature of the solid of the cylinder	[θ]
T_b	: Temperature of the inner cylinder	[θ]
T_∞	: Temperature of the ambient fluid	[θ]
$\bar{u}, \bar{v}$	: Velocity components	$[LT^{-1}]$
u, v	: Dimensionless velocity components	[---]
$\bar{x}, \bar{y}$	: Cartesian coordinates	[L]
x, y	: Dimensionless cartesian coordinates	[---]

13

Greek Symbols

β	: Co-efficient of thermal expansion	$[\theta^{-1}]$
χ	: Conjugate conduction resistant parameter	[---]
ε	: Stress work parameter	[---]
ψ	: Dimensionless stream function	[---]
λ	: Viscosity variation parameter	
ρ	: Density of the fluid inside the boundary layer	$[ML^{-3}]$
ρ_∞	: Density of the ambient fluid	$[ML^{-3}]$
ν	: Kinematic viscosity of the fluid inside the boundary layer	$[L^2T^{-1}]$
ν_∞	: Kinematic viscosity of the ambient fluid	$[L^2T^{-1}]$
μ	: Viscosity of the fluid inside the boundary layer	$[ML^{-1}T^{-1}]$
μ_∞	: Viscosity of the ambient fluid	$[ML^{-1}T^{-1}]$
θ	: Dimensionless temperature	[---]
σ	: Electrical conductivity	$[MLT^{-3}\ \theta^{-1}]$
K_f	: Thermal conductivity of the ambient fluid	$[MLT^{-3}\ \theta^{-1}]$
K_s	: Thermal conductivity of the cylinder solid	$[MLT^{-3}\ \theta^{-1}]$

14

List of Tables

15

16

17

18

List of Figures

19

21

Chapter I

General Introduction

1.1 Overview

Fluid dynamics is one of the most important parts of the recent interdisciplinary activities concerning engineering and technological developments. It is that branch of science which is concerned with the study of the motion of fluids or that of bodies in contact with fluids. Some of the most significant advances have been made in this branch during the last century. These advances have been motivated by exciting development in science and technology and have been facilitated by growth of computer capabilities and developments of sophisticated mathematical techniques.

A fluid element is acted upon by two types of forces, namely body forces and surfaces forces. The surface force may be resolved in two components, one normal and another tangential to the area of the fluid element. The normal force per unit area is known as normal stress while the tangential force per unit area is known as shearing stress. A fluid is said to be viscous (real) when normal as well as shearing stresses exist. On the other hand, a fluid is said to be non-viscous (ideal) when it does not exert any shearing stress.

Theoretical investigations into fluid mechanics in the eighteenth century were mainly based on the ideal fluid. The theory of flows of ideal fluids is mathematically very developed and indeed in many cases gives a satisfactory description of real flows but it is useless when faced with a problem of calculating the drag of a body. For this reason, engineers, on the other side, confronted by the practical problems of fluid mechanics, developed their own strongly empirical science, hydraulics. This relied upon a large amount of experimental data and differed greatly from theoretical hydrodynamics in both methods and goals.

An important contribution to the fluid dynamics is the concept of boundary-layer introduced by Ludwig Prandtl in 1904 (Schlichting and Gersten, 2000). He achieved a high degree of correlation between theory and experiment, which, in the first half of the nineteenth century, has led to unimagined successes in modern fluid mechanics. The concept of boundary layer is the consequence of the fact that flows at high Reynolds numbers can be divided into two unequally spaced regions: A very thin layer close to the body (boundary-layer) where the viscosity is important, and the remaining region outside this layer where the viscosity can be neglected.

Although the boundary layer is very thin, it plays a very important role in the fluid dynamics. One of the most important applications of boundary-layer theory is the calculation of the friction drag of bodies in a flow, e.g. the drag of a flat plate at zero incidence, the friction drag of a ship, an airfoil, the body of an airplane, or a turbine blade. One particular property of the boundary layer is that, under certain conditions, a reverse flow can occur directly at the wall. A separation of the boundary layer from the body and the formation of large or small eddy at the back of the body can then occur. This results in a great change in the pressure distribution at the back of the body, leading to the form or pressure drag of the body. This can also be calculated using boundary layer theory.

Heat has always been perceived to be something that produces in us a sensation of warmth and one would think that the nature of heat is one of the first things understood by the mankind. Heat is that which transfers from one system to another system at lower temperature, by virtue of the temperature difference. It is a transitory quantity which is never contained in a body. Heat transfer to a body increases its thermal energy, just as doing work on a body increases its momentum and kinetic energy. The basic requirement for heat transfer is the presence of temperature difference. There can be no net heat transfer between two bodies that are at the same temperature. The temperature difference is the driving force for heat transfer, just as the voltage difference is the driving force for

23

electric current flow and pressure difference is the driving force for fluid flow. The rate of heat transfer in a certain direction depends on the magnitude of the temperature gradient in that direction. The larger the temperature gradient, the higher the rate of heat transfer.

Heat transfer is commonly encountered in engineering systems and other aspects of life. The human body is constantly rejecting heat to its surroundings, and human comfort is closely tied to the rate of heat rejection. Many ordinary household appliances are designed by using the principles of heat transfer. Some examples include the electric or gas range, the heating and air-conditioning system, the refrigerator and freezer, the water heater, the iron, and even the computer, the television etc. Heat transfer plays a major role in the design of many other devices, such as car radiators, solar collectors, various components of power plants, and even spacecraft. In the design of nuclear-reactor cores, a thorough heat transfer analysis of fuel elements is important for proper sizing of fuel element to prevent burnout. In aerospace technology, heat transfer problems are crucial because of weight limitations and safely considerations. The optimal insulation thickness in the walls and roofs of the houses, on hot water or steam pipes, or on water heaters is again determined on the basis of a heat transfer analysis with economic consideration.

There are three distinct modes of heat transfer, namely conduction, convection and radiation. All mode of heat transfer require the existence of temperature difference, and all modes are from the high temperature medium to a lower-temperature one. In reality, the combined effects of these three modes of heat transfer control temperature distribution in a medium.

Conduction occurs if energy exchange takes place from the region of high temperature to that of low temperature by the kinetic motion or direct impact of molecules, as in the case of fluid at rest, and by the drift of electrons, as in the case of metals. The radiation energy emitted by a body is transmitted in the space

in the form of electromagnetic waves. Energy is emitted from a material due to its temperature level, being larger for a larger temperature, and is then transmitted to another surface, which may be vacuum or a medium, which may absorb, reflect or transmit the radiation depending on the nature and extent of the medium.

Convection is the mode of energy transfer between a solid surface and the adjacent liquid or gas that is in motion, and it involves the combined effects of conduction and fluid motion. Considerable effort has been directed at the convective mode of heat transfer. In this mode, relative motion of the fluid provides an additional mechanism for energy transfer. A study of convective heat transfer involves the mechanism of conduction and, sometimes, those of radiation processes as well. Experience shows that convection heat transfer strongly depends on the fluid properties dynamic viscosity μ, thermal conductivity κ, density ρ, and specific heat C_p, as well as the fluid velocity. It also depends on the geometry and the roughness of the solid surface, in addition to the type of the fluid flow (such as being steady or turbulent). Thus, we expect the convection heat transfer relations to be rather complex because of the dependence of convection on so many variables. This makes the study of convective mode a very complicated one.

The convective mode of heat transfer is divided into two basic processes. If the motion of the fluid arises due to an external agent such as the externally imposed flow of a fluid over a heated object, the process is termed as forced convection. The fluid flow may be the result of a fan, a blower, the wind or the motion of the heated object itself. If the heat transfer to or from a body occurs due to an imposed flow of a fluid at a temperature different from that of the body, problems of forced convection encounters in technology.

On the other hand, if the externally induced flow is provided and flows arising naturally solely due to the effect of the differences in density, caused by temperature or concentration differences in the body force field (such as

gravitational field), then these types of flow are called „free convection" or „natural convection" flows. The density difference causes buoyancy effects and these effects act as „driving forces" due to which the flow is generated. Hence free convection is the process of heat transfer, which occurs due to movement of the fluid particles by density differences associated with temperature difference in a fluid. Natural convection represents a limit on the heat transfer rates and this becomes a very important consideration for problems in which other modes are not practical. It is also relevant for safety consideration under conditions when the usual mode fails and the system has to depend on natural convection to get rid of the generated heat.

Two developed branches of physics, namely electromagnetic theory and fluid dynamics interact to produce hydromagnetics and therefore the field of hydromagnetics is much richer than both the parent branches. The study of hydromagnetic flows is known as magnetohydrodynamics (MHD). Hannes Alfven (1942) was the first to introduce the term "MAGNETOHYDRODYNAMICS" and received the Nobel Prize for his work on MHD.

The motion of an electrically conducting fluid, like mercury, under a magnetic field, in general gives rise to induced electric currents on which mechanical forces are exerted by the magnetic field. On the other hand, the induced electric currents also produce induced magnetic field. Thus there is a two-way interaction between the flow field and the magnetic field: the magnetic field exerts force on the fluid by producing induced currents, and the induced currents change the original magnetic field. Therefore, the hydromagnetic flows (the flows of electrically conducting fluids in the presence of a magnetic field) are more complex than the ordinary hydrodynamic flows. MHD covers phenomena in electrically conducting fluids, where velocity field and magnetic field are coupled.

26

Many natural phenomena and engineering problems are susceptible to MHD analysis. It is useful in astrophysics. Geophysicists encounter MHD phenomena in the interactions of conducting fluids magnetic fields that are presented in and around heavenly bodies. Engineers employ MHD principles in the design of heat exchangers, pumps and flowmeters, in space vehicle propulsion, control and re-entry, in creating novel power generating systems, and in developing confinement schemes for controlled fusion.

Computational fluid dynamics (CFD) is the science of predicting fluid flow, heat transfer, mass transfer, chemical reactions, and related phenomena by solving the mathematical equations which govern these processes using a numerical process. The evaluation of numerical methods, especially finite difference method (FDM) for solving ordinary and partial differential equation, started approximately with the beginning of the twentieth century. Traditionally, both experimental and theoretical methods have been used to develop designs for equipment and vehicles involving fluid flow and heat transfer.

A third method, the numerical approach has become available with the advent of digital computer. Over the years, computer speed has increased much more rapidly than computer costs. The net effect has been a phenomenal decrease in the cost of performing a given calculation. This is illustrated in Figure 1.1, where it is seen that the cost of performing a given calculation has been reduced by approximately a factor of 10 every 8 years.

It is now possible to assign a home work problem in CFD, the solution of which would have represented a major breakthrough. On the other hand, the costs of performing experiments have been steadily increasing over the same period of time. Thus, the importance and progress of CFD is increasing enormously day by day.

27

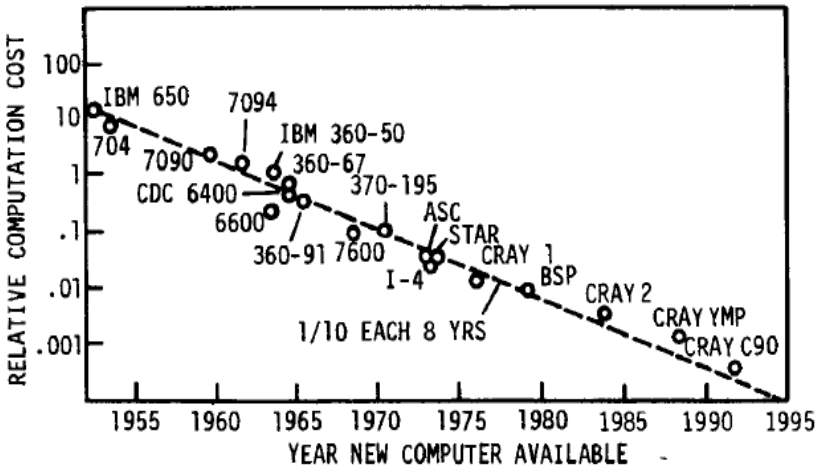

Figure 1.1 Trend of relative computation cost for a given flow and algorithm (based on Chapman, 1979).

1.2 Literature Review

Natural convective flow around heated, horizontal cylinders for various fluids is of great importance due to its extensive industrial applications. These applications have motivated extensive research on the heat transfer and flow characteristics related to natural convection from horizontal cylinders. For example, Saville and Churchill (1967) examined the laminar natural convection boundary-layer flow near horizontal cylinders and vertical axisymmetric bodies. It appears that Merkin (1976, 1977) was the first to apply the finite difference method as proposed by Terrill (1960) to study the steady free convection boundary layers on horizontal circular and elliptical cylinders which are maintained at either a uniform wall temperature or a uniform heat flux. He showed that on starting at the lowest point of the cylinder that the fluid flow reaches the top point without separating and at this point the boundary layer has a finite thickness. The boundary layer approximation usually leads to the neglect of the curvature effects and the pressure difference across the boundary layer and, on using this approximation, Kuehn and Goldstein (1980) solved simplified Navier-Stokes equations and energy equation for laminar natural convection about an isothermal horizontal cylinder using similarity technique and series methods. Natural convection from horizontal circular cylinder-laminar regime was investigated by Farouk and

Guceri (1981). Laminar free convection around horizontal circular cylinders was also analysed by Luciano (1983).

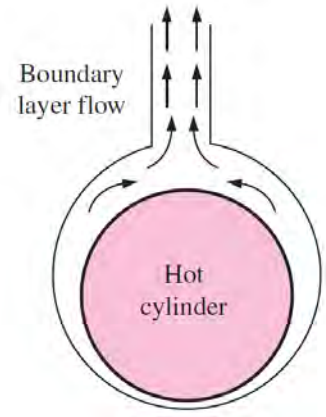

Figure 1.2: Natural convection flow from a horizontal circular cylinder.

In these above studies conduction resistance of the solid of the cylinder for the convective heat transfer between cylinder surface and fluid flow was neglected considering the thickness of the cylinder is infinitesimally small. However, in practical systems conduction resistance may affect natural convection flow in many practical fields especially those concern with thermal insulation.

Perelman (1961) was the first to study the boundary layer equations for the fluid flow over a flat plate of finite thickness considering two-dimensional thermal conduction in the plate. The investigation was then extended by Luikov et al. (1971) and since then various types of conjugate heat transfer (CHT) problems have been studied. The early theoretical and experimental works of the CHT for a viscous fluid have been reviewed by Gdalevich and Fertman (1977) and Miyamoto et al. (1980). They observed that a mixed-problem study of the natural convection has to be performed for an accurate analysis of the thermo-fluid-dynamic (TFD) field if the convective heat transfer depends strongly on the thermal boundary conditions. Pozzi and Lupo (1988) investigated the entire TFD field resulting from the coupling of natural convection along and conduction inside a heated flat plate by means of two expansions, regular series and asymptotic expansions. Moreover, Kimura and Pop (1994) was the first to

investigate conjugate natural convection from a horizontal circular cylinder. Natural convection flow along a vertical flat plate in presence of conduction was also studied by Azim et al. (2008).

On the other hand, a considerable amount of research has been accomplished on the effects of electrically conducting fluids such as liquid metals water mixed with a little acid and others in the presence of transverse magnetic field on the flow and heat transfer characteristics over various geometries. As for example, a natural convection heat transfer from a horizontal cylinder to mercury under a magnetic field was studied by Michiyoshi et al. (1976). Wilks (1976) studied MHD free convection about a semi-infinite vertical plate in a strong cross field. Azim et al. (2007a) investigated MHD laminar free convective flow across a horizontal circular cylinder.

A lot of physical phenomena involve natural convection driven by heat generation, it is necessary to take into account the effect of heat generation to obtain a better estimation of the flow and heat transfer behavior. Possible heat generation effects may alter the temperature distribution. This may occur in such applications related to nuclear reactor cores, fire and combustion modelling, electronic chips and semiconductor wafers. Vajravelu and Hadjinicolaou (1993) studied the heat transfer characteristics in a laminar boundary layer flow of a viscous fluid over a linearly stretching continuous surface with viscous dissipation/frictional heating and internal heat generation. Chamkha and Camille (2000) studied the effect of the heat generation or absorption and thermophoresis on a hydromagnetic flow with heat and mass transfer over a flat plate. Mendez and Trevino (2000) studied the effects of the conjugate conduction natural convection heat transfer along a thin vertical plate with nonuniform heat generation. Molla et al. (2006) studied the natural convection flow from an isothermal horizontal circular cylinder in presence of heat generation. Mamun et al. (2008) studied the MHD conjugate heat transfer for a vertical flat plate in the presence of viscous dissipation and heat generation.

Sparrow and Cess (1961) showed that viscous dissipation and Joule heating are of the same order and as well as negligibly small. But Gebhart (1962) has shown that the viscous dissipation effect plays an important role in natural convection in various devices which are subjected to large deceleration or which operate at high rotative speeds and also in strong gravitational field processes on large scales and in geological processes. With this understanding dissipation effects on MHD free convection flow past a semi-infinite vertical plate was investigated by Takhar and Soundalgekar (1980). Hossain (1992) studied the effects of viscous dissipation and Joule heating on magnetohydrodynamic (MHD) natural convection flow. Aldoss et al. (1996) analysed MHD mixed convection from a horizontal circular cylinder. Hydromagnetic natural convection from an isothermal inclined surface adjacent to a thermally stratified porous medium was analyzed by Chamkha (1997). MHD forced convection flow in the presence of viscous and magnetic dissipations and stress works along a non isothermal wedge was investigated by Yih (1999). Mansour et al. (2000) studied the coupled heat and mass transfer in magnetohydrodynamic flow of micropolar fluid on circular cylinders with uniform heat and mass flux. Combined effect of viscous dissipation and Joule heating on MHD forced convection over a non-isothermal horizontal cylinder embedded in a fluid saturated porous medium was studied by El-Amin (2003). Effect of Joule heating on MHD-Conjugate free convection flow along a vertical flat plate was investigated by Azim et al. (2007b). Alim et al. (2008) presented combined effect of viscous dissipation and joule heating on the coupling of conduction and free convection along a vertical flat plate. Azim et al. (2010c) studied the MHD–conjugate heat transfer for a vertical flat plate in the presence of heat generation with viscous dissipation and Joule heating.

In almost all natural convection studies, pressure stress term is neglected in the energy equation. This is a valid approximation at an ambient temperature of 300 K at 1 atm pressure and at terrestrial gravity, for most gases and low and moderate Prandtl number liquids. However for high gravity, such as in gas turbine blade cooling applications, where the intensity of the body force may be as large as

10^4 g, pressure stress may affect transport even at small downstream distances from the leading edge. Also, the effects on transport may be quite significant at low temperatures for gases and for high Prandtl number liquids. Joshi and Gebhart (1981) studied the effect of pressure stress work and viscous dissipation in some natural convection flows. Pantokratoras (2003) carried out new results of the effect of viscous dissipation and pressure stress work in natural convection along a vertical isothermal plate without any approximation. Alam et al. (2007) investigated free convection from a vertical permeable circular cone with pressure work and non-uniform surface temperature. Barletta and Nield (2009) studied mixed convection with viscous dissipation and pressure work in a lid-driven square enclosure. Very recently, Azim and Chowdhury (2013a) analysed hydromagnetic conjugate free convection flow from an isothermal horizontal circular cylinder with stress work and heat generation.

All the above studies were confined to a fluid with constant viscosity. However, it is known that this physical property may change significantly with temperature. Gray et al. (1982) and Mehta and Sood (1992) showed that when the effect of variation of viscosity considered, the flow characteristics may change substantially. Hossain et al. (2000) studied the flow of viscous incompressible fluid with temperature dependent viscosity and thermal conductivity (Proposed by Charraudeau (1975)) past a permeable wedge with variable heat flux. Molla et al. (2001, 2006) investigated effect of temperature dependent viscosity on natural convection flow from an isothermal horizontal circular cylinder and from a sphere. Ching-Yang Cheng (2006) studied the effect of temperature-dependent viscosity on the natural convection heat transfer from a horizontal isothermal cylinder of elliptic cross section. Recently, Ahmad et al. (2009) studied mixed convection boundary layer flow past an isothermal horizontal circular cylinder with temperature-dependent viscosity.

From the above literature review, it is observed that free convection boundary layer from an isothermal horizontal cylinder was studied by several researchers

[Merkin (1976, 1988), Kuehn and Goldstein (1980), Wang et al. (1990) etc.]. Where as Wilks (1976), Takhar and Soundalgekar(1980), Hossain et al. (1992), studied on MHD free convection flow from vertical plate. Aldoss et al.(1996), studied MHD mixed convection from horizontal cylinder and El-Amin(2003) studied MHD forced convection from horizontal circular cylinder. On the other hand, Kimura and Pop (1994) considered conduction of the cylinder on free convection from horizontal cylinder.

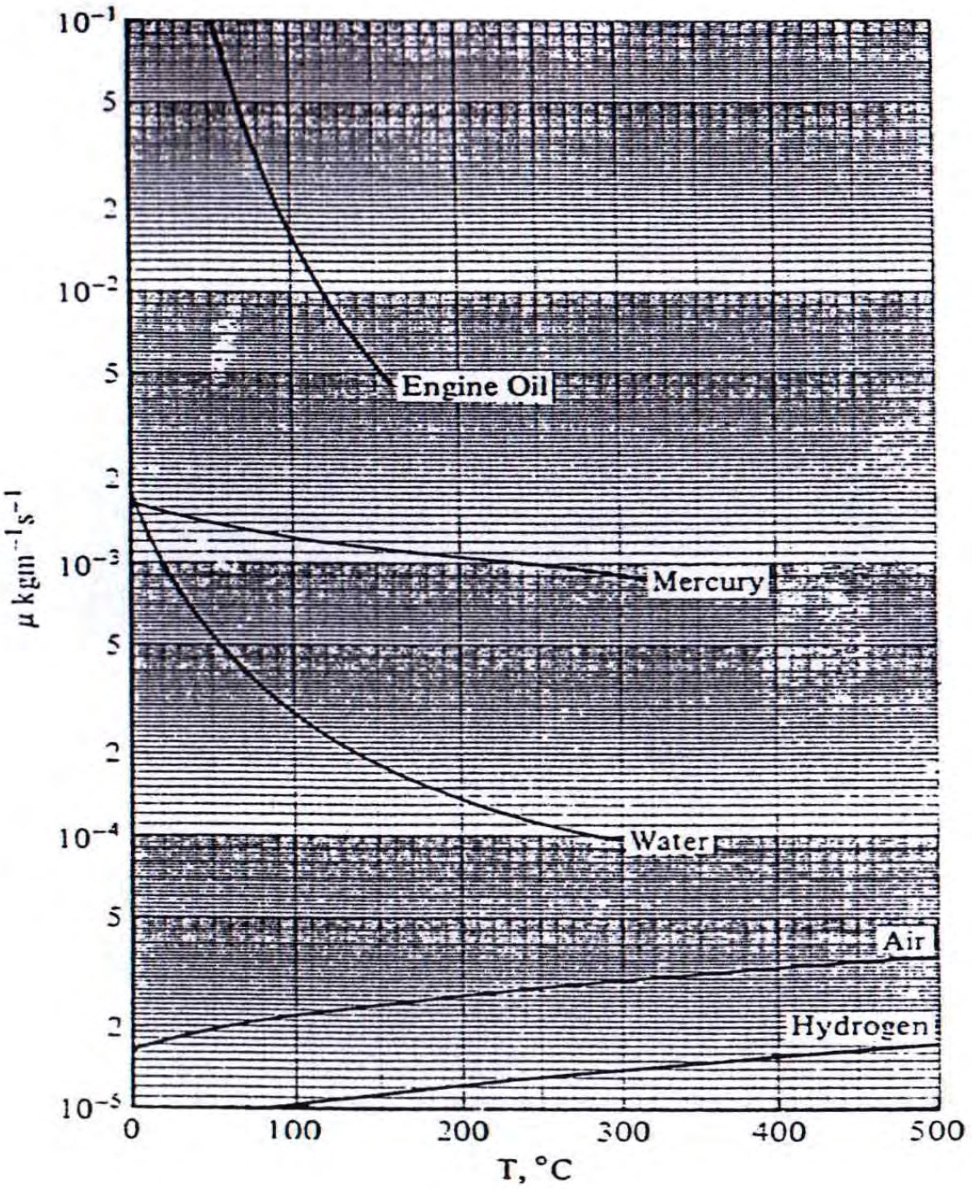

Figure 1.3: Variation of dynamic viscosity of several fluids with temperature (Cebeci and Bradshaw, 1984)

Alim et al. (2008) studied combined effect of viscous dissipation and joule heating on the coupling of conduction and free convection along a vertical flat plate. None of the above researchers considered magnetohydrodynamic (MHD) conjugate free convection flow from an isothermal horizontal circular cylinder. Present study demonstrates this issue.

Heat transfer analysis of MHD conjugate free convection flow from an isothermal horizontal circular cylinder is investigated in this current study. In addition, the problem has been extended considering the presence (i) Joule heating and heat generation (ii) Pressure stress work and viscous dissipation and (iii) Temperature dependent viscosity. To the best of my knowledge, these problems have not been considered before.

34

1.3 Objectives

The proposed research is to investigate the result of MHD-conjugate free convection flow from an isothermal horizontal circular cylinder. Then it is extended considering Joule heating, heat generation, stress work, viscous dissipation and temperature dependent viscosity on the flow field. The basic equations will be transformed to non-dimensional boundary layer equations using the suitable transformations, which will be solved numerically and analyzed in terms of velocity profiles, temperature distributions, skin friction and heat transfer over the whole boundary layer for a variety of parameters such as Prandtl number Pr, magnetic parameter M, conjugate conduction parameter χ, heat generation parameter Q, Joule heating parameter J, viscous dissipation parameter N, stress work parameter ε, temperature ratio parameter T_r and temperature dependent viscosity variation parameter λ.

The major objectives of this study are:

(i) To solve the equations governing MHD conjugate free convection flow from an isothermal horizontal circular cylinder using implicit finite difference method with Keller box scheme.

(ii) To analyse heat and mass transfer characteristics of the MHD conjugate flow from an isothermal horizontal circular cylinder from the obtained solution.

(iii) To compare the present results with some previously published results.

(iv) To study the effects of magnetic parameter M, conjugate conduction parameter χ, heat generation parameter Q, Joule heating parameter J, viscous dissipation parameter N, stress work parameter ε, temperature ratio parameter T_r and temperature dependent viscosity variation parameter λ on the velocity profiles, temperature distributions, skin friction coefficient and heat transfer.

1.4 Applications

The study of heat transfer is of great interest in many branches of science and engineering. In designing heat exchangers such as boilers, condensers and radiators etc. heat transfer analysis is essential for sizing such equipment. For example in the design of nuclear-reactor cores a thorough heat transfer analysis is important for proper sizing of fuel element to prevent burnout. In aerospace technology, heat transfer problems are crucial because of weight limitations and safety considerations. In heating and air conditioning applications for buildings a proper heat transfer analysis is necessary to estimate the amount of insulation needed to prevent excessive heat loses or gains.

The most important application of MHD is in the generation of electrical power with the flow of an electrical conducting fluid through a transverse magnetic field. Beside this MHD is widely applied in astrophysics (planetary magnetic field), MHD pumps, MHD generators, MHD flow meters, Metallurgy (induction furnace and casting of Al and Fe), Ship propulsion, Crystal growth, MHD flow control (reduction of turbulent drag), Magnetic filtration and separation, Jet printers and Fusion reactors etc. Recently, experiments with ionized gases have been performed with the hope of producing power on a large scale in stationary plants with large magnetic fields.

Presently, the concept of heat and mass transfer is applied for security purpose. Security related to transport phenomena include biological and chemical threat detection, aerosol generation and dispersion, distributed power generation, portable power infrastructure and fire protection etc. For example, the World Trade Center (WTC) towers could have sustained the impact of the planes during the attack in September 11, 2001, but the resulting fires caused structure failure and a total collapse. Fire is not considered as a design load in the prediction and evaluation of structural performance in the current design practices. In order to consider fire as a design load, it is imperative to develop science-based set of

verified tools to evaluate the performance of the entire structure under realistic fire conditions.

The study of the thermal sciences contributes significantly to improve health and environment. For example, lasers have been widely used in medical applications for more than three decades. The majority of those applications involve thermal effects. Thus, in the area biomedical engineering, understanding of heat mass transfer plays an important role on design of replacement tissues, and delivery of drugs.

The recent information technology revolution has led to increase generation rates of heat fluxes and volumetric energy. The operating temperatures of devices must be held to reasonably low values to ensure their reliability. Transport phenomena must be used to develop new, more efficient cooling systems. Limitations on maximum chip temperature and constraints on the level of temperature uniformity in electronic components can be resolved with heat pipes, Micro heat pipes, miniature heat pipes, heat sinks and heat spreaders etc.

Human body has had to devise a „second skin" called clothing, a product made from a material called fabric. Properly engineered (designed) fabrics and clothing permit people to live in most of the locations on planet earth from Sahara Desert to Polar region environmental conditions explore lake and ocean depths as well as travel in interplanetary space. For thermal equilibrium of man in his environment, it is convenient for the parameters related to the ambiance and for those concerning man to compensate their effects. It should be noted that, the total heat loss from skin is made up of two parts, the heat loss by evaporation and the heat loss by conduction, convection and radiation. Now, new technologies are permitting the production of „intelligent" textiles; textiles capable of sensing changes in environmental conditions or body functioning and responding to those changes. In this century, textile fabrics have been improved to assist in thermal and moisture regulation to and from human body through engineering of fibers,

37

yarns and fabric construction, and developing fabric finishes. Accordingly, the knowledge of heat transfer is a crucial area under discussion in textile engineering.

1.5 Motivation

The study of convective heat and mass transfer has gained serious momentum during recent years due to increased demands by industry for heat exchange equipment that is less expensive to build and operate. Savings in energy use also provide strong motivation for the development of improved methods of convective heat transfer. Constant efforts have been made to produce more efficient heat exchangers by employing various methods of heat transfer augmentation. When designing heat exchangers for air conditioning and refrigeration applications, it is imperative that they are made as compact and lightweight as possible. This is also true for cooling system in automobiles and spacecrafts, where volume and weight constraints are particularly important.

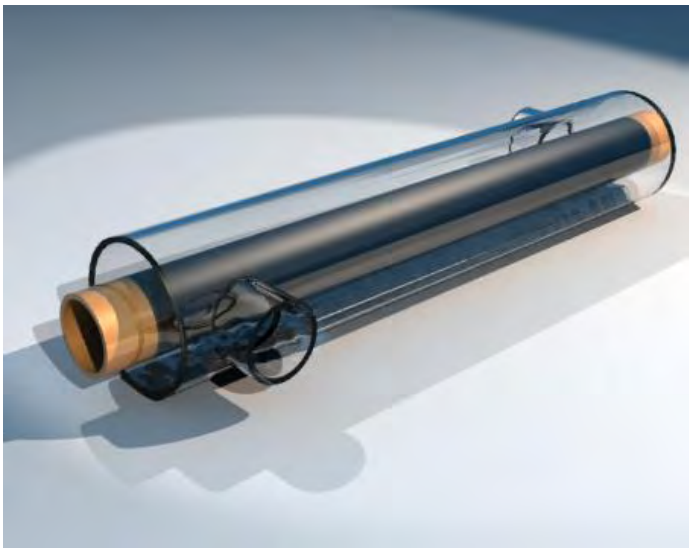

Figure 1.4: Heat exchanger

Numerous methods have been developed to increase the rates of heat transfer in
38 compact heat exchange devices operated in laminar regime. The objective behind these methods is to efficiently interrupt the boundary layer that forms on the

exchanger surface and replace it with fluid from the core, thereby creating a fresh boundary layer that has increased near wall temperature gradients. This leads not only the higher rate of heat transfer but also to greater frictional losses.

Horizontal circular cylinder is a very simple and useful structure which is frequently used to design a heat exchanger or a heat pipe. In a heat exchanger thermal energy moves from hot fluid to a surface by convection, through the wall by conduction. On the other hand, there are many industrial and engineering applications concern with magnetohydrodynamics (MHD). Magnetic field is also used to control heat transfer rate. Therefore MHD conjugate free convection from an isothermal horizontal circular cylinder is considered in the present study.

1.6 Outline of the thesis

The chapter I is an introductory chapter which includes physical phenomena of natural convection, magnetohydrodynamics, conduction, Joule heating, volumetric rate of heat generation, viscous dissipation, stress work and temperature dependent viscosity with applications. An extensive literature review of the past studies on the above physical facts is included with the aim of the present studies. The author also gives an explanation why and how did he motivated to do this research with a list of objectives.

Chapter II is a presentation of detailed derivation of the governing equations for the flow field and heat transfer from standard vector form to the case by case form. The dimensionless form of the governing equations is presented with careful discussion. At the end of this chapter a comprehensive discussion regarding the method of solution of the non-linear dimensionless governing equations is introduced.

MHD-conjugate free convection flow from an isothermal horizontal circular cylinder is investigated in chapter III. Three parameters are found from the governing equations and boundary conditions, namely magnetic parameter,

Prandtl number and conjugate conduction parameter. The heat transfer characteristics are analysed with a rigorous discussion. The results obtained in this chapter have been published in the Journal of energy, heat and mass transfer [see Azim and Chowdhury (2012a)].

The effects of the Joule heating and heat generation on MHD-conjugate free convection from an isothermal horizontal circular cylinder has been considered in chapter IV. Numerical solutions have been obtained for Joule heating parameter, heat generation parameter, magnetic parameter, Prandtl number and conjugate conduction parameter. The results obtained in chapter IV has been presented partially in different conferences such as 16th Mathematic conference 2009 [see Azim et al. (2009a)], ICME 2009 [Azim et al. (2009b)], ACFM 2010 [Azim and Chowdhury (2010b)] and published in the Journal of Computational Methods in Physics [Azim and Chowdhury (2013b)].

In Chapter V, stress work and viscous dissipation is introduced with the problem discussed in chapter III. Three new parameters are present in chapter V, namely stress work parameter, viscous dissipation parameter and temperature ratio parameters. The characteristics of these new parameters are presented graphically and discussed elaborately. The results are presented partially in conference MERTEC 2010 [see Azim et al. (2010a)] and published in the Journal of Dhaka International University [see Azim (2012b)].

Temperature dependent viscosity is taken into account in chapter VI as a result a new parameter is added with the parameters introduced in chapter III, namely viscosity variation parameter. The properties of this parameter on the fluid flow and heat transfer are widely explained in chapter VI.

Finally, a general conclusion and possible future work on this thesis has been discussed in chapter VII.

40

Chapter II

Mathematical Modeling of the problem

2.1 Magnetohydrodynamic equations

Magnetohydrodynamic equations are the ordinary electromagnetic and hydrodynamic equations modified to take account of the interaction between the motion of the fluid and electromagnetic field. Formulation of the electromagnetic theory in mathematical form is known as Maxwell‟s equations. Maxwell‟s basic equations show the relation of basic field quantities and their production. The basic laws of electromagnetic theory are all contained in special theory of relativity. In this study it is assumed that all velocities are small in comparison with the speed of light. Before writing down the MHD equations it is essential to know the ordinary electromagnetic and hydro-magnetic equations (Cramer and Pai(1974)).

The electromagnetic equations are:

Charge continuity: $$\nabla.\vec{D} = \rho_e \qquad (2.1)$$

Current continuity: $$\nabla.\vec{J} = -\frac{\partial \rho_e}{\partial t} \qquad (2.2)$$

Magnetic field continuity: $$\nabla.\vec{B} = 0 \qquad (2.3)$$

Ampere‟s Law: $$\nabla \wedge B_0 = \vec{J} + \frac{\partial \vec{D}}{\partial t} \qquad (2.4)$$

Faraday‟s Law: $$\nabla \wedge \vec{E} = -\frac{\partial \vec{B}}{\partial t} \qquad (2.5)$$

Constitutive (transport) equations for $\vec{D}$ and $\vec{B}$:

$$\vec{D} = \varepsilon' \vec{E} \text{ and } \vec{B} = \mu_e B_0 \qquad (2.6)$$

Total current density flow: $$\vec{J} = \sigma\left(\vec{E} + \vec{q} \wedge \vec{B}\right) + \rho_e \vec{q} \qquad (2.7)$$

The above equations (2.1) to (2.7) are Maxwell‟s equations where $\vec{D}$ is the electron displacement, ρ_e is the charge density, $\vec{E}$ is the electric field, $\vec{B}$ is the magnetic field, B_0 is the magnetic field strength, $\vec{J}$ is the current density, $\frac{\partial \vec{D}}{\partial t}$ is the displacement current density, ε' is the electric permeability of the medium, μ_e is the magnetic permeability of the medium, $\vec{q}$ is the vector field, σ is the

41

electric conductivity and $\rho_e \vec{q}$ is the convection current due to charge moving with the field.

The electromagnetic equations shown above are not usually applied in their present form and require interpretation and several assumptions to provide the set to be used in MHD. In MHD a fluid is considered as grossly neutral. The charge density ρ_e in Maxwell"s equations must then be interpreted, as an excess charge density, which is generally not large. If it is disregard the excess charge density then it must disregard the displacement current. In most problems the displacement current, the excess charge density and the current due to convection of the excess charge are small. Taking into this effect the electromagnetic equations can be reduced to the following form:

Charge continuity:	$\nabla.\vec{D} = 0$	(2.8)
Current continuity:	$\nabla.\vec{J} = 0$	(2.9)
Ampere"s Law:	$\nabla \wedge B_0 = \vec{J}$	(2.10)
Total current density flow:	$\vec{J} = \sigma\left(\vec{E} + \vec{q} \wedge \vec{B}\right)$	(2.11)

Following are the presentation of the fluid dynamics equations considering electromagnetic phenomena.

2.1.1 The continuity Equation

The MHD continuity equation for viscous incompressible electrically conduction fluid remains as that of usual continuity equation:

$$\nabla.\vec{q} = 0 \qquad (2.12)$$

2.1.2 The Navier-Stokes equation

The motion of conducting fluid across the magnetic field generates electric currents, which change the magnetic field and the action of the magnetic field on these current give rises to mechanical forces, which modify the flow of the fluid.

42

Thus, the fundamental equation of the magneto-fluid combines the equations of the motion from the fluid mechanics with Maxwell"s equations from electrodynamics.

Then the Navier-Stokes equation for a steady laminar viscous incompressible fluid with constant viscosity may be written in the following form:

$$\rho(\vec{q}.\nabla)\vec{q} = -\nabla P + \mu\nabla^2\vec{q} + \rho\vec{g} + \vec{J}\times\vec{B} \qquad (2.13)$$

Where ρ is the density, μ is the viscosity of the fluid and P is the pressure. The Navier-Stokes equation for a steady laminar viscous incompressible fluid with variable viscosity may be written in the following form:

$$\rho(\vec{q}.\nabla)\vec{q} = -\nabla P + \nabla.\tau + \rho\vec{g} + \vec{J}\times\vec{B} \qquad (2.14)$$

$$\tau = 2\mu\dot{\varepsilon}$$

and

$$\dot{\varepsilon} = \begin{pmatrix} \dot{\varepsilon}_x & \dot{\varepsilon}_{xy} & \dot{\varepsilon}_{xz} \\ \dot{\varepsilon}_{yx} & \dot{\varepsilon}_y & \dot{\varepsilon}_{yz} \\ \dot{\varepsilon}_{zx} & \dot{\varepsilon}_{zy} & \dot{\varepsilon}_z \end{pmatrix}$$

$$= \begin{pmatrix} \dfrac{\partial u}{\partial x} & \dfrac{1}{2}\left(\dfrac{\partial v}{\partial x}+\dfrac{\partial u}{\partial y}\right) & \dfrac{1}{2}\left(\dfrac{\partial w}{\partial x}+\dfrac{\partial u}{\partial z}\right) \\ \dfrac{1}{2}\left(\dfrac{\partial u}{\partial y}+\dfrac{\partial v}{\partial x}\right) & \dfrac{\partial u}{\partial y} & \dfrac{1}{2}\left(\dfrac{\partial w}{\partial y}+\dfrac{\partial v}{\partial z}\right) \\ \dfrac{1}{2}\left(\dfrac{\partial u}{\partial z}+\dfrac{\partial w}{\partial x}\right) & \dfrac{1}{2}\left(\dfrac{\partial v}{\partial z}+\dfrac{\partial w}{\partial y}\right) & \dfrac{\partial u}{\partial z} \end{pmatrix}$$

The left side of the equation (2.13) is the mass time acceleration; the first term on the right hand side is the pressure gradient, second term is the viscous force, third term is the body force per unit volume and the last term is the electromagnetic force due to motion of the fluid.

2.1.3 The energy equation

The energy equation for a viscous incompressible fluid is obtained by adding the
43 electromagnetic energy term into the classical gas dynamic energy equation. This equation can be written as:

$$\rho C_p(\vec{q}.\nabla)T = \nabla.(\kappa\nabla T) + (\vec{J}\times\vec{q})\bar{u} + Q_0(T-T_\infty) + \varphi + \beta T(\vec{q}.\nabla)P \qquad (2.15)$$

Where κ is the thermal conductivity of the fluid, C_p is the specific heat at constant pressure, β is the coefficient of thermal expansion, Q_0 is the heat generation/absorption coefficient and φ is the viscous dissipation function.

The left side of the equation (2.15) represents the net energy transfer due to mass transfer; the first term of the right hand side represents conductive heat transfer, the second term is the Joule heating term due to resistance of the electric current flowing through the fluid, the third term is the volumetric rate of heat generation, the fourth term is the viscous dissipation term and the last term is the rate of work done by the share stress force.

In the above equations ∇ is the vector differential operator and for two dimensional case it is defined as:

$$\nabla = \hat{i}\frac{\partial}{\partial x} + \hat{j}\frac{\partial}{\partial y}$$

Where $\hat{i}$ and $\hat{j}$ are the unit vectors along $\bar{x}$ and $\bar{y}$ axes respectively. If it is considered that the external electric field is zero and induced magnetic field is negligible, then the current density is related to the velocity by Ohm"s law as follows:

$$\vec{J} = \sigma(\vec{q}\wedge\vec{B}) \qquad (2.16)$$

Where $\vec{q}\wedge\vec{B}$ is the electrical fluid vector and σ denotes the electric conductivity of the fluid. This condition is usually well satisfied in terrestrial applications, especially so in (low- velocity) free convection flows. So, we can write

$$\vec{B} = \hat{j}B_0 \qquad (2.17)$$

Using equations (2.16) and (2.17) the force per unit volume $\vec{J}\times\vec{B}$ acting along the $\bar{x}$ axis takes the following form:

$$\vec{J}\times\vec{B} = -\sigma B_0{}^2\bar{u} \qquad (2.18)$$

44

2.2 Physical Model

Let us consider an isothermal horizontal circular cylinder of radius a placed in a fluid of uniform temperature T_∞. The cylinder has a heated core region of temperature T_b and the normal distance from inner surface to the outer surface is b with $T_b > T_\infty$. A uniform magnetic field having strength B_0 is acting normal to the cylinder surface. The physical model is shown in Figure 2.1, where the $\bar{x}$-axis is taken along the circumference of the cylinder measured from the lower stagnation point to the upper stagnation point and the $\bar{y}$-axis is taken normal to the surface. The gravitational force g is acting in downward direction.

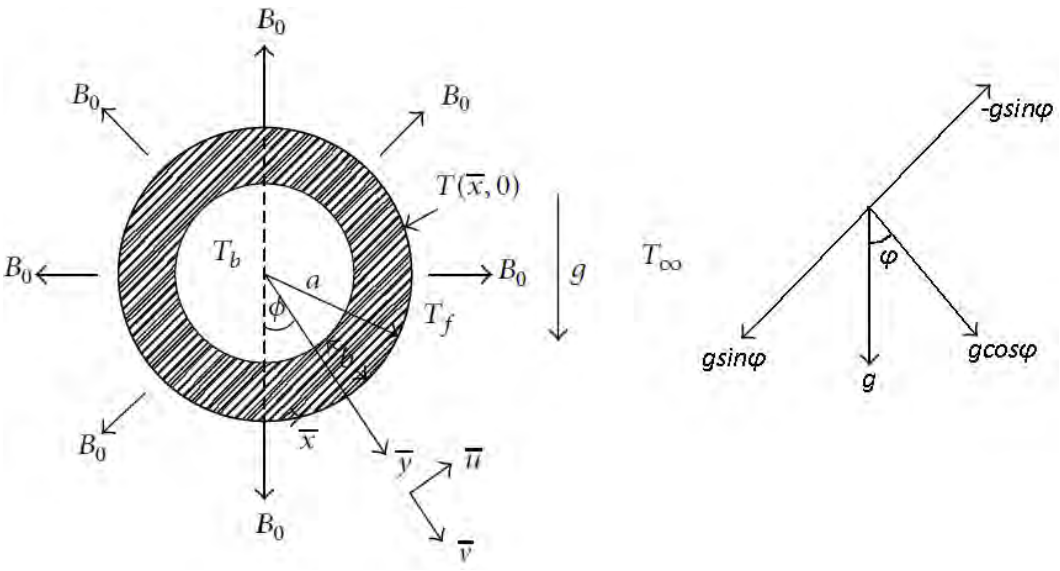

Figure 2.1: Physical Model and coordinate system

2.3 Assumptions

The present research is based on the following assumptions.

1. The flow is steady, laminar, two-dimensional, incompressible, and electrically conducting.
2. The fluid may be treated as continuous and is describable in terms of local properties.

3. The cylinder surface is impermeable, with no injection or withdrawal at the wall.
4. The induced magnetic field is small enough to be negligible.
5. The Boussinesq approximation is applicable, which treats density as a constant in all terms in the governing equations except for the buoyancy term in the momentum equation. The density variation is mainly caused by the thermal expansion of the fluid and can be expressed as:

   $\rho(T) = \rho_\infty \left[1 - \beta\left(T - T_\infty\right)\right]$

   where $\beta = -\frac{1}{\rho}\left(\frac{\partial \rho}{\partial T}\right)_p$ denotes the coefficient of thermal expansion.
6. The boundary layer thickness is very small compared with the external radius „a" of the cylinder (Boundary layer approximation).

2.4 Mathematical analysis

The mathematical formulation of the present problem has been discussed in this section. As there are four cases considered in the current study for the same physical model shown in Figure 2.1, therefore the case by case mathematical formulation of the analysis are presented in the following sub-sections.

2.4.1 Case I: MHD conjugate free convection flow

Under the assumptions in section 2.3 and with the help of equation (2.18) reduced form of the governing boundary-layer equations (2.12) and (2.13) are:

Continuity equation:

$$\frac{\partial\left(\rho\bar{u}\right)}{\partial\bar{x}} + \frac{\partial\left(\rho\bar{v}\right)}{\partial\bar{y}} = 0$$

This implies:
$$\frac{\partial\bar{u}}{\partial\bar{x}} + \frac{\partial\bar{v}}{\partial\bar{y}} = 0 \qquad (2.19)$$

46

$\bar{x}$ -momentum equation

$$\rho\left(\bar{u}\frac{\partial\bar{u}}{\partial\bar{x}}+\bar{v}\frac{\partial\bar{u}}{\partial\bar{y}}\right)=-\frac{\partial P}{\partial\bar{x}}+\mu\frac{\partial^2\bar{u}}{\partial\bar{y}^2}-\rho g\sin\phi-\sigma{B_0}^2\bar{u} \tag{2.20}$$

Where $\phi=\frac{\bar{x}}{a}$. The $\bar{x}$ -momentum equation in the quiescent fluid out side the boundary layer can be obtained from equation (2.20) as a special case by setting $\bar{u}=0$. It gives

$$\frac{\partial P_\infty}{\partial\bar{x}}=-\rho_\infty g\sin\phi=-\rho_\infty g\sin\left(\frac{\bar{x}}{a}\right) \tag{2.21}$$

It is noted that $\bar{v}<<\bar{u}$ in the boundary layer and thus $\frac{\partial\bar{v}}{\partial\bar{x}}\approx\frac{\partial\bar{v}}{\partial\bar{y}}\approx 0$ and that there are no body forces in the $\bar{y}$ direction, the force balance in that direction gives $\frac{\partial P}{\partial\bar{y}}=0$. That is the variation of pressure in that direction normal to the surface is negligible and for a given $\bar{x}$ the pressure in the boundary layer is equal to the pressure in the inactive fluid. Therefore $P=P(\bar{x})=P_\infty(\bar{x})$ and

$$\frac{\partial P}{\partial\bar{x}}=\frac{\partial P_\infty}{\partial\bar{x}}=-\rho_\infty g\sin\left(\frac{\bar{x}}{a}\right) \tag{2.22}$$

Now adding the first term (pressure gradient) and the third term (body force) of the right of the equation (2.20) we have:

$$-\frac{\partial P}{\partial\bar{x}}-\rho g\sin\phi=-\left(-\rho_\infty g\sin\left(\frac{\bar{x}}{a}\right)\right)-\rho(T)g\sin\left(\frac{\bar{x}}{a}\right)$$

$[\because \rho \text{ is a function of temperature for the body force term}]$

$$\Rightarrow-\frac{\partial P}{\partial\bar{x}}-\rho g\sin\phi=\rho_\infty g\sin\left(\frac{\bar{x}}{a}\right)-\rho(T)g\sin\left(\frac{\bar{x}}{a}\right)$$

$$\therefore-\frac{\partial P}{\partial\bar{x}}-\rho g\sin\phi=-[\rho(T)-\rho_\infty]g\sin\left(\frac{\bar{x}}{a}\right) \tag{2.23}$$

47

The density function $\rho(T)$ is expanded at the position $T = T_\infty$ in a Taylor series as

$$\rho(T) = \rho_\infty + \left(\frac{d\rho}{dT}\right)_\infty (T - T_\infty) + \ldots \tag{2.24}$$

If we break off this series after the linear term, using (2.24) in equation (2.23) yields:

$$-\frac{\partial P}{\partial \bar{x}} - \rho g \sin\phi = -\left[\rho_\infty + \left(\frac{d\rho}{dT}\right)_\infty (T - T_\infty) - \rho_\infty\right] g \sin\left(\frac{\bar{x}}{a}\right)$$

$$= -\left[-\beta_\infty \rho_\infty (T - T_\infty)\right] g \sin\left(\frac{\bar{x}}{a}\right)$$

$$= g\beta_\infty \rho_\infty (T - T_\infty) \sin\left(\frac{\bar{x}}{a}\right)$$

$$\left[\text{Where } \beta_\infty = -\frac{1}{\rho_\infty}\left(\frac{d\rho}{dT}\right)_\infty \text{ is the coefficient of thermal expansion}\right]$$

Using above results and symbolized β, ρ and T_f instead of β_∞, ρ_∞ and T, the modified form of the momentum equation (2.20) can be written as:

$$\rho\left(\bar{u}\frac{\partial \bar{u}}{\partial \bar{x}} + \bar{v}\frac{\partial \bar{u}}{\partial \bar{y}}\right) = \mu\frac{\partial^2 \bar{u}}{\partial \bar{y}^2} + g\beta\rho(T_f - T_\infty)\sin\left(\frac{\bar{x}}{a}\right) - \sigma {B_0}^2 \bar{u}$$

This implies

$$\bar{u}\frac{\partial \bar{u}}{\partial \bar{x}} + \bar{v}\frac{\partial \bar{u}}{\partial \bar{y}} = \nu\frac{\partial^2 \bar{u}}{\partial \bar{y}^2} + g\beta(T_f - T_\infty)\sin\left(\frac{\bar{x}}{a}\right) - \frac{\sigma {B_0}^2 \bar{u}}{\rho} \tag{2.25}$$

Where $\nu = \dfrac{\mu}{\rho}$ is the kinematic viscosity of the surrounding fluid.

Joule heating term, heat generation term, viscous dissipation term and stress work term in the energy equation (2.15) should be neglected for case I. The reduced energy equation is

48

$$\bar{u}\frac{\partial T_f}{\partial \bar{x}}+\bar{v}\frac{\partial T_f}{\partial \bar{y}}=\frac{\kappa_f}{\rho c_p}\frac{\partial^2 T_f}{\partial \bar{y}^2} \tag{2.26}$$

The energy equation in the solid of the cylinder is given by

$$\frac{\partial^2 T_s}{\partial \bar{x}^2}+\frac{\partial^2 T_s}{\partial \bar{y}^2}=0 \text{ for } 0\le \mathrm{x}\le \pi,\ -\mathrm{b}\le \bar{\mathrm{y}}\le 0 \tag{2.27}$$

The equation (2.27) is coupled to the energy equation in the fluid region by the condition that the temperature and heat flux are continuous at the solid –fluid interface, namely

$$T_s = T_f \qquad \text{on} \quad \bar{\mathrm{y}}=0,\ 0\le \mathrm{x}\le \pi \tag{2.28a}$$

$$\kappa_s \frac{\partial T_s}{\partial \bar{y}}=\kappa_f \frac{\partial T_f}{\partial \bar{y}}=0 \qquad \text{on} \quad \bar{\mathrm{y}}=0,\ 0\le \mathrm{x}\le \pi \tag{2.28b}$$

In general axial, the axial conduction of heat along the wall is negligible when compared with the normal conduction across the wall and this assumption is consistent with the boundary-layer theory (Luikov (1974)). In this case equation (2.27) reduces to

$$\frac{\partial^2 T_s}{\partial \bar{y}^2}=0 \qquad \text{for} \quad 0\le \mathrm{x}\le \pi,\ -\mathrm{b}\le \bar{\mathrm{y}}\le 0 \tag{2.29}$$

The assumption of the neglecting the axial heat conduction is only valid for $\frac{b}{a}<<1$. Thus on applying the condition that $T_s = T_b$ on $\bar{y}=-b$, Equation (2.29) gives

$$T_s(\bar{x},\bar{y})=T(\bar{x},0)-\frac{T_b-T(\bar{x},0)}{b}\bar{y} \qquad \text{for } 0\le \mathrm{x}\le \pi,\ -\mathrm{b}\le \bar{\mathrm{y}}\le 0 \tag{2.30}$$

Applying equation (2.30) in (2.28b) we have

$$\frac{\partial T_f}{\partial \bar{y}}=\frac{\kappa_s}{b\kappa_f}\left(T_f-T_b\right) \text{ on } \bar{y}=0,\ \bar{x}>0$$

49

Thus the problem is governed by the boundary-layer equations (2.19), (2.25) and (2.26) and the physical situation of the system suggests the following boundary conditions [Kimura and Pop (1994), Pop and Ingham (2001)]

$$\bar{u} = \bar{v} = 0,\ T_f = T(\bar{x}, 0),\ \ \frac{\partial T_f}{\partial \bar{y}} = \frac{\kappa_s}{b\kappa_f}\left(T_f - T_b\right) \text{ on } \bar{y} = 0,\ \bar{x} > 0$$
$$\bar{u} \to 0,\ T_f \to T_\infty \ as\ \bar{y} \to \infty,\ \bar{x} > 0 \tag{2.31}$$

Dimensionless governing equations

The governing equations (2.19), (2.25) and (2.26) and the boundary conditions (2.31) can be made non-dimensional, using the Grashof number $Gr = [g\beta a^3 (T_b - T_\infty)]/\nu^2$ which is assumed large and the following non-dimensional variables:

$$x = \frac{\bar{x}}{a},\ \ y = \frac{\bar{y}}{a} Gr^{1/4},\ \ u = \frac{\bar{u}a}{\nu} Gr^{-1/2},\ \ v = \frac{\bar{v}a}{\nu} Gr^{-1/4},\ \ \theta = \frac{T_f - T_\infty}{T_b - T_\infty} \tag{2.32}$$

Where θ is the dimensionless temperature.

From equation (2.32) we have:

$$\bar{x} = ax\ ;\ \bar{y} = aGr^{-\frac{1}{4}} y\ ;\ \bar{u} = \frac{\nu Gr^{\frac{1}{2}}}{a} u\ ;\ \bar{v} = \frac{\nu Gr^{\frac{1}{4}}}{a} v\ ;\ T_f = T_\infty + \left(T_b - T_\infty\right)\theta \tag{2.33}$$

This implies

$$\partial\bar{x} = a\partial x\ ;\ \partial\bar{y} = aGr^{-\frac{1}{4}}\partial y\ ;\ \partial\bar{u} = \frac{\nu Gr^{\frac{1}{2}}}{a}\partial u\ ;\ \partial\bar{v} = \frac{\nu Gr^{\frac{1}{4}}}{a}\partial v\ ;\ \partial T_f = \left(T_b - T_\infty\right)\partial\theta \tag{2.34}$$

$$\frac{\partial\bar{u}}{\partial\bar{x}} = \frac{\nu Gr^{\frac{1}{2}}}{a^2}\frac{\partial u}{\partial x} \tag{2.35}$$

$$\frac{\partial\bar{v}}{\partial\bar{y}} = \frac{\nu Gr^{\frac{1}{2}}}{a^2}\frac{\partial v}{\partial y} \tag{2.36}$$

$$\bar{u}\frac{\partial\bar{u}}{\partial\bar{x}} = \frac{\nu Gr^{\frac{1}{2}}}{a} u . \frac{\nu Gr^{\frac{1}{2}}}{a^2}\frac{\partial u}{\partial x} = \frac{\nu^2 Gr}{a^3} u\frac{\partial u}{\partial x} \tag{2.37}$$

$$\bar{v}\frac{\partial \bar{u}}{\partial \bar{y}} = \frac{\nu Gr^{\frac{1}{4}}}{a} v. \frac{\nu Gr^{\frac{1}{2}}}{a^2 Gr^{-\frac{1}{4}}} \frac{\partial u}{\partial y} = \frac{\nu^2 Gr}{a^3} v \frac{\partial u}{\partial y} \tag{2.38}$$

$$\frac{\partial^2 \bar{u}}{\partial \bar{y}^2} = \frac{\nu Gr}{a^3} \frac{\partial^2 u}{\partial y^2} \tag{2.39}$$

$$g\beta\left(T_f - T_\infty\right)\sin\left(\frac{\bar{x}}{a}\right) = g\beta(T_b - T_\infty)\,\theta \sin x \tag{2.40}$$

$$\frac{\sigma {B_0}^2 \bar{u}}{\rho} = \frac{\sigma {B_0}^2}{\rho} \frac{\nu Gr^{\frac{1}{2}}}{a} u \tag{2.41}$$

$$\frac{\partial T_f}{\partial \bar{x}} = \frac{\left(T_b - T_\infty\right)\partial\theta}{a\,\partial x} = \frac{\left(T_b - T_\infty\right)}{a} \frac{\partial\theta}{\partial x} \tag{2.42}$$

$$\frac{\partial T_f}{\partial \bar{y}} = \frac{\left(T_b - T_\infty\right)\partial\theta}{a\,Gr^{\frac{-1}{4}}\,\partial y} = \frac{\left(T_b - T_\infty\right)Gr^{\frac{1}{4}}}{a} \frac{\partial\theta}{\partial y} \tag{2.43}$$

$$\bar{u}\frac{\partial T_f}{\partial \bar{x}} = \frac{\nu Gr^{\frac{1}{2}}}{a} u \frac{\left(T_b - T_\infty\right)}{a} \frac{\partial\theta}{\partial x} = \frac{\nu Gr^{\frac{1}{2}}\left(T_b - T_\infty\right)}{a^2} .u \frac{\partial\theta}{\partial x} \tag{2.44}$$

$$\bar{v}\frac{\partial T_f}{\partial \bar{y}} = \frac{\nu Gr^{\frac{1}{4}}}{a} v. \frac{\left(T_b - T_\infty\right)Gr^{\frac{1}{4}}}{a} \frac{\partial\theta}{\partial y} = \frac{\nu Gr^{\frac{1}{2}}\left(T_b - T_\infty\right)}{a^2} .v \frac{\partial\theta}{\partial y} \tag{2.45}$$

Left Side of the momentum equation:

$$\bar{u}\frac{\partial \bar{u}}{\partial \bar{x}} + \bar{v}\frac{\partial \bar{u}}{\partial \bar{y}} = \frac{\nu^2 Gr}{a^3} u \frac{\partial u}{\partial x} + \frac{\nu^2 Gr}{a^3} v \frac{\partial v}{\partial y} = \frac{\nu^2 Gr}{a^3}\left(u \frac{\partial u}{\partial x} + v \frac{\partial v}{\partial y}\right) \tag{2.46}$$

Right Side of the momentum equation

$$\nu \frac{\partial^2 \bar{u}}{\partial \bar{y}^2} + g\beta\left(T_f - T_\infty\right)\sin\left(\frac{\bar{x}}{a}\right) - \frac{\sigma {B_0}^2 \bar{u}}{\rho}$$

$$= \frac{\nu^2 Gr}{a^3} \frac{\partial^2 u}{\partial y^2} + g\beta(T_b - T_\infty)\,\theta \sin x - \frac{\sigma {B_0}^2}{\rho} \frac{\nu Gr^{\frac{1}{2}}}{a} u \tag{2.47}$$

51

Left side of the energy equation

$$\bar{u}\frac{\partial T_f}{\partial \bar{x}} + \bar{v}\frac{\partial T_f}{\partial \bar{y}} = \frac{\nu Gr^{\frac{1}{2}}(T_b - T_\infty)}{a^2}.u\frac{\partial \theta}{\partial x} + \frac{\nu Gr^{\frac{1}{2}}(T_b - T_\infty)}{a^2}.v\frac{\partial \theta}{\partial y}$$

$$= \frac{\nu Gr^{\frac{1}{2}}(T_b - T_\infty)}{a^2}\left(u\frac{\partial \theta}{\partial x} + v\frac{\partial \theta}{\partial y}\right) \tag{2.48}$$

Right side of the energy equation

$$\frac{\kappa}{\rho c_p}\frac{\partial^2 T_f}{\partial \bar{y}^2} = \frac{\kappa}{\rho c_p}\frac{\partial}{\partial \bar{y}}\left(\frac{\partial T_f}{\partial \bar{y}}\right)$$

$$= \frac{\kappa}{\rho c_p}\frac{\partial}{aGr^{-\frac{1}{4}}\partial y}\left(\frac{(T_b - T_\infty)Gr^{\frac{1}{4}}}{a}\frac{\partial \theta}{\partial y}\right)$$

$$= \frac{\kappa(T_b - T_\infty)Gr^{\frac{1}{2}}}{\rho c_p a^2}\frac{\partial^2 \theta}{\partial y^2} \tag{2.49}$$

Using equations (2.32) to (2.49) following are the dimensionless form of the governing equations (2.19), (2.25) and (2.26) respectively

$$\frac{\partial u}{\partial x} + \frac{\partial v}{\partial y} = 0 \tag{2.50}$$

$$u\frac{\partial u}{\partial x} + v\frac{\partial u}{\partial y} + Mu = \frac{\partial^2 u}{\partial y^2} + \theta \sin x \tag{2.51}$$

$$u\frac{\partial \theta}{\partial x} + v\frac{\partial \theta}{\partial y} = \frac{1}{\Pr}\frac{\partial^2 \theta}{\partial y^2} \tag{2.52}$$

Where $M = \frac{\sigma a^2 B_0^{\ 2}}{\nu \rho Gr^{1/2}}$ is the magnetic parameter and $Pr = \frac{\mu c_p}{\kappa}$ is the Prandtl number and the boundary conditions in (2.31) can be written as:

$$u = v = 0,\ \theta - 1 = \chi\frac{\partial \theta}{\partial y},\ on\ y = 0,\ x > 0$$
$$u \to 0,\ \theta \to 0\ as\ y \to \infty,\ x > 0 \tag{2.53}$$

52

Where $\chi = \left(\frac{b\kappa_f}{a\kappa_s}\right) Gr^{1/4}$ is the conjugate conduction parameter. The present problem is governed by the magnitude of magnetic parameter M, Prandtl number Pr and conjugate conduction parameter χ. The values of χ depends on the ratios of $\frac{b}{a}$ and $\frac{\kappa_f}{\kappa_s}$ and Grashof number Gr. The ratios $\frac{b}{a}$ and $\frac{\kappa_f}{\kappa_s}$ are less than unity where as Gr is large for free convection. Therefore the value of χ is greater than zero. Present analysis will refer to free convection problem without conduction for $\chi = 0$.

To solve equation (2.50)-(2.52), subject to the boundary condition (2.53), we assume following transformations:

$$\psi = x f(x, y),\ \theta = \theta(x, y) \tag{2.54}$$

where θ is the dimensionless temperature and ψ is the stream function usually defined as:

$$u = \partial\psi / \partial y \text{ and } v = -\partial\psi / \partial x \tag{2.55}$$

The equations (2.54) and (2.55) implies that

$$u = \frac{\partial\psi}{\partial y} = \frac{\partial(xf)}{\partial y} = xf' \tag{2.56}$$

$$v = -\frac{\partial\psi}{\partial x} = -\frac{\partial(xf)}{\partial x} = -x\frac{\partial f}{\partial x} - f \tag{2.57}$$

$$\frac{\partial u}{\partial x} = \frac{\partial(xf')}{\partial x} = x\frac{\partial f'}{\partial x} + f' \tag{2.58}$$

$$\frac{\partial u}{\partial y} = \frac{\partial(xf')}{\partial y} = xf'' \tag{2.59}$$

$$\frac{\partial v}{\partial y} = \frac{\partial}{\partial y}\left(-x\frac{\partial f}{\partial x} - f\right) = -x\frac{\partial f'}{\partial x} - f' \tag{2.60}$$

53

$$u\frac{\partial u}{\partial x} = x^2 f'\frac{\partial f'}{\partial x} + xf'^2 \tag{2.61}$$

$$v\frac{\partial u}{\partial y} = \left(-x\frac{\partial f}{\partial x} - f\right).xf'' = -x^2 f''\frac{\partial f}{\partial x} - xff'' \tag{2.62}$$

$$Mu = Mxf' \tag{2.63}$$

$$\frac{\partial^2 u}{\partial y^2} = \frac{\partial}{\partial y}\left(\frac{\partial u}{\partial y}\right) = \frac{\partial}{\partial y}\left(xf''\right) = xf''' \tag{2.64}$$

$$\theta \sin x = \theta \sin x \tag{2.65}$$

From equation (2.58) and equation (2.60) it is observed that the stream function defined at equation (2.54) satisfies the continuity equation. i.e.

$$\frac{\partial u}{\partial x} + \frac{\partial v}{\partial y} = x\frac{\partial f'}{\partial x} + f' - x\frac{\partial f'}{\partial x} - f' = 0$$

Substituting equations (2.56) to (2.65) into the equations (2.50)-(2.52), new forms of the dimensionless governing equations (2.51) and (2.52) are:

$$f''' + ff'' - f'^2 - Mf' + \theta\frac{\sin x}{x} = x\left(f'\frac{\partial f'}{\partial x} - f''\frac{\partial f}{\partial x}\right) \tag{2.66}$$

$$\frac{1}{\Pr}\theta'' + f\theta' = x\left(f'\frac{\partial \theta}{\partial x} - \theta'\frac{\partial f}{\partial x}\right) \tag{2.67}$$

The corresponding boundary conditions as mentioned in equation (2.53) take the following form:

$$\begin{aligned} &f = f' = 0,\ \theta - 1 = \chi\frac{\partial \theta}{\partial y}\ at\ \ y = 0,\ x > 0 \\ &f' \to 0,\ \theta \to 0\ as\ \ y \to \infty,\ x > 0 \end{aligned} \tag{2.68}$$

In the above equations primes denote differentiation with respect to y only.

54

Most important physical quantities, the shearing stress and the rate of heat transfer in terms of skin friction coefficient and Nusselt number respectively can be written as:

$$C_f = \frac{\tau_w}{\rho U_\infty^2} \text{ and } Nu = \frac{aq_w}{\kappa(T_w - T_\infty)} \tag{2.69}$$

Where U_∞ is the characteristic velocity and for natural convection flows defined as $U_\infty^2 = ga\beta(T_b - T_\infty)$.

The skin friction $\tau_w = \mu\left(\frac{\partial \bar{u}}{\partial \bar{y}}\right)_{\bar{y}=0} = \frac{\rho \nu^2 Gr^{\frac{3}{4}}}{a^2} x f^{//}(x,0)$

and the rate of heat transfer, $q_w = -\kappa\left(\frac{\partial T}{\partial \bar{y}}\right)_{\bar{y}=0} = -\kappa \frac{(T_w - T_\infty) Gr^{\frac{1}{4}}}{a} \theta^{/}(x,0)$

Using the variables in equation (2.32) with the equations (2.54) and (2.55) and the boundary conditions into (2.68), we have

$$C_f\, Gr^{1/4} = x f''(x,0),\ Nu\, Gr^{-1/4} = -\theta(x,0) \tag{2.70}$$

The results of the velocity profiles and temperature distributions can be calculated by the following relations:

$$u = f'(x,y),\ \theta = \theta(x,y) \tag{2.71}$$

2.4.2 Case II: The effect of Joule heating and heat generation

In this case, the effects of Joule heating and volumetric rate of heat generation in the energy equation (2.15) are taking into account. The energy equation for this case is

$$\bar{u}\frac{\partial T_f}{\partial \bar{x}} + \bar{v}\frac{\partial T_f}{\partial \bar{y}} = \frac{\kappa}{\rho c_p}\frac{\partial^2 T_f}{\partial \bar{y}^2} + \frac{\sigma {B_0}^2 \bar{u}^2}{\rho c_p} + \frac{Q_0}{\rho c_p}(T_f - T_\infty) \tag{2.72}$$

55

Applying non-dimensional variables, which are described in equation (2.32) last two terms, can be written as:

$$\frac{\sigma B_0^{\,2}\bar{u}^{2}}{\rho c_p}=\frac{\sigma B_0^{\,2}}{\rho c_p}\left(\frac{\nu Gr^{\frac{1}{2}}}{a}u\right)^2=\frac{\sigma \nu^{\,2} B_0^{\,2} Gr}{a^2 \rho c_p}u^2 \tag{2.73}$$

$$\frac{Q_0}{\rho c_p}\left(T_f-T_\infty\right)=\frac{Q_0}{\rho c_p}\left(T_b-T_\infty\right)\theta \tag{2.74}$$

Using above relations and equations (2.42) to (2.45), the dimensionless form of the energy equation can be written as:

$$u\frac{\partial\theta}{\partial x}+v\frac{\partial\theta}{\partial y}=\frac{1}{\Pr}\frac{\partial^2\theta}{\partial y^2}+Ju^2+Q\theta \tag{2.75}$$

Where $J=\dfrac{\sigma \nu B_0^{\,2} Gr^{1/2}}{\rho c_p\left(T_b-T_\infty\right)}$ is the Joule heating parameter, $Q=\dfrac{Q_0 a^2}{\mu c_p Gr^{1/2}}$ is the heat generation parameter and $Pr=\dfrac{\mu c_p}{\kappa}$ is the Prandtl number.

The continuity equation, momentum equation and the boundary conditions remain same as equations (2.50), (2.51) and (2.53) as case I. This problem is governed by the magnitude of magnetic parameter M, Prandtl number Pr, Joule heating parameter J, heat generation parameter Q and conjugate conduction parameter χ.

The energy equation (2.75) has the following form by means of stream function and dimensionless temperature as defined in equation (2.54) and (2.55).

$$\frac{1}{\Pr}\theta''+f\theta'+Jx^2 f'^2+Q\theta=x\left(f'\frac{\partial\theta}{\partial x}-\theta'\frac{\partial f}{\partial x}\right) \tag{2.76}$$

The shearing stress and the rate of heat transfer in terms of skin friction coefficient and Nusselt number respectively and the velocity and temperature distributions within the boundary-layer can be calculated by the relations (2.70) and (2.71) respectively.

56

2.4.3 Case III: The study on viscous dissipation and stress work

The effects of viscous dissipation and pressure stress work are neglected in the above cases and therefore viscous dissipation and stress work terms also disappear in the energy equations of the above cases. If viscous dissipation and stress work terms are considered and Joule heating and heat generation terms are neglected in the energy equation (2.15) then the energy equation for this circumstance is

$$\bar{u}\frac{\partial T_f}{\partial \bar{x}}+\bar{v}\frac{\partial T_f}{\partial \bar{y}}=\frac{\kappa_f}{\rho c_p}\frac{\partial^2 T_f}{\partial \bar{y}^2}+\frac{\nu}{c_p}\left(\frac{\partial \bar{u}}{\partial \bar{y}}\right)^2+\frac{T\beta\bar{u}}{\rho c_p}\frac{\partial p}{\partial \bar{x}} \tag{2.77}$$

According to equation (2.32) last two terms, can be written as:

$$\frac{\nu}{c_p}\left(\frac{\partial \bar{u}}{\partial \bar{y}}\right)^2=\frac{\nu}{c_p}\left(\frac{\nu Gr^{\frac{1}{2}}}{a^2 Gr^{-\frac{1}{4}}}\frac{\partial u}{\partial y}\right)^2=\frac{\nu^3 Gr}{c_p a^4 Gr^{-\frac{1}{2}}}\left(\frac{\partial u}{\partial y}\right)^2$$

$$\therefore \frac{\nu}{c_p}\left(\frac{\partial \bar{u}}{\partial \bar{y}}\right)^2=\frac{\nu^3 Gr^{\frac{3}{2}}}{c_p a^4}\left(\frac{\partial u}{\partial y}\right)^2 \tag{2.78}$$

$$\frac{T_f\beta\bar{u}}{\rho c_p}\frac{\partial p}{\partial \bar{x}}=\frac{T_f\beta\bar{u}}{\rho c_p}(-\rho g)=-\frac{\{T_\infty+(T_b-T_\infty)\theta\}\beta\frac{\nu Gr^{\frac{1}{2}}}{a}u}{c_p}g$$

$$=-\frac{\{T_\infty+(T_b-T_\infty)\theta\}\beta\nu Gr^{\frac{1}{2}}u}{ac_p}g$$

$$=-\frac{\{T_\infty+(T_b-T_\infty)\theta\}\beta\nu Gr^{\frac{1}{2}}u}{ac_p}g$$

$$\therefore \frac{T_f\beta\bar{u}}{\rho c_p}\frac{\partial p}{\partial \bar{x}}=-\frac{g\beta\nu Gr^{\frac{1}{2}}}{ac_p}\left[T_\infty u+(T_b-T_\infty)\theta u\right] \tag{2.79}$$

Using above relations (2.78) and (2.79) and equations (2.42) to (2.45), the dimensionless form of the energy equation can be written as:

$$u\frac{\partial\theta}{\partial x}+v\frac{\partial\theta}{\partial y}=\frac{1}{\mathrm{Pr}}\frac{\partial^2\theta}{\partial y^2}+N\left(\frac{\partial u}{\partial y}\right)^2-\varepsilon(T_r u+u\theta) \tag{2.80}$$

57

Where $\Pr = \frac{\mu c_p}{\kappa}$ is the Prandtl number, $N = \frac{\nu^2 Gr}{a^2 c_p (T_b - T_\infty)}$ is the viscous dissipation parameter, $\varepsilon = \frac{g\beta a}{c_p}$ is the stress work parameter and $T_r = \frac{T_\infty}{T_b - T_\infty}$ is the temperature ratio parameter.

The continuity equation, momentum equation and the boundary conditions remain same as equations (2.50), (2.51) and (2.53). This problem is governed by the magnitude of magnetic parameter *M*, Prandtl number Pr, conjugate conduction parameter χ, viscous dissipation parameter *N*, stress work parameter ε and temperature ratio parameter T_r. By means of stream function and dimensionless temperature as defined in equation (2.54) and (2.55) the energy equation (2.80) has the following form:

$$\frac{1}{\Pr}\theta'' + f\theta' + Nx^2 f''^2 - \varepsilon\left(T_r x f' - x f'\theta\right) = x\left(f'\frac{\partial\theta}{\partial x} - \theta'\frac{\partial f}{\partial x}\right) \qquad (2.81)$$

From equation (2.70) one can calculate the shearing stress and the rate of heat transfer in terms of skin friction coefficient and Nusselt number respectively and the equation (2.71) is responsible for the velocity and temperature distributions within the boundary-layer.

2.4.4 Case IV: Temperature dependent viscosity

In the above cases the studies are confined with constant viscosity but it is observed from Figure 1.3 that viscosity is function of temperature. For some liquids like engine oil, mercury and water it is inversely proportional with temperature and for air and hydrogen it is directly proportional with temperature. Gray et al. (1982) and Mehta and Sood (1992) showed that when the effect of variation of viscosity considered, the flow characteristics may change substantially. The momentum equation (2.14) can be written as:

$$\rho_\infty\left(\bar{u}\frac{\partial\bar{u}}{\partial\bar{x}} + \bar{v}\frac{\partial\bar{u}}{\partial\bar{y}}\right) = \frac{\partial}{\partial\bar{y}}\left(\mu\frac{\partial\bar{u}}{\partial\bar{y}}\right) - \frac{dP}{d\bar{x}} - \rho_\infty g\sin\left(\frac{\bar{x}}{a}\right) - \sigma B_0{}^2\bar{u} \qquad (2.82)$$

58

Where ρ_∞ is the density of the ambient fluid. There are a very few forms of viscosity variation available in the literature, among them the following form of viscosity variation is considered in this case which is proposed by Lings and Dybbs (1987):

$$\mu = \frac{\mu_\infty}{1+\gamma\left(T_f - T_\infty\right)} \tag{2.83}$$

Where μ_∞ is the viscosity of the ambient fluid and γ is a constant. The equation (2.83) can be written as

$$\mu = \frac{\mu_\infty}{1+\gamma\left(\frac{T_f - T_\infty}{T_b - T_\infty}\right)T_b - T_\infty} = \frac{\mu_\infty}{1+\gamma\left(T_b - T_\infty\right)\theta} = \frac{\mu_\infty}{1+\lambda\theta} \tag{2.84}$$

Where $\lambda = \gamma\left(T_b - T_\infty\right)$ is the viscosity variation parameter.

Using dimensionless variables describe in equation (2.32) and equation (2.84) the first term of the right side of the equation (2.82) is

$$\frac{\partial}{\partial \bar{y}}\left(\mu\frac{\partial \bar{u}}{\partial \bar{y}}\right) = \frac{\partial}{\partial \bar{y}}\left(\frac{\mu_\infty}{1+\lambda\theta}\frac{\partial \bar{u}}{\partial \bar{y}}\right) = \mu_\infty\left(\frac{1}{1+\lambda\theta}\frac{\partial^2 \bar{u}}{\partial \bar{x}^2} + \frac{\partial \bar{u}}{\partial \bar{y}}\frac{\partial}{\partial \bar{y}}\left(1+\lambda\theta\right)^{-1}\right)$$

$$= \mu_\infty\left(\frac{1}{1+\lambda\theta}\frac{\nu_\infty Gr}{a^3}\frac{\partial^2 u}{\partial y^2} - \frac{\nu_\infty Gr^{\frac{1}{2}}}{a^2 Gr^{-\frac{1}{4}}}\frac{\partial u}{\partial y}\frac{1}{aGr^{-\frac{1}{4}}}\left(1+\lambda\theta\right)^{-2}\lambda\frac{\partial \theta}{\partial y}\right)$$

$$\frac{\partial}{\partial \bar{y}}\left(\mu\frac{\partial \bar{u}}{\partial \bar{y}}\right) = \mu_\infty\frac{\nu_\infty Gr}{a^3}\left(\frac{1}{1+\lambda\theta}\frac{\partial^2 u}{\partial y^2} - \frac{\lambda}{\left(1+\lambda\theta\right)^2}\frac{\partial u}{\partial y}\frac{\partial \theta}{\partial y}\right) \tag{2.85}$$

Applying equations (2.23) and (2.85) in (2.82), new form of the momentum equation is:

$$u\frac{\partial u}{\partial x} + v\frac{\partial u}{\partial y} + Mu = \frac{1}{1+\lambda\theta}\frac{\partial^2 u}{\partial y^2} - \frac{\lambda}{\left(1+\lambda\theta\right)^2}\frac{\partial u}{\partial y}\frac{\partial \theta}{\partial y} + \theta\sin x \tag{2.86}$$

where $M = \left(\sigma a^2 {B_0}^2\right)/\left(\nu_\infty \rho_\infty Gr^{1/2}\right)$ is the magnetic parameter and $\lambda = \gamma\left(T_b - T_\infty\right)$ is the temperature dependent viscosity variation parameter.

The continuity equation, energy equation and the boundary conditions are same as equations (2.50), (2.52) and (2.53). This problem is governed by the magnitude of magnetic parameter M, Prandtl number Pr, conjugate conduction parameter χ and viscosity variation parameter λ.

Considering stream function and dimensionless temperature as defined in equation (2.54) and (2.55) the momentum equation (2.86) has the following form:

$$\frac{1}{1+\lambda\theta} f''' + ff'' - f'^2 - \frac{\lambda}{(1+\lambda\theta)^2}\theta' f'' - Mf' + \frac{\sin x}{x}\theta = x\left(f'\frac{\partial f'}{\partial x} - f''\frac{\partial f}{\partial x}\right) \tag{2.87}$$

The shearing stress in terms of skin friction coefficient is

$$C_f = \frac{\tau_w}{\rho_\infty U_\infty^2} \tag{2.88}$$

Where U_∞ is the characteristic velocity and for free convection flows defined as

$$U_\infty^2 = ga\beta(T_b - T_\infty) \tag{2.89}$$

Where, the skin friction

$$\tau_w = \mu\left(\frac{\partial \bar{u}}{\partial \bar{y}}\right)_{\bar{y}=0} = \frac{\mu_\infty}{1+\lambda\theta}\frac{\nu_\infty Gr^{\frac{1}{2}}}{a^2 Gr^{-\frac{1}{4}}}\frac{\partial u}{\partial y} = \frac{\mu_\infty}{1+\lambda\theta}\frac{\nu_\infty Gr^{\frac{3}{4}}}{a^2} xf''(x,0) \tag{2.90}$$

Above relations in equations (2.88), (2.89) and (2.90) gives

$$C_f Gr^{\frac{1}{4}} = \frac{x}{1+\lambda\theta} f''(x,0) \tag{2.91}$$

From equation (2.91) we can calculate the shearing stress in terms of skin friction coefficient. The rate of heat transfer in terms of Nusselt number can be determined by equation (2.70) and the equation (2.71) is responsible for the velocity and temperature distributions within the boundary-layer.

60

2.5 Method of Solutions

In all cases of this thesis the author has applied implicit finite difference method to get the numerical solution for the velocity and temperature distributions within boundary-layer and the skin friction and heat transfer rate along the surface of the cylinder, which was first, introduced by Keller (1978) and elaborately describe by Cebeci and Bradshaw (1984). A complete discussion on the development of algorithm of implicit finite difference method together with Keller-box elimination scheme for case I of this thesis is given below.

2.5.1 Numerical approach

The Equations (2.66) and (2.67) based on the boundary conditions described in equation (2.68) are written in terms of first order equations in y, which are then expressed in finite difference form by approximating the functions and their derivatives in terms of the central differences in both coordinate directions. Denoting the mesh points in the (x, y) plane by x_i and y_j, where $i = 1,2,3, \ldots, M$ and $j = 1,2,3, \ldots, N$, central difference approximations are made such that the equations involving x explicitly are centred at $\left(x_{i-1/2}, y_{j-1/2}\right)$and the remainder at $\left(x_i, y_{j-1/2}\right)$, where $y_{j-1/2} = \left(y_j + y_{j-1}\right)/2$, etc. This results in a set of nonlinear difference equations for the unknowns at x_i in terms of their values at x_{i-1}. These equations are then linearised by the Newton"s method and are solved using a block-tridiagonal algorithm, taking as the initial iteration of the converged solution at $x = x_{i-1}$. Now to initiate the process at x = 0, we first provide guess profiles for all five variables (arising the reduction to the first order form) and use the Keller box method to solve the governing ordinary differential equations. Having obtained the lower stagnation point solution it is possible to march step by step along the boundary layer. For a given value of x, the iterative procedure is stopped when the difference in computing the velocity and the temperature in the next iteration is less than 10^{-6}, i.e. when $\left|\delta f^{i}\right| \le 10^{-6}$, where the superscript denotes the iteration number. The computations were not performed using a uniform grid

61

in the y direction, but a non-uniform grid was used and defined by $y_j = \sinh((j-1)/p)$, with j = 1,2,. . . ,301 and p = 100.

2.5.2 Implicit Finite Difference Method (IFDM)

To describe the numerical solution for case-I, we start with the transformed boundary-layer equations and boundary conditions given by equations (2.66), (2.67) and (2.68) respectfully.

$$f''' + ff'' - f'^2 - Mf' + \theta \frac{\sin x}{x} = x\left(f' \frac{\partial f'}{\partial x} - f'' \frac{\partial f}{\partial x} \right) \tag{2.66}$$

$$\frac{1}{\Pr}\theta'' + f\theta' = x\left(f' \frac{\partial \theta}{\partial x} - \theta' \frac{\partial f}{\partial x} \right) \tag{2.67}$$

Boundary conditions:

$$\begin{aligned} &f = f' = 0,\ \theta - 1 = \chi \frac{\partial \theta}{\partial y}\ at\ y = 0,\ x > 0 \\ &f' \to 0,\ \theta \to 0\ as\ y \to \infty,\ x > 0 \end{aligned} \tag{2.68}$$

First we write equations (2.66) and (2.67) and their boundary conditions (2.68) in terms of first order system. For this purpose, new dependent variables $u(x,y)$, $v(x,y)$ and $p(x,y)$ has been introduced so that the transformed momentum and energy equations can be written as:

$$f' = u \tag{2.92}$$

$$f'' = u' = v \tag{2.93}$$

$$\theta' = p \tag{2.94}$$

$$v' + p_1 . fv - p_2 . u^2 - p_4 u + p_3 \theta = x\left(u \frac{\partial u}{\partial x} - v \frac{\partial f}{\partial x} \right) \tag{2.95}$$

$$\frac{1}{\Pr} p' + p_1 . fp = x\left(u \frac{\partial \theta}{\partial x} - p \frac{\partial f}{\partial x} \right) \tag{2.96}$$

Where,

$$p_1 = 1,\ p_2 = 1,\ p_3 = \frac{\sin x}{x}\ \text{ and }\ p_4 = M \tag{2.97}$$

62

And the boundary condition in terms of new dependent variables:

$$f(x,0) = u(x,0) = 0, \quad \theta(x,0) - 1 = \chi.p(x,0)$$
$$f'(x,\infty) \to 0,\ \theta(x,\infty) \to 0 \tag{2.98}$$

The flow calculation program utilizes a finite difference scheme in solving the governing equations at specified boundary conditions. The computation employs 181 nodal points in the x direction and 301 nodal points and y direction. Since the boundary layer thickness changes more rapidly near the leading edge, more attention was given to this area of the domain. The computations are performed using a uniform grid in the x direction and a non uniform grid in the y direction. The non-uniform grid is defined by $y_j = \sinh((j-1)/p)$, with j = 1,2,. . . ,301 and p = 100. For a given value of x, the iterative procedure is stopped when the difference in computing the velocity in the next iteration is less than 10^{-6}, i.e. when $|\delta f^i| \le 10^{-6}$, where the superscript denotes the iteration number. In Figure 2.2 a portion of the computational grid consisting 31 nodal points in x direction and 50 nodal points in y direction is shown.

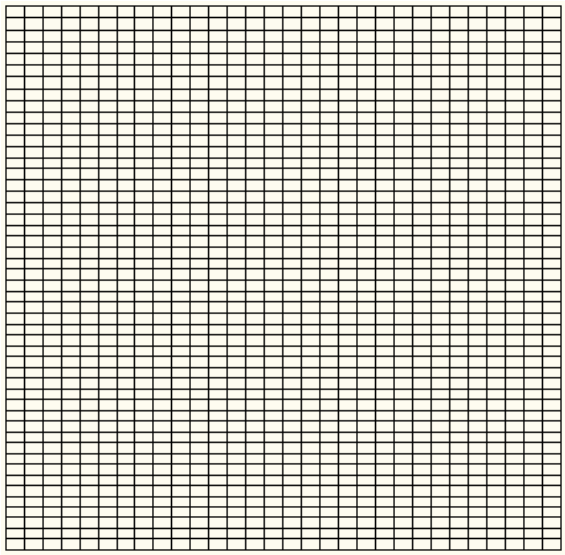

Figure 2.2: Computational grid structure

63

Now we consider the net rectangle in the *xy* plane shown in the Figure 2.3 and the net points defined in the *xy* plane as:

$$x_0 = 0, \quad x_n = x_{n-1} + k_n, \quad n = 1,2,...,N$$
$$y_0 = 0, \quad y_j = y_{j-1} + h_j, \quad j = 1,2,...,J \tag{2.99}$$

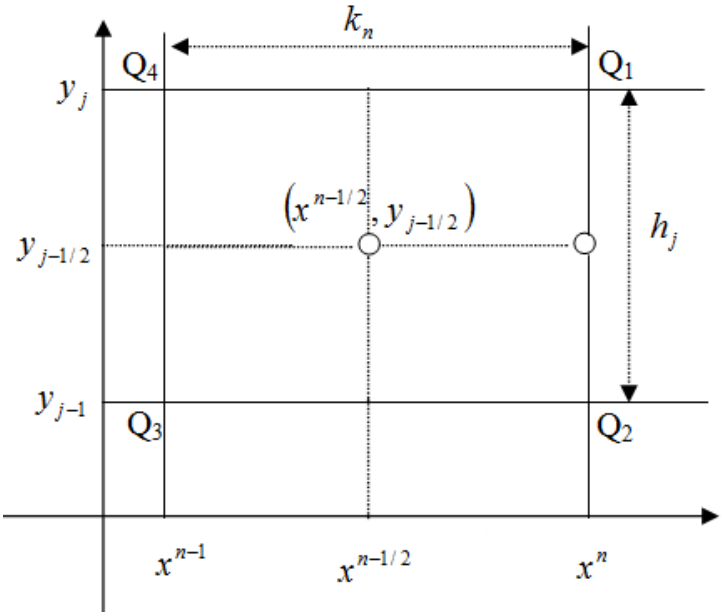

Figure 2.3: Net rectangle of the difference approximation for the Box scheme.

The quantities (f, u, v, θ, p) at the points (x^n, y_j) of the net are approximated by ($f_j^n, u_j^n \quad v_j^n, \quad \theta_j^n, p_j^n$) which we call net function . We also employ the following notation for the quantities midway between net points shown in Figure 2.3 and for any net function as

$$x^{n-1/2} = \frac{1}{2}(x^n + x^{n-1}) \tag{2.100a}$$

$$y_{j-1/2} = \frac{1}{2}(y_j - y_{j-1}) \tag{2.100b}$$

$$\theta_j^{n-1/2} = \frac{1}{2}(\theta_j^n + \theta_j^{n-1}) \tag{2.100c}$$

$$\theta_{j-1/2}^n = \frac{1}{2}(\theta_j^n + \theta_{j-1}^n) \tag{2.100d}$$

64

Now we write the difference equations that are to approximate the three first order ordinary differential equations (2.92)-(2.94) according to Box method by considering one mesh rectangle. We start by writing the finite difference approximation of the above three equations using central difference quotients and average about the mid-point $(x^n, y_{j-1/2})$ of the segment Q_1Q_2 shown in the Figure 2.3 and the finite difference approximations to the two first order differential equations (2.95)-(2.96) are written for the mid point $(x^{n-1/2}, y_{j-1/2})$ of the rectangle $Q_1Q_2Q_3Q_4$. This procedure yields.

$$h_j^{-1}(f_j^n - f_{j-1}^n) = u_{j-1/2}^n = \frac{u_{j-1}^n + u_j^n}{2} \tag{2.101}$$

$$h_j^{-1}(u_j^n - u_{j-1}^n) = v_{j-1/2}^n = \frac{v_{j-1}^n + v_j^n}{2} \tag{2.102}$$

$$h_j^{-1}(\theta_j^n - \theta_{j-1}^n) = p_{j-1/2}^n = \frac{p_{j-1}^n + p_j^n}{2} \tag{2.103}$$

$$\begin{aligned} &\frac{1}{2}\left[\frac{v_j^n - v_{j-1}^n}{h_j} + \frac{v_j^{n-1} - v_{j-1}^{n-1}}{h_j}\right] + (p_1 fv)_{j-1/2}^{n-1/2} - (p_2 u^2)_{j-1/2}^{n-1/2} - (p_4 u)_{j-1/2}^{n-1/2} \\ &+ (p_3\theta)_{j-1/2}^{n-1/2} = x_{j-1/2}^{n-1/2}\left[u_{j-1/2}^{n-1/2}\left\{\frac{u_{j-1/2}^n - u_{j-1/2}^{n-1}}{k_n}\right\} - v_{j-1/2}^{n-1/2}\left\{\frac{f_{j-1/2}^n - f_{j-1/2}^{n-1}}{k_n}\right\}\right] \end{aligned} \tag{2.104}$$

$$\begin{aligned} &\frac{1}{2\,\mathrm{Pr}}\left[\frac{p_j^n - p_{j-1}^n}{h_j} + \frac{p_j^{n-1} - p_{j-1}^{n-1}}{h_j}\right] + (p_1 fp)_{j-1/2}^{n-1/2} \\ &= x_{j-1/2}^{n-1/2}\left[u_{j-1/2}^{n-1/2}\left\{\frac{\theta_{j-1/2}^n - \theta_{j-1/2}^{n-1}}{k_n}\right\} - p_{j-1/2}^{n-1/2}\left\{\frac{f_{j-1/2}^n - f_{j-1/2}^{n-1}}{k_n}\right\}\right] \end{aligned} \tag{2.105}$$

65

Now from the equation (2.104) yields

$$\frac{1}{2}\left(\frac{v_j^n - v_{j-1}^n}{h_j}\right)+\frac{1}{2}\left(\frac{v_j^{n-1} - v_{j-1}^{n-1}}{h_j}\right)+\frac{1}{2}\left\{(p_1 fv)_{j-1/2}^n+(p_1 fv)_{j-1/2}^{n-1}\right\}$$
$$-\frac{1}{2}\left\{(p_2 u^2)_{j-1/2}^n+(p_2 u^2)_{j-1/2}^{n-1}\right\}-\frac{1}{2}\left\{(p_4 u)_{j-1/2}^n+(p_4 u)_{j-1/2}^{n-1}\right\}$$
$$+\frac{1}{2}\left\{(p_3\theta)_{j-1/2}^n+(p_3\theta)_{j-1/2}^{n-1}\right\}=\frac{1}{2k_n}x_{j-1/2}^{n-1/2}\left(u_{j-1/2}^n+u_{j-1/2}^{n-1}\right)\left(u_{j-1/2}^n-u_{j-1/2}^{n-1}\right)$$
$$-\frac{1}{2k_n}x_{j-1/2}^{n-1/2}\left(v_{j-1/2}^n+v_{j-1/2}^{n-1}\right)\left(f_{j-1/2}^n-f_{j-1/2}^{n-1}\right)$$

$$\Rightarrow h_j^{-1}(v_j^n - v_{j-1}^n)+h_j^{-1}(v_j^{n-1} - v_{j-1}^{n-1})+(p_1)_{j-1/2}^n(fv)_{j-1/2}^n+(p_1)_{j-1/2}^{n-1}(fv)_{j-1/2}^{n-1}$$
$$-(p_2)_{j-1/2}^n(u^2)_{j-1/2}^n-(p_2)_{j-1/2}^{n-1}(u^2)_{j-1/2}^{n-1}-(p_4)_{j-1/2}^n(u)_{j-1/2}^n-(p_4)_{j-1/2}^{n-1}(u)_{j-1}^{n-1}$$
$$+(p_3)_{j-1/2}^n(\theta)_{j-1/2}^n+(p_3)_{j-1/2}^{n-1}\theta_{j-1/2}^{n-1}=\alpha_n\{(u^2)_{j-1/2}^n-(u^2)_{j-1/2}^{n-1}-(fv)_{j-1/2}^n$$
$$+v_{j-1/2}^n f_{j-1/2}^{n-1}-v_{j-1/2}^{n-1}f_{j-1/2}^n+(fv)_{j-1/2}^{n-1}\},\ \textit{Where}\ \alpha_n=x_{j-1/2}^{n-1/2}/k_n$$

$$\Rightarrow h_j^{-1}(v_j^n - v_{j-1}^n)+\left\{(p_1)_{j-1/2}^n+\alpha_n\right\}(fv)_{j-1/2}^n-\left\{(p_2)_{j-1/2}^n+\alpha_n\right\}(u^2)_{j-1/2}^n$$
$$-(p_4)_{j-1/2}^n u_{j-1/2}^n+(p_3)_{j-1/2}^n(\theta)_{j-1/2}^n=\alpha_n[-(u^2)_{j-1/2}^{n-1}+v_{j-1/2}^n f_{j-1/2}^{n-1}-v_{j-1/2}^{n-1}f_{j-1}^n$$
$$+(fv)_{j-1/2}^{n-1}]-h_j^{-1}(v_j^{n-1} - v_{j-1}^{n-1})-(p_1)_{j-1/2}^{n-1}(fv)_{j-1/2}^{n-1}+(p_2)_{j-1/2}^{n-1}(u^2)_{j-1/2}^{n-1}$$
$$+(p_4)_{j-1/2}^{n-1}u_{j-1/2}^{n-1}-(p_3)_{j-1/2}^{n-1}\theta_{j-1/2}^{n-1}$$

$$\Rightarrow h_j^{-1}(v_j^n - v_{j-1}^n)+\left\{(p_1)_{j-1/2}^n+\alpha_n\right\}(fv)_{j-1/2}^n-\left\{(p_2)_{j-1/2}^n+\alpha_n\right\}(u^2)_{j-1/2}^n$$
$$+(p_3)_{j-1/2}^n(\theta)_{j-1/2}^n-(p_4)_{j-1/2}^n u_{j-1/2}^n+\alpha_n(v_{j-1/2}^{n-1}f_{j-1/2}^n-v_{j-1/2}^n f_{j-1/2}^{n-1})$$
$$=\alpha_n\left\{(fv)_{j-1/2}^{n-1}-(u^2)_{j-1/2}^{n-1}\right\}-h_j^{-1}(v_j^{n-1} - v_{j-1}^{n-1})-(p_1)_{j-1/2}^{n-1}(fv)_{j-1/2}^{n-1}$$
$$+(p_2)_{j-1/2}^{n-1}(u^2)_{j-1/2}^{n-1}+(p_4)_{j-1/2}^{n-1}u_{j-1/2}^{n-1}-(p_3)_{j-1/2}^{n-1}(\theta)_{j-1/2}^{n-1}$$

$$\Rightarrow h_j^{-1}(v_j^n - v_{j-1}^n)+\left\{(p_1)_{j-1/2}^n+\alpha_n\right\}(fv)_{j-1/2}^n-\left\{(p_2)_{j-1/2}^n+\alpha_n\right\}(u^2)_{j-1/2}^n$$
$$-(p_4)_{j-1/2}^n u_{j-1/2}^n+(p_3)_{j-1/2}^n(\theta)_{j-1/2}^n+\alpha_n(v_{j-1/2}^{n-1}f_{j-1/2}^n-v_{j-1/2}^n f_{j-1/2}^{n-1})$$
$$=-L_{j-1/2}^{n-1}+\alpha_n\left\{(fv)_{j-1/2}^{n-1}-(u^2)_{j-1/2}^{n-1}\right\}$$

$$L_{j-1/2}^{n-1}=h_j^{-1}(v_j^{n-1} - v_{j-1}^{n-1})+(p_1)_{j-1/2}^{n-1}(fv)_{j-1/2}^{n-1}-(p_2)_{j-1/2}^{n-1}(u^2)_{j-1/2}^{n-1}$$
$$-(p_4)_{j-1/2}^{n-1}u_{j-1/2}^{n-1}+(p_3)_{j-1/2}^{n-1}(\theta)_{j-1/2}^{n-1}$$

66

$$\Rightarrow h_j^{-1}(v_j^n - v_{j-1}^n) + \{(p_1)_{j-1/2}^n + \alpha_n\}(fv)_{j-1/2}^n - \{(p_2)_{j-1/2}^n + \alpha_n\}(u^2)_{j-1/2}^n$$
$$-(p_4)_{j-1/2}^n u_{j-1/2}^n + (p_3)_{j-1/2}^n (\theta)_{j-1/2}^n + \alpha_n (v_{j-1/2}^{n-1} f_{j-1/2}^n - v_{j-1/2}^n f_{j-1/2}^{n-1})$$
$$= R_{j-1/2}^{n-1} \qquad (2.106)$$
$$where \quad R_{j-1/2}^{n-1} = -L_{j-1/2}^n + \alpha_n \{(fv)_{j-1/2}^{n-1} - (u^2)_{j-1/2}^{n-1}\}$$

Since $p_i = p_i(x)$, so we may write the above equation as

$$h_j^{-1}(v_j^n - v_{j-1}^n) + \{(p_1)^n + \alpha_n\}(fv)_{j-1/2}^n - \{(p_2)^n + \alpha_n\}(u^2)_{j-1/2}^n$$
$$-(p_4)^n u_{j-1/2}^n + (p_3)^n (\theta)_{j-1/2}^n + \alpha_n (v_{j-1/2}^{n-1} f_{j-1/2}^n - v_{j-1/2}^n f_{j-1/2}^{n-1}) = R_{j-1/2}^{n-1} \qquad (2.107)$$

Again from the equation (2.105) we get

$$\frac{1}{2\,\mathrm{Pr}}\left[\frac{p_j^n - p_{j-1}^n}{h_j} + \frac{p_j^{n-1} - p_{j-1}^{n-1}}{h_j}\right] + (p_1 fp)_{j-1/2}^{n-1/2}$$
$$= x_{j-1/2}^{n-1/2}\left[u_{j-1/2}^{n-1/2}\left\{\frac{\theta_{j-1/2}^n - \theta_{j-1/2}^{n-1}}{k_n}\right\} - p_{j-1/2}^{n-1/2}\left\{\frac{f_{j-1/2}^n - f_{j-1/2}^{n-1}}{k_n}\right\}\right]$$

$$\Rightarrow \frac{1}{\mathrm{Pr}} h_j^{-1}(p_j^n - p_{j-1}^n) + \frac{1}{\mathrm{Pr}} h_j^{-1}(p_j^{n-1} - p_{j-1}^{n-1}) + (p_1)_{j-1/2}^{n-1/2}(fp)_{j-1/2}^n$$
$$+ (p_1)_{j-1/2}^{n-1/2}(fp)_{j-1/2}^{n-1} = \alpha_n \begin{Bmatrix} (u_{j-1/2}^n + u_{j-1/2}^{n-1})(\theta_{j-1/2}^n - \theta_{j-1/2}^{n-1}) \\ -(p_{j-1/2}^n + p_{j-1/2}^{n-1})(f_{j-1/2}^n - f_{j-1/2}^{n-1}) \end{Bmatrix}$$

$$\Rightarrow \frac{1}{\mathrm{Pr}} h_j^{-1}(p_j^n - p_{j-1}^n) + (p_1)_{j-1/2}^{n-1/2}(fp)_{j-1/2}^n = -M_{j-1/2}^{n-1} + \alpha_n\{(u\theta)_{j-1/2}^n - u_{j-1/2}^n \theta_{j-1/2}^{n-1}$$
$$+ u_{j-1/2}^{n-1}\theta_{j-1/2}^n - (fp)_{j-1/2}^n + p_{j-1/2}^n f_{j-1/2}^{n-1} - p_{j-1/2}^{n-1} f_{j-1/2}^n\} + \alpha_n\{(fp)_{j-1/2}^{n-1} - (u\theta)_{j-1/2}^{n-1}\}$$
$$Where, \; M_{j-1/2}^{n-1} = \frac{1}{\mathrm{Pr}} h_j^{-1}(p_j^{n-1} - p_{j-1}^{n-1}) + (p_1)_{j-1/2}^{n-1/2}(fp)_{j-1/2}^{n-1}$$

$$\Rightarrow \frac{1}{\mathrm{Pr}} h_j^{-1}(p_j^n - p_{j-1}^n) + \{(p_1)_{j-1/2}^{n-1/2} + \alpha_n\}(fp)_{j-1/2}^n - \alpha_n (u\theta)_{j-1/2}^n$$
$$-\alpha_n(u_{j-1/2}^{n-1}\theta_{j-1/2}^n - u_{j-1/2}^n \theta_{j-1/2}^{n-1} + p_{j-1/2}^n f_{j-1/2}^{n-1} - p_{j-1/2}^{n-1} f_{j-1/2}^n) = T_{j-1/2}^{n-1} \qquad (2.108)$$
$$T_{j-1/2}^{n-1} = -M_{j-1/2}^{n-1} + \alpha_n\{(fp)_{j-1/2}^{n-1} - (u\theta)_{j-1/2}^{n-1}\}$$

The boundary conditions become

$$f_0^n = u_0^n = 0, \quad \theta_0^n - 1 = \chi . p_0^n$$
$$u_J^n = 0, \; \theta_J^n = 0 \qquad (2.109)$$

If we assume $f_j^{n-1}, u_j^{n-1}, v_j^{n-1}, \theta_j^{n-1}, p_j^{n-1}$ to be known for $0 \le j \le J$, equations (2.101) to (2.103) and (2.107)–(2.109) form a system of 5J + 5 non linear equations for the solutions of the 5J + 5 unknowns ($f_j^n, u_j^n, v_j^n, \theta_j^n, p_j^n$) , j=0,1,2 …J. This non linear system of algebraic equations is to be linearized by Newton"s quassy linearization method. We define the iterates [$f_j^{(i)}, u_j^{(i)}, v_j^{(i)}, \theta_j^{(i)}, p_j^{(i)}$] , i=0,1,2 …N with initial values equal those at the previous x-station, which are usually the best initial guess available. For the higher iterates we set:

$$f_j^{(i+1)} = f_j^{(i)} + \delta f_j^{(i)} \tag{2.110a}$$

$$u_j^{(i+1)} = u_j^{(i)} + \delta u_j^{(i)} \tag{2.110b}$$

$$v_j^{(i+1)} = v_j^{(i)} + \delta v_j^{(i)} \tag{2.110c}$$

$$\theta_j^{(i+1)} = \theta_j^{(i)} + \delta \theta_j^{(i)} \tag{2.110d}$$

$$p_j^{(i+1)} = p_j^{(i)} + \delta p_j^{(i)} \tag{2.110e}$$

Now we substitute the right hand sides of the above equations in place of f_j^n, u_j^n, v_j^n, θ_j^n and p_j^n in equations (2.101) to (2.108) and (2.109) and omitting the terms that are quadratic in δf_j^i , $\delta u_j^i, \delta v_j^i, \delta \theta_j^{\,i}$ and δp_j^i we get the equations (2.101) to (2.103) and (2.107) to (2.109) in the following form:

$$\delta f_j^{(i)} - \delta f_{j-1}^{(i)} - \frac{h_j}{2}(\delta u_j^{(i)} + \delta u_{j-1}^{(i)}) = (r_1)_j \tag{2.111a}$$

$$\delta u_j^{(i)} - \delta u_{j-1}^{(i)} - \frac{h_j}{2}(\delta v_j^{(i)} + \delta v_{j-1}^{(i)}) = (r_4)_j \tag{2.111b}$$

$$\delta \theta_j^{(i)} - \delta \theta_{j-1}^{(i)} - \frac{h_j}{2}(\delta p_j^{(i)} + \delta p_{j-1}^{(i)}) = (r_5)_j \tag{2.111c}$$

Where, $(r_1)_j = f_{j-1}^{(i)} - f_j^{(i)} + h_j u_{j-1/2}^{(i)}$ (2.112a)

$$(r_4)_j = u_{j-1}^{(i)} - u_j^{(i)} + h_j v_{j-1/2}^{(i)} \tag{2.112b}$$

68 $$(r_5)_j = \theta_{j-1}^{(i)} - \theta_j^{(i)} + h_j p_{j-1/2}^{(i)} \tag{2.112c}$$

Now using the equations (2.110) in the equation (2.107) we get the following form:

$$h_j^{-1}(v_j^n - v_{j-1}^n) + \{(p_1)^n + \alpha_n\}(fv)_{j-1/2}^n - \{(p_2)^n + \alpha_n\}(u^2)_{j-1/2}^n$$
$$-(p_4)^n u_{j-1/2}^n + (p_3)^n(\theta)_{j-1/2}^n + \alpha_n(v_{j-1/2}^{n-1} f_{j-1/2}^n - v_{j-1/2}^n f_{j-1/2}^{n-1}) = R_{j-1/2}^{n-1}$$

$$\Rightarrow h_j^{-1}(v_j^{(i)} + \delta v_j^{(i)} - v_{j-1}^{(i)} - \delta v_{j-1}^{(i)}) + \{(p_1)_{j-1/2}^n + \alpha_n\}\{(fv)_{j-1/2}^{(i)} + \delta(fv)_{j-1/2}^{(i)}\}$$
$$-\{(p_2)_{j-1/2}^n + \alpha_n\}\{(u^2)_{j-1/2}^{(i)} + \delta(u^2)_{j-1/2}^{(i)}\} + (p_3)_{j-1/2}^n\{(\theta)_{j-1/2}^{(i)} + \delta(\theta)_{j-1/2}^{(i)}\}$$
$$-(p_4)^n\{u_{j-1/2}^{(i)} + \delta u_{j-1/2}^{(i)}\} + \alpha_n(f_{j-1/2}^{(i)} + \delta f_{j-1/2}^{(i)})v_{j-1/2}^{n-1} - \alpha_n(v_{j-1/2}^{(i)} + \delta v_{j-1/2}^{(i)})f_{j-1/2}^{n-1}$$
$$= R_{j-1/2}^{n-1}$$

$$\Rightarrow h_j^{-1}(v_j^{(i)} + \delta v_j^{(i)} - v_{j-1}^{(i)} - \delta v_{j-1}^{(i)}) + \{(p_1)_{j-1/2}^n + \alpha_n\}$$
$$\left\{(fv)_{j-1/2}^{(i)} + \frac{1}{2}(f_j^{(i)}\delta(v)_j^{(i)} + v_j^{(i)}\delta(f)_j^{(i)} + f_{j-1}^{(i)}\delta(v)_{j-1}^{(i)} + v_{j-1}^{(i)}\delta(f)_{j-1}^{(i)})\right\}$$
$$-\{(p_2)_{j-1/2}^n + \alpha_n\}\left\{(u^2)_{j-1/2}^{(i)} + \frac{1}{2}\{\delta(u^2)_j^{(i)} + \delta(u^2)_{j-1}^{(i)}\}\right\}$$
$$+(p_3)_{j-1/2}^n\left\{(\theta)_{j-1/2}^{(i)} + \frac{1}{2}(\delta(\theta)_j^{(i)} + \delta(\theta)_{j-1}^{(i)})\right\} - (p_4)^n\left\{u_{j-1/2}^{(i)} + \frac{1}{2}(\delta u_j^{(i)} + \delta u_{j-1}^{(i)})\right\}$$
$$+\alpha_n\left[\left\{v_{j-1/2}^{n-1}(f_{j-1/2}^{(i)} + \frac{1}{2}(\delta f_j^{(i)} + \delta f_{j-1}^{(i)}))\right\} - \left\{f_{j-1/2}^{n-1}(v_{j-1/2}^{(i)} + \frac{1}{2}(\delta v_j^{(i)} + \delta v_{j-1}^{(i)}))\right\}\right] = R_{j-1/2}^{n-1}$$

$$\Rightarrow (s_1)_j \delta v_j^{(i)} + (s_2)_j \delta v_{j-1}^{(i)} + (s_3)_j \delta f_j^{(i)} + (s_4)_j \delta f_{j-1}^{(i)} + (s_5)_j \delta u_j^{(i)} \quad (2.111d)$$
$$+(s_6)_j \delta u_{j-1}^{(i)} + (s_7)_j \delta\theta_j^{(i)} + (s_8)_j \delta\theta_{j-1}^{(i)} + (s_9)_j \delta p_j^i + (s_{10})_j \delta p_{j-1}^i$$
$$= (r_2)_j$$

Where $(s_1)_j = (h_j^{-1} + \frac{(p_1)_{j-1/2}^n + \alpha_n}{2} f_j^{(i)} - \frac{1}{2}\alpha_n f_{j-1/2}^{n-1})$ (2.113a)

$$(s_2)_j = (-h_j^{-1} + \frac{(p_1)_{j-1/2}^n + \alpha_n}{2} f_{j-1}^{(i)} - \frac{1}{2}\alpha_n f_{j-1/2}^{n-1}) \quad (2.113b)$$

$$(s_3)_j = (\frac{(p_1)_{j-1/2}^n + \alpha_n}{2} v_j^{(i)} + \frac{1}{2}\alpha_n v_{j-1/2}^{n-1} \quad (2.113c)$$

69

$$(s_4)_j = \left(\frac{(p_1)^n_{j-1/2} + \alpha_n}{2} v^{(i)}_{j-1} + \frac{1}{2}\alpha_n\, v^{n-1}_{j-1/2}\right) \tag{2.113d}$$

$$(s_5)_j = -\{(p_2)^n_{j-1/2} + \alpha_n\}\, u^{(i)}_j - \frac{(p_4)^n_{j-1/2}}{2} \tag{2.113e}$$

$$(s_6)_j = -\{(p_2)^n_{j-1/2} + \alpha_n\}\, u^{(i)}_{j-1} - \frac{(p_4)^n_{j-1/2}}{2}\ ) \tag{2.113f}$$

$$(s_7)_j = (p_3)^n/2 \tag{2.113g}$$

$$(s_8)_j = (p_3)^n/2 \tag{2.113h}$$

$$(s_9)_j = 0 \tag{2.113i}$$

$$(s_{10})_j = 0 \tag{2.113j}$$

$$\begin{aligned}(r_2)_j = {} & R^{n-1}_{j-1/2} - \left\{h_j^{-1}\,(v^{(i)}_j - v^{(i)}_{j-1}) + ((p_1)^n_{j-1/2} + \alpha_n)(fv)^{(i)}_{j-1/2}\right\} \\ & + ((p_2)^n_{j-1/2} + \alpha_n)(u^2)^{(i)}_{j-1/2} - \alpha_n\{f^{(i)}_{j-1/2}\, v^{n-1}_{j-1/2} - f^{n-1}_{j-1/2} v^{(i)}_{j-1/2}\} \\ & - \left\{(p_3)^n_{j-1/2}\,\theta^{(i)}_{j-1/2} - (p_4)^n u^{(i)}_{j-1/2}\right\}\end{aligned} \tag{2.112d}$$

Here the coefficients $(s_9)_j$ and $(s_{10})_j$, which are zero in this case, are included here for the generality.

Similarly by using the equations (2.110) in the equation (2.108) we get the following form:

$$\begin{aligned}& \frac{1}{\mathrm{Pr}} h_j^{-1}\,(p^n_j - p^n_{j-1}) + \left\{(p_1)^{n-1/2}_{j-1/2} + \alpha_n\right\}(fp)^n_{j-1/2} - \alpha_n (u\theta)^n_{j-1/2} \\ & - \alpha_n (\,u^{n-1}_{j-1/2}\,\theta^n_{j-1/2} - u^n_{j-1/2}\,\theta^{n-1}_{j-1/2} + p^n_{j-1/2}\, f^{n-1}_{j-1/2} - p^{n-1}_{j-1/2}\, f^n_{j-1/2}\,) = T^{n-1}_{j-1/2} \\ & T^{n-1}_{j-1/2} = -M^{n-1}_{j-1/2} + \alpha_n \left\{(fp)^{n-1}_{j-1/2} - (u\theta)^{n-1}_{j-1/2}\right\}\end{aligned}$$

70

$$
\begin{aligned}
&\Rightarrow \frac{1}{\mathrm{Pr}} h_j^{-1}\left\{p_j^{(i)}+\delta p_j^{(i)}-p_{j-1}^{(i)}-\delta p_{j-1}^{(i)}\right\} \\
&+\left\{(p_1)_{j-1/2}^{n-1/2}+\alpha_n\right\}\left\{(fp)_{j-1/2}^{(i)}+\frac{1}{2}\left(f_j^{(i)}\delta p_j^{(i)}+p_j^{(i)}\delta f_j^{(i)}+f_{j-1}^{(i)}\delta p_{j-1}^{(i)}+p_{j-1}^{(i)}\delta f_{j-1}^{(i)}\right)\right\} \\
&-\frac{\alpha_n}{2}\left\{(u\theta)_j^{(i)}+u_j^{(i)}\delta\theta_j^{(i)}+\theta_j^{(i)}\delta u_j^{(i)}+(u\theta)_{j-1}^{(i)}+u_{j-1}^{(i)}\delta\theta_{j-1}^{(i)}+\theta_{j-1}^{(i)}\delta u_{j-1}^{(i)}\right\} \\
&-\frac{\alpha_n}{2}\left\{\begin{array}{l} u_{j-1/2}^{n-1}\left(\theta_j^{(i)}+\delta\theta_j^{(i)}+\theta_{j-1}^{(i)}+\delta\theta_{j-1}^{(i)}\right)-\left(u_j^{(i)}+\delta u_j^{(i)}+u_{j-1}^{(i)}+\delta u_{j-1}^{(i)}\right)\theta_{j-1/2}^{n-1} \\ +\left(p_j^{(i)}+\delta p_j^{(i)}+p_{j-1}^{(i)}+\delta p_{j-1}^{(i)}\right)f_{j-1/2}^{n-1}-p_{j-1/2}^{n-1}\left(f_j^{(i)}+\delta f_j^{(i)}+f_{j-1}^{(i)}+\delta f_{j-1}^{(i)}\right) \end{array}\right\} \\
&=T_{j-1/2}^{n-1}
\end{aligned}
$$

$$
\begin{aligned}
&\Rightarrow (t_1)_j\,\delta p_j^{(i)}+(t_2)_j\,\delta p_{j-1}^{(i)}+(t_3)_j\,\delta f_j^{(i)}+(t_4)_j\,\delta f_{j-1}^{(i)}+(t_5)_j\,\delta u_j^{(i)} \\
&+(t_6)_j\,\delta u_{j-1}^{(i)}+(t_7)_j\,\delta\theta_j^{(i)}+(t_8)_j\,\delta\theta_{j-1}^{(i)}+(t_9)_j\,\delta v_j^{(i)}+(t_{10})_j\,\delta v_{j-1}^{(i)} \qquad (2.111e) \\
&=(r_3)_j
\end{aligned}
$$

where $(t_1)_j=\dfrac{1}{\mathrm{Pr}}h_j^{-1}+\dfrac{(p_1)_{j-1/2}^{n-1/2}+\alpha_n}{2}f_j^{(i)}-\dfrac{1}{2}\alpha_n f_{j-1/2}^{n-1}$ (2.114a)

$$(t_2)_j=-\frac{1}{\mathrm{Pr}}h_j^{-1}+\frac{(p_1)_{j-1/2}^{n-1/2}+\alpha_n}{2}f_{j-1}^{(i)}-\frac{1}{2}\alpha_n f_{j-1/2}^{n-1} \qquad (2.114b)$$

$$(t_3)_j=\frac{(p_1)_{j-1/2}^{n-1/2}+\alpha_n}{2}p_j^{(i)}+\frac{1}{2}\alpha_n p_{j-1/2}^{n-1} \qquad (2.114c)$$

$$(t_4)_j=\frac{(p_1)_{j-1/2}^{n-1/2}+\alpha_n}{2}p_{j-1}^{(i)}+\frac{1}{2}\alpha_n p_{j-1/2}^{n-1} \qquad (2.114d)$$

$$(t_5)_j=-\frac{\alpha_n}{2}\theta_j^{(i)}+\frac{1}{2}\alpha_n\theta_{j-1/2}^{n-1} \qquad (2.114e)$$

$$(t_6)_j=-\frac{\alpha_n}{2}\theta_{j-1}^{(i)}+\frac{1}{2}\alpha_n\theta_{j-1/2}^{n-1} \qquad (2.114f)$$

$$(t_7)_j=-\frac{\alpha_n}{2}u_j^{(i)}-\frac{1}{2}\alpha_n u_{j-1/2}^{n-1} \qquad (2.114g)$$

$$(t_8)_j=-\frac{\alpha_n}{2}u_{j-1}^{(i)}-\frac{1}{2}\alpha_n u_{j-1/2}^{n-1} \qquad (2.114h)$$

$$(t_9)_j=0 \qquad (2.114i)$$

$$(t_{10})_j=0 \qquad (2.114j)$$

71

$$
\begin{aligned}
(r_3)_j = & T^{n-1}_{j-1/2} - \frac{1}{P_r} h_j^{-1} (p_j^{(i)} - p_{j-1}^{(i)}) - \frac{(p_1)^{n-1/2}_{j-1/2} + \alpha_n}{2} (fp)^{(i)}_{j-1/2} \\
& + \alpha_n \{(u\theta)^{(i)}_{j-1/2} + u^{n-1}_{j-1/2} \theta^{(i)}_{j-1/2} - \theta^{n-1}_{j-1/2} u^{i}_{j-1/2}\} \\
& + \alpha_n \{f^{n-1}_{j-1/2} p^{(i)}_{j-1/2} - p^{n-1}_{j-1/2} f^{(i)}_{j-1/2}\}
\end{aligned}
\tag{2.112e}
$$

The boundary conditions (2.109) become

$$
\begin{aligned}
& \delta f_0^n = 0,\ \delta u_0^n = 0,\ \delta\theta_0^n - \chi \delta p_0^n = 0 \\
& \delta u_J^n = 0,\ \delta\theta_J^n = 0
\end{aligned}
\tag{2.115}
$$

which just express the requirement for the boundary conditions to remain during the iteration process.

Now the system of linear equations (2.111) together with the boundary conditions (2.115) can be written in a block matrix from as:

$$\mathbf{A.\delta = r} \tag{2.116}$$

Where,

$$
\mathrm{A} = \begin{bmatrix}
\mathrm{A}_0 & \mathrm{C}_0 & & & & & \\
\mathrm{B}_1 & \mathrm{A}_1 & \mathrm{C}_1 & & & & \\
 & & & & & & \\
 & & \mathrm{B}_j & \mathrm{A}_j & \mathrm{C}_j & & \\
 & & & \mathrm{B}_{J-1} & \mathrm{A}_{J-1} & \mathrm{C}_{J-1} & \\
 & & & & \mathrm{B}_J & \mathrm{A}_J
\end{bmatrix};\quad
\delta = \begin{bmatrix} \delta_0 \\ \delta_1 \\ . \\ \delta_j \\ . \\ \delta_J \end{bmatrix};\quad \text{and}\quad
\mathrm{r} = \begin{bmatrix} \mathrm{r}_0 \\ \mathrm{r}_1 \\ . \\ \mathrm{r}_j \\ . \\ \mathrm{r}_J \end{bmatrix}
$$

We now define $\delta_j,\ \mathrm{r}_j, \mathrm{A}_j,\ \mathrm{B}_j$ and C_j as follows:

$$
\delta_j = \begin{bmatrix} \delta f_j \\ \delta u_j \\ \delta v_j \\ \delta\theta_j \\ \delta p_j \end{bmatrix} \quad \text{for } 0 \le j \le J
$$

72

$$\mathrm{r}_0 = \begin{bmatrix} 0 \\ 0 \\ 0 \\ (r_4)_1 \\ (r_5)_1 \end{bmatrix}, \quad \mathrm{r}_J = \begin{bmatrix} (r_1)_J \\ (r_2)_J \\ (r_3)_J \\ 0 \\ 0 \end{bmatrix} \text{ and } \mathrm{r}_j = \begin{bmatrix} (r_1)_j \\ (r_2)_j \\ (r_3)_j \\ (r_4)_j \\ (r_5)_j \end{bmatrix} \text{ for } 0 \le j \le J-1,$$

$$\mathrm{A}_0 = \begin{bmatrix} 1 & 0 & 0 & 0 & 0 \\ 0 & 1 & 0 & 0 & 0 \\ 0 & 0 & 0 & 1 & -\chi \\ 0 & -1 & -\frac{h_1}{2} & 0 & 0 \\ 0 & 0 & 0 & -1 & -\frac{h_1}{2} \end{bmatrix}$$

$$\mathrm{A}_J = \begin{bmatrix} 1 & -\frac{h_J}{2} & 0 & 0 & 0 \\ (s_3)_J & (s_5)_J & (s_1)_J & (s_7)_J & 0 \\ (t_3)_J & (t_5)_J & (t_9)_J & (t_7)_J & (t_1)_J \\ 0 & 1 & 0 & 0 & 0 \\ 0 & 0 & 0 & 1 & 0 \end{bmatrix}$$

$$\mathrm{A}_j = \begin{bmatrix} 1 & -\frac{h_j}{2} & 0 & 0 & 0 \\ (s_3)_j & (s_5)_j & (s_1)_j & (s_7)_j & 0 \\ (t_3)_j & (t_5)_j & (t_9)_j & (t_7)_j & (t_1)_j \\ 0 & -1 & -\frac{h_{j+1}}{2} & 0 & 0 \\ 0 & 0 & 0 & -1 & -\frac{h_{j+1}}{2} \end{bmatrix} \text{ for } 1 \le j \le J-1$$

$$\mathrm{B}_j = \begin{bmatrix} -1 & -\frac{h_j}{2} & 0 & 0 & 0 \\ (s_4)_j & (s_6)_j & (s_2)_j & (s_8)_j & 0 \\ (t_4)_j & (t_6)_j & (t_{10})_j & (t_8)_j & (t_2)_j \\ 0 & 0 & 0 & 0 & 0 \\ 0 & 0 & 0 & 0 & 0 \end{bmatrix} \text{ for } 1 \le j \le J$$

73

$$C_j = \begin{bmatrix} 0 & 0 & 0 & 0 & 0 \\ 0 & 0 & 0 & 0 & 0 \\ 0 & 0 & 0 & 0 & 0 \\ 0 & 1 & -\frac{h_{j+1}}{2} & 0 & 0 \\ 0 & 0 & 0 & 1 & -\frac{h_{j+1}}{2} \end{bmatrix} \quad \text{for } 0 \le j \le J-1$$

The solution of the equation (2.116) by block-elimination method consists of two sweeps. In forward sweep we compute Γ_j, Δ_j and w_j from the recursion formulas given by:

$$\Delta_0 = A_0 \tag{2.117a}$$

$$\Gamma_j \Delta_{j-1} = B_j \qquad for \quad 1 \le j \le J \tag{2.117b}$$

$$\Delta_j = A_j - \Gamma_j C_{j-1} \quad for \quad 1 \le j \le J \tag{2.117c}$$

$$w_0 = r_0 \tag{2.117d}$$

$$w_j = r_j - \Gamma_j w_{j-1} \qquad for \quad 1 \le j \le J \tag{2.117e}$$

Here Γ_j has the same structure as B_j.

In the backward sweep, δ_j is computed from the recursion formulas:

$$\Delta_J \delta_J = w_J \tag{2.118a}$$

$$\Delta_j \delta_j = w_j - C_j \delta_{j+1} \quad \text{for } j = J-1, J-2, ..., 0 \tag{2.118b}$$

This numerical method of solution has been applied with the required modification for the other three cases, which are discussed in subsections 2.4.2, 2.4.3 and 2.4.4.

74

Chapter III

MHD Conjugate Free Convection Flow from an Isothermal Horizontal Circular Cylinder

3.1 Introduction

The specific problem selected for study is the flow and heat transfer in an electrically conducting fluid around an isothermal horizontal circular cylinder. In this study, the steady laminar MHD conjugate free convection flow of a viscous and incompressible fluid due to an isothermal horizontal circular cylinder with an axial uniform magnetic field is considered. Mathematical analysis of this problem is discussed in section 2.4.1 as case I of chapter II. The equations (2.50), (2.51) and (2.52) are the dimensionless form of the continuity equation, momentum equation and energy equation. Further we have the equations (2.66) and (2.67) as the momentum equation and energy equation using stream function defined in equation (2.54) and (2.55) which satisfies dimensionless continuity equation (2.50). The final form of the momentum and energy equations (2.66) and (2.67) are solved using implicit finite difference method based on the boundary condition defined in equation (2.68).

$$f''' + ff'' - f'^2 - Mf' + \theta\frac{\sin x}{x} = x\left(f'\frac{\partial f'}{\partial x} - f''\frac{\partial f}{\partial x}\right)$$

$$\frac{1}{\Pr}\theta'' + f\theta' = x\left(f'\frac{\partial \theta}{\partial x} - \theta'\frac{\partial f}{\partial x}\right)$$

$$f = f' = 0,\ \theta - 1 = \chi\frac{\partial \theta}{\partial y}\ at\ y = 0,\ x > 0$$

$$f' \to 0,\ \theta \to 0\ as\ y \to \infty,\ x > 0$$

If we consider M=0.0 in equation (2.66) and χ= 0 in equation (2.68) then the present analysis will refer to free convection problem with no conduction and the momentum equation (2.66) the boundary conditions in (2.68) becomes:

$$f''' + ff'' - f'^2 + \theta \frac{\sin x}{x} = x\left(f' \frac{\partial f'}{\partial x} - f'' \frac{\partial f}{\partial x} \right) \tag{3.1}$$

$$\begin{aligned} &u = v = 0,\ \theta = 1,\ \ on\ \ y = 0,\ x > 0 \\ &u \to 0,\ \theta \to 0\ as\ \ y \to \infty,\ x > 0 \end{aligned} \tag{3.2}$$

The reduced form of the momentum equation (3.1), the energy equation (2.67) and the boundary conditions in equation (3.2) are considered by Merkin in 1976 (Pop and Ingham, 2001) and Nazar et al. (2002). Later on we compare the present numerical results with the results obtained by Merkin and Nazar et al..

3.2 Numerical Results

The numerical results of the equations (2.66) and (2.67) based on the boundary condition (2.68) are presented in the following sub-sections. In section 3.2.1, a grid refinement test is given. A comparison of the local Nusselt number and the local skin friction factor obtained in the present work and obtained by Merkin (1976) and Nazar et al. (2002) is shown in section 3.2.2 and the graphical presentation of the numerical results for the velocity and temperature distribution within the boundary layer and the skin friction coefficient and local heat transfer along the surface with an elaborate discussion are presented in section 3.2.3.

3.2.1 Grid independent test

The grid independent test has been shown by taking three different grid configurations, 181×305, 361×405 and 451×505 in Figures 3.1(a) and 3.1(b) as the skin-friction coefficient and the rate of heat transfer while Pr=1.0, M=0.1 and χ=1.0. From these Figures, it can be concluded that the numerical solutions are completely independent of the grid orientations. In the present investigation 181 × 305 grid configuration has been chosen for the numerical computation.

3.2.2 Comparison

The present results have been compared with the previous studies in the literature, which are shown in Table 3.1 and Table 3.2 respectively. The comparison of the local Nusselt number and the comparison of the local skin friction factor obtained

in the present work with M=0.0, *J*=0.0 and Pr=1.0 and obtained by Merkin (1976) and Nazar et al. (2002) are made available in Table 3.1 and Table 3.2 respectively. It is clear from these two tables that there is an excellent agreement among these three results.

3.2.3 Discussion

The main objective of the present work is to analyze the flow of the fluid and the conjugate heat transfer processes due to the conduction inside the solid of the cylinder and natural convection from the isothermal horizontal circular cylinder in presence of magnetic field. The effects of the relevant parameters, such as magnetic parameter, conjugate conduction parameter and Prandtl number on the surface share stress in terms of the skin friction coefficient, the rate of heat transfer in terms of Nusselt number, the velocity due to natural convection and the temperature distribution over the whole boundary layer are shown graphically.

The Prandtl numbers are considered to be 1.63, 1.44, 1.0 and 0.733 for the simulation that correspond to glycerin at 50^0C, water at 120^0C, steam at 700^0K and hydrogen at 1300^0K, respectively. The magnetic parameter is the ratio of the magnetic force to the inertia force. Hence the magnetic force is important when it is the order of one and the flow is considered as hydromagnetic flow. The flow is hydrodynamic for the value of the magnetic parameter $M << 1$. For small value of the magnetic parameter M, the motion is hardly affected by the magnetic field and for large value of the magnetic parameter M, the motion is largely controlled by the magnetic field. The values of the magnetic parameter are chosen as (M=0.0, 0.1, 0.3, 0.5, 0.7) throughout the thesis. From the equation (2.68) it has been observed that the conjugate conduction parameter χ is derived as $\chi = (b\kappa_f)/(a\kappa_s).Gr^{1/4}$. According to the definition of the conjugate conduction parameter χ, it can be easily understood that the values of the conjugate conduction parameter χ depend upon the ratios of b/a and κ_f / κ_s and Grashof number Gr. The ratios b/a and κ_f / κ_s are less than one where as, the Grashof

number Gr is large for free convection. Therefore, the value of χ is greater than zero. Present analysis will refer to the free convection problem without conduction for $\chi = 0$. In this study, the values of the conjugate conduction parameter taken as (χ = 0.0, 0.75, 1.0, 1.5, 2.0, 2.5).

The skin friction coefficients and the rate of heat transfer obtained from the relation (2.70) are illustrated in Figures 3.5-3.7 and the velocity profiles and temperature distributions obtained from the relations (2.71) are presented in Figures 3.2-3.4. Since the velocity and the temperature are the function of x and y, thus, Figures 3.2-3.4 illustrate the velocity and temperature distributions at $x=\pi/2$ against y, the direction along the normal to the surface of the cylinder.

From all figures of velocity profiles it is observed that the fluid velocity is zero at the surface of the cylinder i.e. at y=0 as well as at the outer edge of the velocity boundary layer. This is expected since the fluid beyond the boundary layer is motionless. Thus, the fluid velocity increases with the distance from the surfaces, reaches a maximum, and gradually decreases to zero at a distance sufficiently far from the surface. Again, it is found from figures of the temperature profiles that the temperature is maximum at the surface i.e. y=0 and gradually decreases to the temperature of the surrounding fluid at distance sufficiently far from the surface.

The boundary layer around the horizontal circular cylinder starts to develop at the bottom of the cylinder, increasing the thickness along the circumference, therefore, the velocity gradient is zero at the lower stagnation point, thus it increases with the increasing value of x, reaches a maximum, due to the curvature effect it started to decrease gradually just after a critical value of x. As the heated fluid surrounding the cylinder is rising up within the boundary layer, the temperature of the upper region also increases gradually with the increased value of x. Thus the temperature difference between the surface and the fluid within the boundary layer is lower in the upper region than that of in the lower region. Therefore the rate of heat transfer is the highest at the bottom, and lowest at the

78

top of the cylinder. These common phenomenon for the skin friction coefficient and the rate of heat transfer are observed in all Figures 3.5-3.7.

Numerical values of the velocity $f'(x,y)$ and the temperature $\theta(x,y)$ are illustrated in Figure 3.2(a) and Figure 3.2(b) respectively against the axial distance y for different values of magnetic parameter (M=0.1, 0.3, 0.5, 0.7) for the fluid having Prandtl number Pr=1.0 with conjugate conduction parameter χ =1.0. From Figure 3.2 it is seen that, as the magnetic parameter M increases, the velocity profile decreases and the temperature profile increases. The reason of this practical scenario is that the interaction of the magnetic field and the moving electric charge carried by the fluid induces a force which tends to oppose the fluid motion. But near the surface of the cylinder, velocity increases and after a distance from the surfaces it decreases slowly and finally approaches to zero. This implies that there exists a local maximum of the velocity within the boundary-layer. The local maximums for different values of magnetic parameter M while Pr=1.0 and χ =1.0 are shown in the Table 3.3 and it has been observed that the maximum velocity come closer to the surface for increasing value of the magnetic parameter. The maximum values of the velocities are found as 0.284157, 0.254927, 0.230954 and 0.211052 for M=0.1, M=0.3, M=0.5 and M=0.7 respectively. It is noted that the velocity decreases by approximately 25.73% as magnetic parameter increases from 0.1 to 0.7.

Figures 3.3(a) and 3.3(b) are the graphical representation of the velocity $f'(x,y)$ and the temperature $\theta(x,y)$ respectively against y axis for different values of conjugate conduction parameter (χ =0.75, 1.0, 1.5, 2.0) for the fluid having Prandtl number Pr=1.0 with magnetic parameter M=0.1. It can be concluded, From Figure 3.3 that as the value of the conjugate conduction parameter χ increases, the velocity profile and the temperature profile both decrease. The physical fact behind it is that the increasing value of the conjugate conduction parameter χ resists thermal energy transfer by conductive mode from core region of the cylinder to the boundary layer in the vicinity of the cylinder, so

79

that the temperature distribution within the boundary layer decreases for the increasing values of the conjugate conduction parameter χ as observed in Figure 3.3(b). Since the temperature within the boundary layer decreases for increasing values of the conjugate conduction parameter χ, it must decelerates convection at the surface of the cylinder and finally the flow of the surrounding fluid is reduced which are illustrated in Figure 3.3(a). The local maximums for different values of values of the conjugate conduction parameter χ while Pr=1.0 and M=0.1 are shown in the Table 3.4. It is clear from Table 3.4 that the local maximums for the velocity profiles go away from the surface for increasing value of the magnetic parameter. The maximum values of the velocities are found as 0.294869, 0.284157, 0.266868 and 0.252827 for χ = 0.75, χ = 1.0, χ = 1.5 and χ=2.0 respectively. The velocity decreases by approximately 14.26% as conjugate conduction parameter χ increases from 0.75 to 2.0.

The velocity profiles and temperature distributions against y for different values of Prandtl number (Pr=0.733, 1.0, 1.440, 1.630) with magnetic parameter M=0.1 and conjugate conduction parameter χ =1.0 are presented graphically in Figure 3.4(a) and Figure 3.4(b) respectively. The maximum velocities for different values of Prandtl number Pr while magnetic parameter M=0.1 and conjugate conduction parameter χ =1.0 are provided in Table 3.5. It is noted that the maximum velocities are closer to the surface for increasing value of the Prandtl number. The maximum values of the velocities are found as 0.314559, 0.284157, 0.250420 and 0.239484 at y=1.564468, y=1.509461, y=1.438224and y=1.420778 for Pr=0.733, Pr=1.0, Pr=1.44 and Pr=1.63 respectively. It is seen that the velocity decreases by approximately 23.87% as Prandtl number increases from 0.733 to 1.630. Besides that the velocity decreases for the increasing values of the Prandtl number Pr and the temperature also decreases for the increasing values of the Prandtl number which are observed from Figure 3.4(a) and Figure 3.4(b) respectively. Moreover, it is observed that the thickness of the velocity boundary layer and thermal boundary layer become thinner for increasing values of the Prandtl number. The above are the predictable physical significance of the Prandtl

number as it is known that the Prandtl number Pr is the ratio of viscous force and thermal action. Thus the increasing value of the Prandtl number Pr represents a fluid with increasing viscosity or decreasing thermal conductivity. Therefore the increasing viscosity decreases the flow of the fluid and lower thermal conductivity decreases temperature within the boundary layer.

The effect of magnetic parameter (M=0.1, 0.3, 0.5, 0.7) for the fluid having Prandtl number Pr=1.0 with conjugate conduction parameter χ =1.0 on the surface shear stress in terms of the local skin friction coefficient and the rate of heat transfer in terms of local Nusselt number are depicted in Figures 3.5(a) and 3.5(b) respectively against x. The increasing values of magnetic parameter increase magnetic field strength which is acting normal to the surface of the cylinder and reduces fluid motion, as discussed earlier as a result the skin friction at the surface of the cylinder is decreased for increasing values of magnetic parameter which is illustrated in Figure 3.5 (a). Heat produces due to the interaction between magnetic field and fluid motion, consequently, temperature within the thermal boundary layer increases for increasing value of magnetic parameter consequently, it reduces temperature difference between core region and boundary layer region which ultimately decreases heat transfer rate as illustrated in Figure 3.5(b). Moreover, it has been observed from Table 3.6 that the maximum values of the skin friction coefficient are 0.738048, 0.681999, 0.637196 and 0.600514 for M=0.1, M=0.3, M=0.5 and M=0.7 and which are occurred at x=1.850049, x=1.797689, x=1.762783 and x=1.727876 that is maximum values of skin friction are shifted closer to the lower stagnation point for the increasing values of magnetic parameter. Furthermore it has been calculated that the maximum value of the skin friction coefficient decreases by 18.63% as magnetic parameter M increases from 0.1 to 0.7.

The values of the skin friction coefficient and the rate of heat transfer have been presented in Figure 3.6(a) and Figure 3.6(b) respectively for different values of conjugate conduction parameter (χ=0.75, 1.0, 1.5, 2.0) while the other controlling

81

parameters are: Prandtl number Pr=1.0 and magnetic parameter M=0.1. Increasing value of conjugate conduction parameter χ resists heat transfer by conduction from the inner region to the boundary layer region of the cylinder as observed in Figure 3.6(b). Consequently, decelerates convection within the boundary layer. As a result velocity decreases for increasing values of conjugate conduction parameter at a particular value of y, as the velocity decreases, the skin friction at the surface decreases for increasing value of conjugate conduction parameter χ, as observed in Fig 3.6(a). It can be noted from Table 3.7 that the maximum values of the skin friction coefficient are 0.778009 for χ=0.75, 0.738048 for χ =1.0, 0.673587 for χ =1.5 and 0.622761 for χ =2.0 at x=1.850049. Finally it is observed that the maximum value of the skin friction coefficient decreases by 19.95% as conjugate conduction parameter χ increases from 0.75 to 2.0.

The variation of the skin friction coefficients and the variation of rate of heat transfer against x for different values of the Prandtl number (Pr=0.733, Pr=1.0, Pr=1.44, Pr=1.63) with magnetic parameter M=0.1 and conjugate conduction parameter χ = 1.0 are shown in Figures 3.7(a) and 3.7(b) respectively. It is discussed earlier that the increasing values of Prandtl number decreases velocity, which leads to decrease skin friction coefficient as illustrated in Figure 3.7(a). From Figure 3.7(b) it is observed that the rate of heat transfer increases for increasing values of Prandtl number. Beside this, one can reveal that the rates of heat transfer are almost same for all the values of the Prandtl numbers at x=π.

The Table 3.8 shows the maximum values of the skin friction coefficient $xf''(x,0)$ against x for different values of Prandtl number Pr while M=0.1 and χ=1.0. It is observed that the maximum values of the skin friction coefficient are 0.790054, 0.738048, 0.678296 and 0.658416 which are obtained for Pr=0.733, Pr=1.0, Pr =1.44 and Pr=1.63 at x=1.850049, x=1.850049, x=1.832596 and x=1.832596 respectively. Moreover it is calculated that the maximum value of the

82

skin friction coefficient decreases by 16.66% as Prandtl number Pr increases from 0.733 to 1.630.

TABLES

Table 3.1: Comparisons of the present numerical values of $-\theta'(x,0)$ with Merkin (1976) and Nazar et al. (2002) for different values of x while with Pr=1.0, $M = 0.0$ and $\chi = 0.0$.

$Nu\,Gr^{-1/4} = -\theta'(x,0)$			
x	Merkin (1976)	Nazar et al. (2002)	Present
0.0	0.4214	0.4214	0.4216
π/6	0.4161	0.4161	0.4163
π/3	0.4007	0.4005	0.4006
π/2	0.3745	0.3741	0.3741
2π/3	0.3364	0.3355	0.3355
5π/6	0.2825	0.2811	0.2811
π	0.1945	0.1916	0.1912

Table 3.2: Comparisons of the present numerical values of $x f''(x,0)$ with Merkin (1976) and Nazar et al. (2002) for different values of x while Pr=1.0, M = 0.0 and $\chi = 0.0$.

$C_f\,Gr^{1/4} = x f''(x,0)$			
x	Merkin (1976)	Nazar et al. (2002)	Present
0.0	0.0000	0.0000	0.0000
π/6	0.4151	0.4148	0.4139
π/3	0.7558	0.7542	0.7528
π/2	0.9579	0.9545	0.9526
2π/3	0.9756	0.9698	0.9678
5π/6	0.7822	0.7740	0.7718
π	0.3391	0.3265	0.3239

83

Table 3.3: Maximum velocity $f'(x, y)$ against y for different values of magnetic parameter M while with Pr=1.0 and χ = 1.0.

Magnetic parameter M	y	Maximum Velocity
0.1	1.509461	0.284157
0.3	1.491429	0.254927
0.5	1.473548	0.230954
0.7	1.455813	0.211052

Table 3.4: Maximum velocity $f'(x, y)$ against y for different values of conjugate conduction parameter χ while Pr=1.0 and M = 0.1.

Conjugate conduction parameter χ	y	Maximum Velocity
0.75	1.473548	0.294869
1.0	1.509461	0.284157
1.5	1.545979	0.266868
2.0	1.583115	0.252827

Table 3.5: Maximum velocity $f'(x, y)$ against y for different values of Prandtl number Pr while M=0.1 and χ = 1.0.

Prandtl number Pr	y	Maximum Velocity
0.733	1.564468	0.314559
1.000	1.509461	0.284157
1.440	1.438224	0.250420
1.630	1.420778	0.239484

84

Table 3.6: Maximum value of the skin friction coefficient $xf''(x,0)$ against x for different values of magnetic parameter M while Pr=1.0 and χ = 1.0.

Magnetic parameter M	x	Maximum $C_f Gr^{1/4} = xf''(x,0)$
0.1	1.850049	0.738048
0.3	1.797689	0.681999
0.5	1.762783	0.637196
0.7	1.727876	0.600514

Table 3.7: Maximum value of the skin friction coefficient $xf''(x,0)$ against x for different values of conjugate conduction parameter χ while Pr=1.0 and M=0.1.

Conjugate conduction parameter χ	x	Maximum Skin friction coefficient
0.75	1.850049	0.778009
1.0	1.850049	0.738048
1.5	1.850049	0.673587
2.5	1.850049	0.622761

Table 3.8: Maximum value of the skin friction coefficient $xf''(x,0)$ against x for different values of Prandtl number Pr while M=0.1 and χ =1.0.

Prandtl number Pr	x	Maximum Skin friction coefficient
0.733	1.850049	0.790054
1.000	1.850049	0.738048
1.440	1.832596	0.678296
1.630	1.832596	0.658416

FIGURES

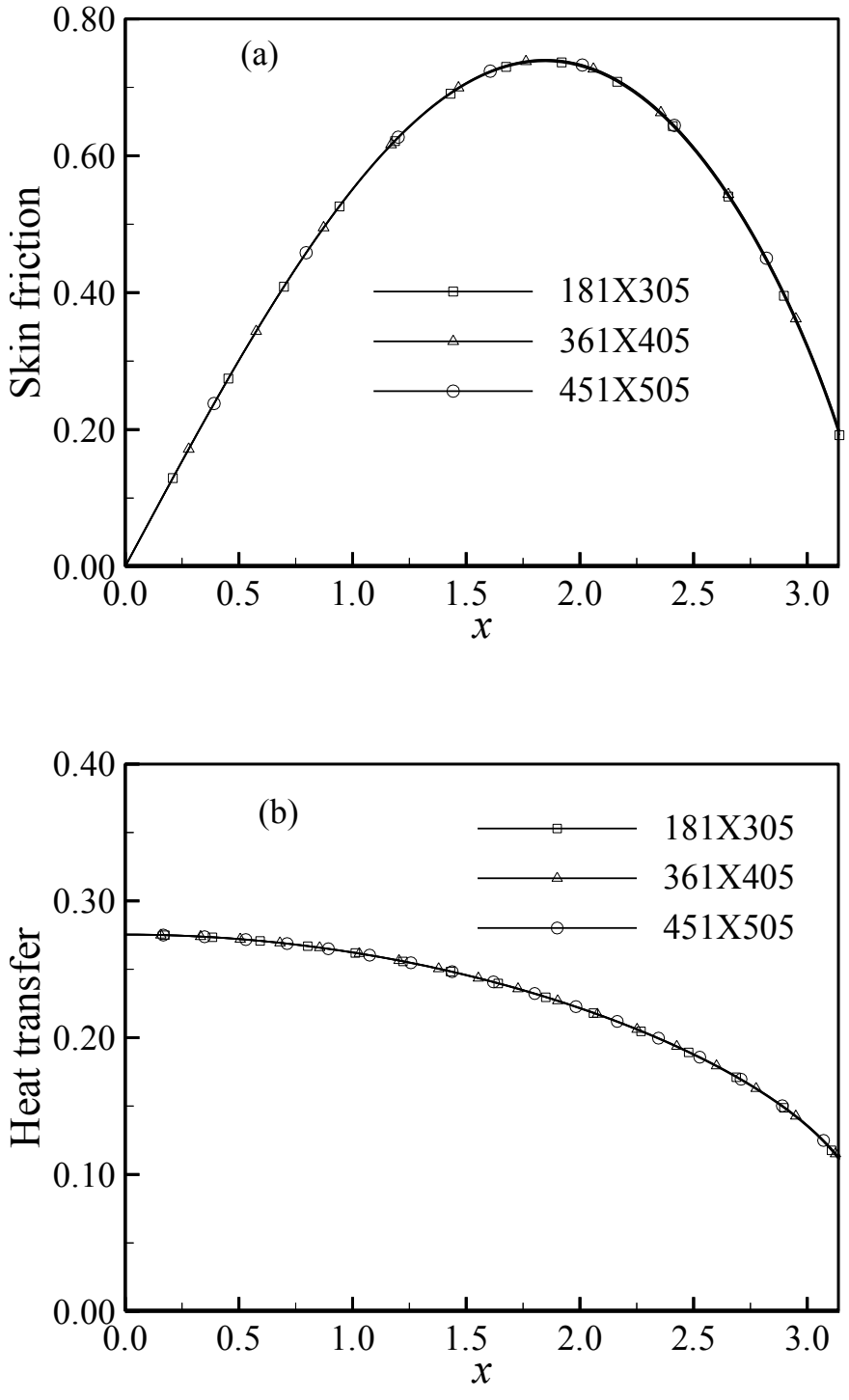

86 **Figure 3.1:** (a) The skin friction coefficient and (b) the rate of heat transfer against x for different mesh configurations while Pr=1.0, M=0.1, χ=1.0.

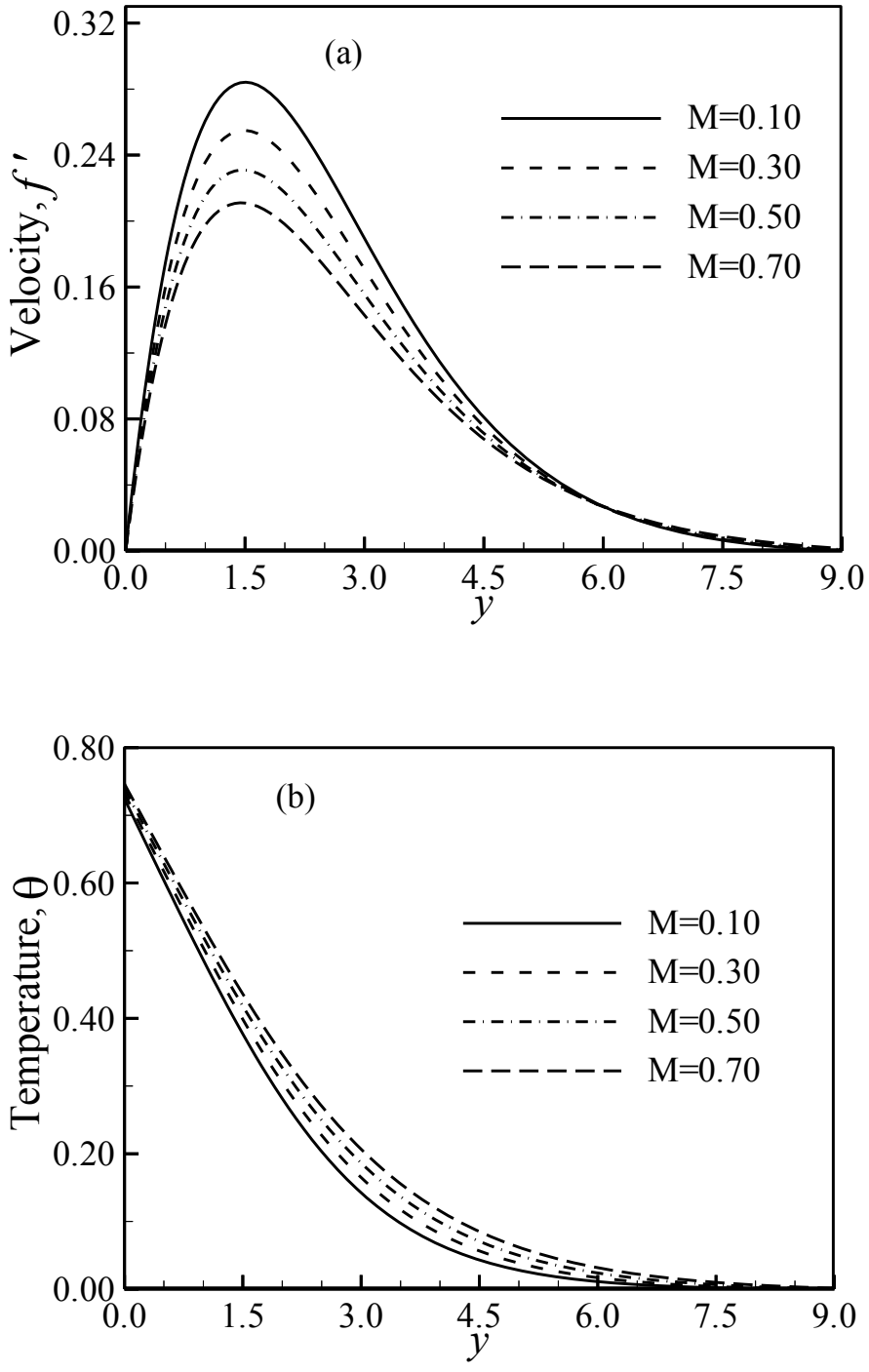

Figure 3.2: (a) Variation of velocity profiles and (b) variation of temperature distributions against y for varying of magnetic parameter M with Pr =1.0 and χ=1.0.

87

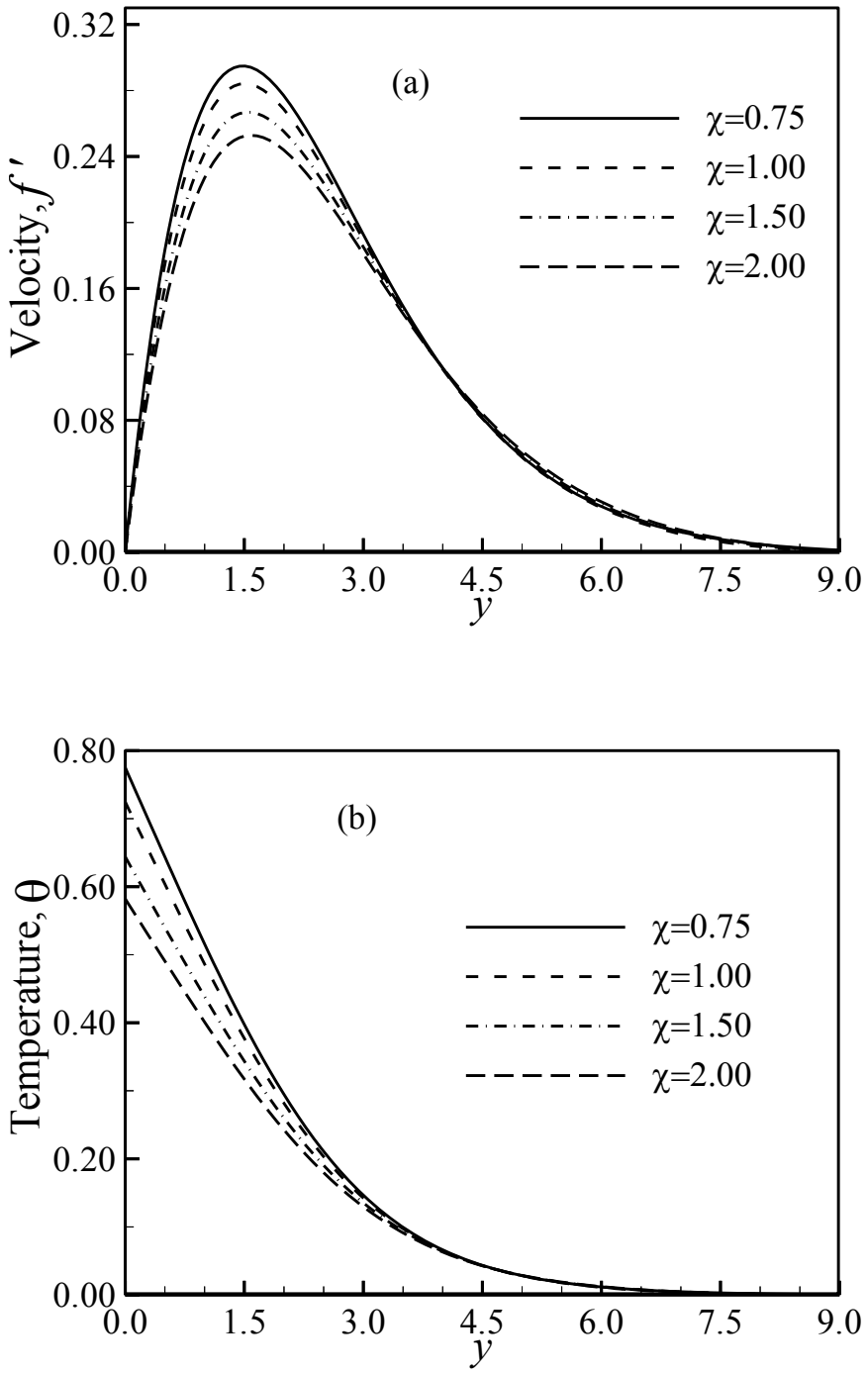

Figure 3.3: (a) Variation of velocity profiles and (b) variation of temperature distributions against y for varying of conjugate conduction parameter χ with Pr=1.0 and M = 0.1.

88

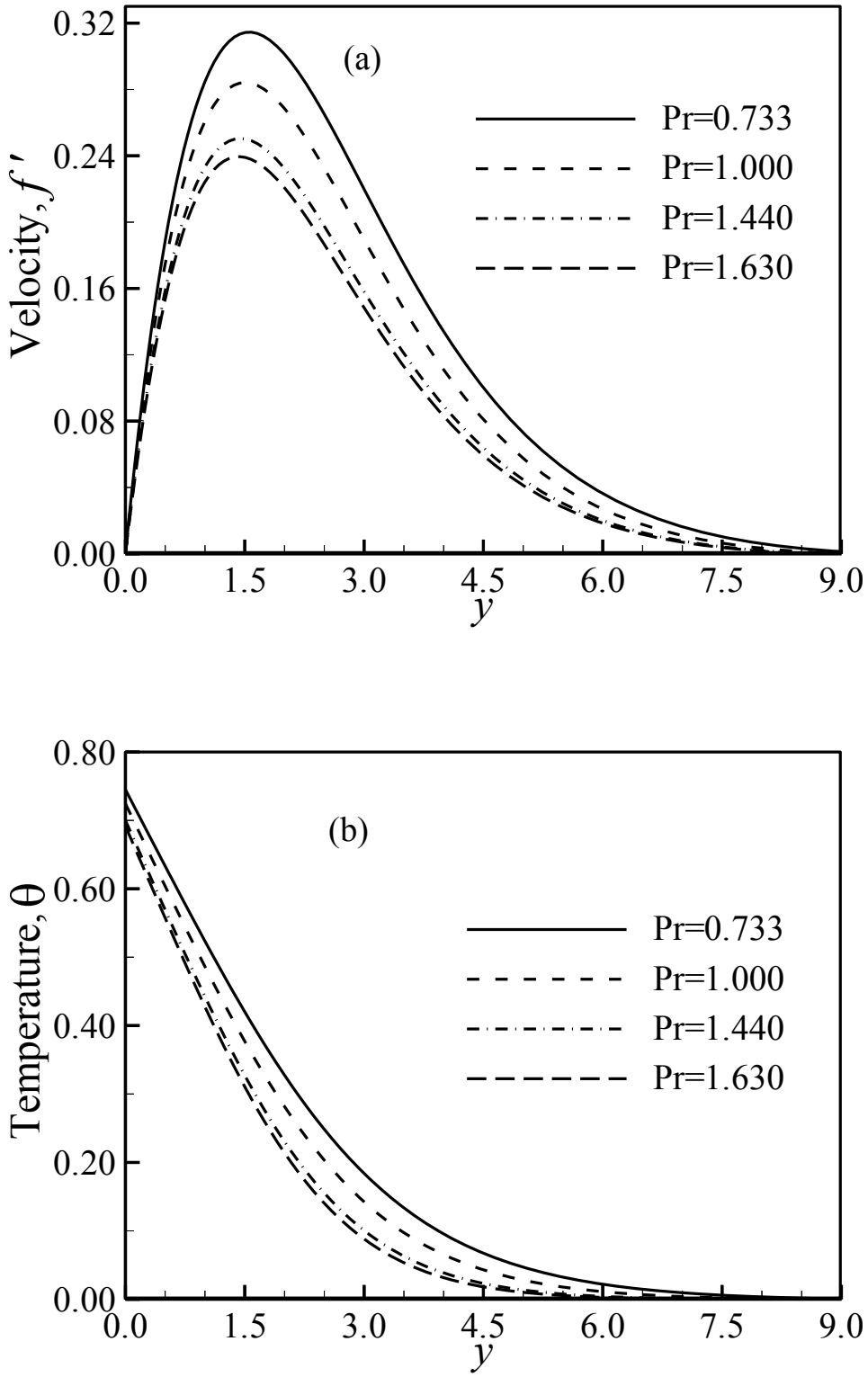

89 **Figure 3.4:** (a) Variation of velocity profiles and (b) variation of temperature distributions against y for varying of Pr with M = 0.1 and χ = 1.0.

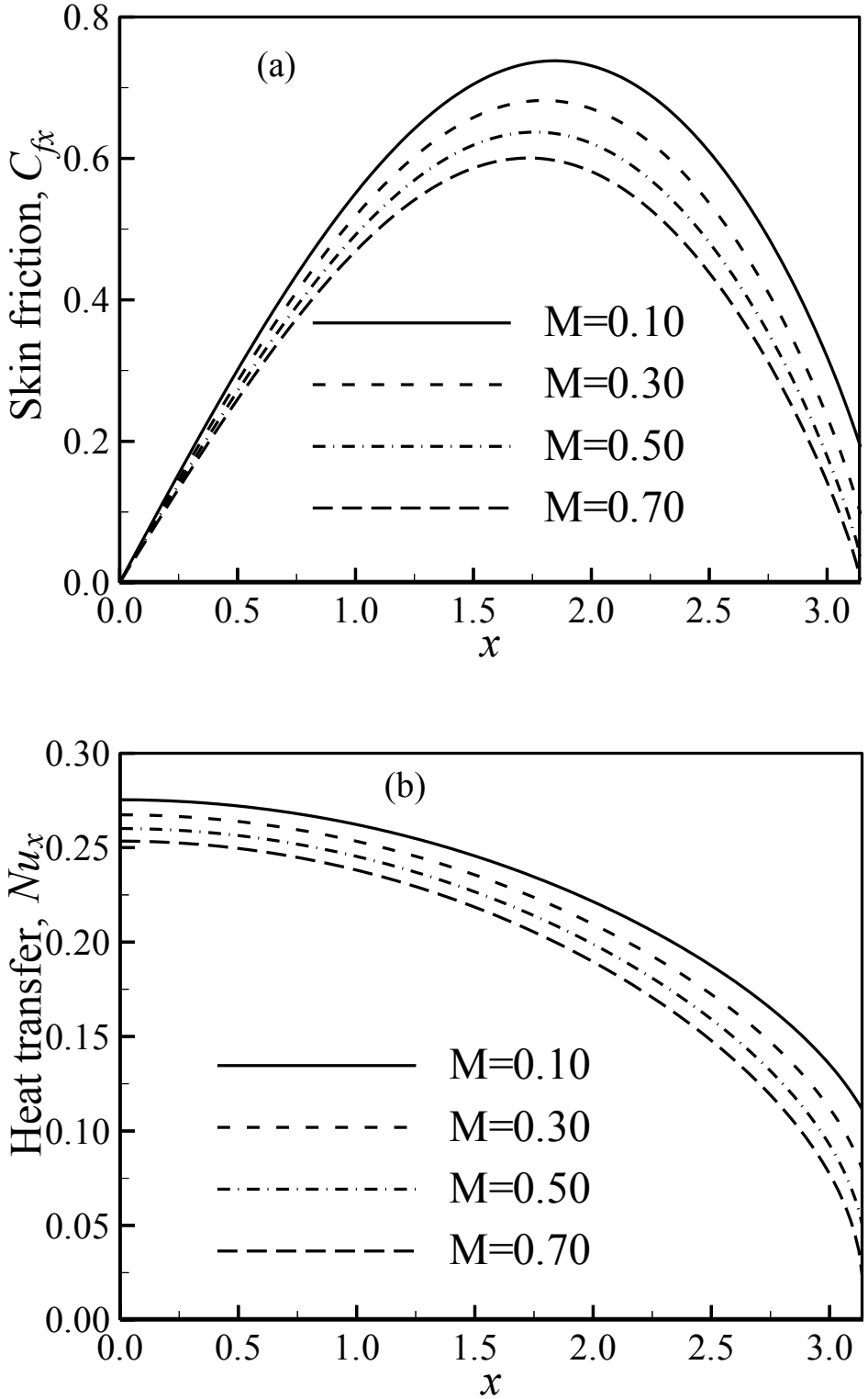

Figure 3.5: (a) Variation of skin friction coefficients and (b) variation of rate of heat transfer against x for varying of M with Pr = 1.0 and χ = 1.0.

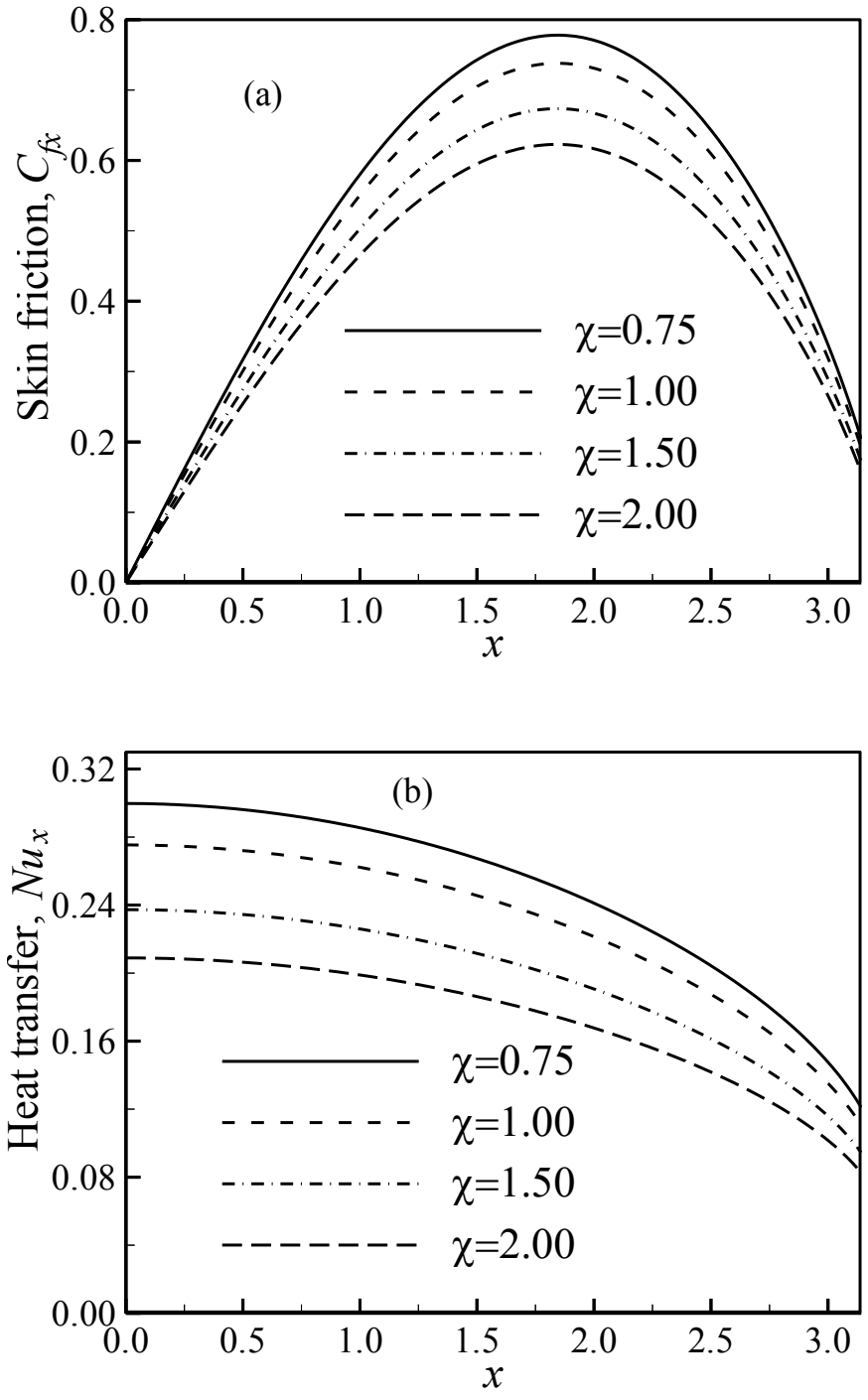

Figure 3.6: (a) Variation of skin friction coefficients and (b) variation of rate of heat transfer against x for varying of conjugate conduction parameter χ with Pr = 1.0 and M = 0.1.

91

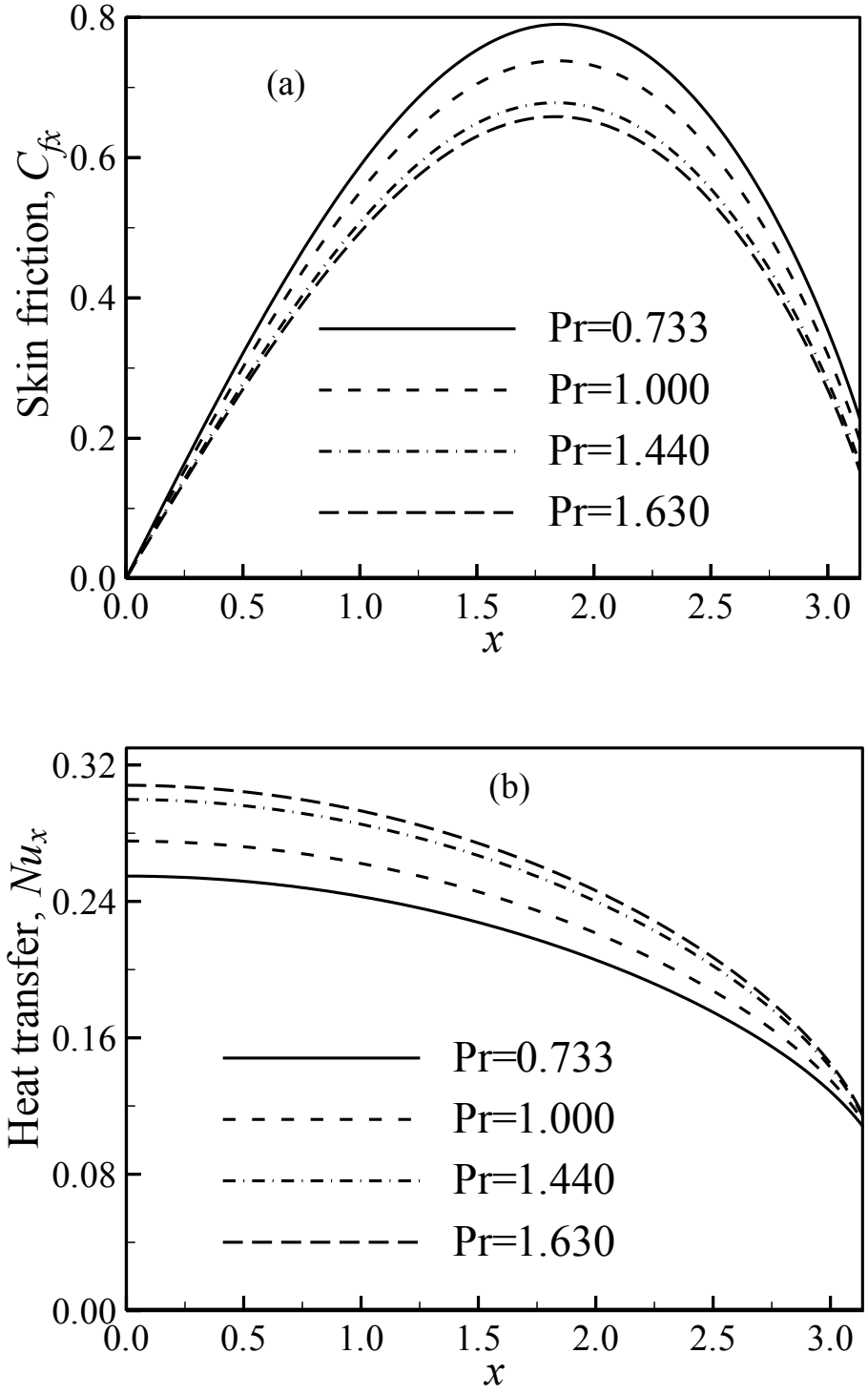

Figure 3.7: (a) Variation of skin friction coefficients and (b) variation of rate of heat transfer against x for varying of Pr with M = 0.1 and χ = 1.0.

92

3.3 Conclusion

A steady, two dimensional, MHD-conjugate free convection flow from an isothermal horizontal circular cylinder is studied. The effects of the magnetic parameter, conjugate conduction parameter and Prandtl number are analysed. From the present study following conclusion may be drawn:

- The velocity of the fluid within the boundary layer decreases with increasing magnetic parameter, conjugate conduction parameter and Prandtl number.

- The temperature of the fluid within the boundary layer increases for increasing magnetic parameter whereas it decreases for increasing conjugate conduction parameter and Prandtl number.

- The skin friction along the surface of the cylinder decreases for increasing magnetic parameter, conjugate conduction parameter and Prandtl number.

- The rate of heat transfer along the surface decreases for increasing value of the magnetic parameter and conjugate conduction parameter while it increases for increasing Prandtl number.

93

Chapter IV

MHD-Conjugate Free Convection Flow from an Isothermal Horizontal Circular Cylinder with Joule heating and Heat Generation

4.1 Introduction

In the physical model of this thesis, it was considered that the cylinder is placed in a fluid which is electrically conducting. It is known that, some electric energy is transformed into thermal energy as an electric current flowing through a solid or liquid with finite conductivity, through resistive losses in the material. This phenomenon is known as Joule heating. At an atomic level, Joule heating is the result of moving electrons colliding with atoms in a conductor, whereupon momentum is transferred to the atom, increasing its kinetic energy. Joule heating is named for James Prescott Joule, the first to articulate what is now Joule's law, relating the amount of heat released from an electrical resistor to its resistance and the charge passed through it. Joule heating increases for increasing current. If the current is large enough, Joule heating can start a fire. When the conduction electrons transfer energy to the conductor‟s atoms through collisions the heat is generated in this process is on the micro scale. The Joule heating effect is in some cases unwanted, and efforts are made to reduce it. However, many applications rely on Joule heating; some of these use the effect directly, such as cooking plates, while other applications, such as micro valves for fluid control, use the effect indirectly through thermal expansion. Hossain (1992) studied viscous and Joule heating effects on MHD free convection flow with variable plate temperature. El-Amin (2003) found out the combined effect of viscous dissipation and Joule heating on MHD forced convection over a non-isothermal horizontal circular cylinder embedded in a fluid saturated porous medium.

Many practical heat transfer applications involve the conversion of some form of mechanical, electrical, nuclear or chemical energy to thermal energy in the

94

medium. Such mediums are said to involve internal heat generation. For example, a large amount of heat is generated in the fuel elements from atomic reactors as a result of atomic fission that serves as the heat source for the nuclear power plants. The heat generated in the sun as a result of fusion of hydrogen into helium makes the sun a large nuclear reactor that supplies heat to the earth. Possible heat generation effects may modify temperature distribution and, therefore, the particle deposition rate. The heat transfer in a laminar boundary layer flow of a viscous fluid over a linearly stretching continuous surface with viscous dissipation/frictional heating and internal heat generation was analyzed by Vajravelu and Hadjinicolaou (1993). They considered the volumetric rate of heat generation, q''' [W/m3], as:

$$q''' = \begin{cases} Q_0 \left(T_f - T_\infty\right), for\ T_f \geq T_\infty \\ 0 \quad for\ T_f < T_\infty \end{cases} \tag{4.1}$$

where Q_0 is the heat generation constant. The above relation is valid for the state of some exothermic processes having T_∞ as onset temperature. Effects of heat generation/absorption and thermophorosis on hydromagnetic flow along a flat plate were studied by Chamkha and Camille (2000). Molla et al. (2006) studied natural convection flow from an isothermal horizontal circular cylinder in presence of heat generation considering above term as heat generation. Moreover, natural convection heat transfer from a horizontal isothermal elliptical cylinder with internal heat generation was studied by Ching-Yang cheng (2009).

Two physical phenomena, one Joule heating and another volumetric rate of heat generation are taken into account in this chapter.

4.2 Boundary layer equations

Mathematical formulation of the present investigation has been discussed elaborately in section 2.4.2 as case II of chapter II. The equations (2.50), (2.51) and (2.75) are the dimensionless form of the continuity equation, momentum equation and energy equation. Further we have the equations (2.66) and (2.76) as

95

the momentum equation and energy equation using stream function defined in equation (2.54) and (2.55) which satisfies dimensionless continuity equation (2.50). The final form of the momentum and energy equations (2.66) and (2.76) are solved using implicit finite difference method based on the boundary condition defined in equation (2.68).

$$f''' + ff'' - f'^2 - Mf' + \theta \frac{\sin x}{x} = x\left(f' \frac{\partial f'}{\partial x} - f'' \frac{\partial f}{\partial x} \right)$$

$$\frac{1}{\Pr}\theta'' + f\theta' + Jx^2 f'^2 + Q\theta = x\left(f' \frac{\partial \theta}{\partial x} - \theta' \frac{\partial f}{\partial x} \right)$$

$$f = f' = 0,\ \theta - 1 = \chi \frac{\partial \theta}{\partial y}\ at\ y = 0,\ x > 0$$

$$f' \to 0,\ \theta \to 0\ as\ y \to \infty,\ x > 0$$

If we consider M =0.0 in equation (2.66); J=0.0 and Q=0.0 in equation (2.76) and χ = 0 in equation (2.68) then the present study will refer to free convection problem which was considered by Merkin (1976) and Nazar et al. (2002). A comparison will be provided in section 4.3 with a complete discussion.

The effects of Joule heating and volumetric rate of heat generation on MHD-conjugate natural convection flow from a horizontal circular cylinder has been considered in this chapter. The governing momentum equation (2.66) and energy equation (2.76) are solved numerically using the implicit finite difference method together with the Keller box technique. The shearing stress and the rate of heat transfer in terms of skin friction coefficient and Nusselt number respectively and the velocity and temperature distributions within the boundary-layer can be calculated by the relations (2.70) and (2.71) respectively.

4.2 Results and discussion

The dimensionless governing equations (2.66) and (2.76) and the boundary conditions (2.68) contain a set of physical parameters: Prandtl number Pr,

magnetic parameter M, conjugate conduction parameter χ, Joule heating parameter J and heat generation parameter Q. The Prandtl numbers are considered to be 1.63, 1.44, 1.0 and 0.733 that correspond to Glycerin, water, steam, and hydrogen, respectively. The remaining parameters are taken as follows: magnetic parameter M=0.10-0.70; conjugate conduction parameter χ=1.0-2.5; Joule heating parameter J=0.01–1.0; and heat generation parameter Q=0.01–0.12.

A comparison of the local Nusselt number and the local skin friction factor obtained in the present work with M = 0.0, χ = 0.0, J=0.0, Q=0.0 and Pr = 1.0 and obtained by Merkin (1976) and Molla et al. (2006) have been shown in Table 4.1 and Table 4.2, respectively and it has been observed that there is an excellent agreement among these three results.

In this stage, a grid independent test has been provided for three different grid configurations, 181×305, 361×405 and 451×505 in Figures 4.1(a) and 4.1(b) as the skin friction coefficient and the rate of heat transfer respectively while Pr=1.0, M = 0.1, χ = 1.0, J=0.01 and Q=0.01. From these Figures, it can be concluded that the numerical solutions are completely independent of these three grid orientations. In this chapter 181×305 grid configuration has been chosen for the numerical computation.

Figures 4.2, 4.4, 4.6, 4.8 and 4.10 illustrate the velocity and temperature distributions at $x=\pi/2$ against y, the direction along the normal to the surface of the cylinder, and Figures 4.3, 4.5, 4.7, 4.9 and 4.11 depict the skin friction coefficients and heat transfer rates against x at y=0 (along the surface of the cylinder) for different values of the magnetic parameter M, conjugate conduction parameter χ, Prandtl number Pr, Joule heating parameter J and heat generation parameter Q, respectively.

The magnetic parameter is the ratio of the magnetic force to the inertia force. Hence the magnetic force is important when it is of the order of one, and the flow is considered as hydromagnetic flow. The flow is hydrodynamic for $M<<1$. For

97

small value of M, the motion is hardly affected by the magnetic field and for large value of M, the motion is largely controlled by the magnetic field. The increasing values of the magnetic parameters increase magnetic-field strength, which is acting normal to the cylinder surface that reduces fluid motion as observed in Figure 4.2(a). As a result the skin friction at the surface to the cylinder is decreased, which is shown from Figure 4.3(a). Heat is produced due to the interaction between magnetic field and fluid motion; consequently, temperature within the thermal boundary-layer increases for increasing value of the magnetic parameters as revealed from Figure 4.2(b). Increasing thermal energy within the boundary layer reduces the temperature difference between core region and boundary layer region, which ultimately decreases the heat transfer rate as illustrated in Figure 4.3(b). The maximum values of the velocity are recorded to be 0.289429, 0.260270, 0.236298 and 0.216355 for magnetic parameter M=0.1, 0.3, 0.5 and 0.7 at y=1.509461, 1.491429, 1.473548 and 1.455813 respectively with Joule heating parameter J=0.01 and heat generation parameter Q=0.01, which are presented in Table 4.3. It is also observed from Table 4.8 that the maximum values of the skin friction coefficient are 0.749931, 0.693555, 0.648461 and 0.611517 for magnetic parameter M=0.1, 0.3, 0.5 and 0.7 with Joule heating parameter J=0.01 and heat generation parameter Q=0.01 at x=1.850049, 1.797689, 1.762783 and 1.745329 respectively. Here it is observed that the velocity decreased by 25.25% and the skin friction coefficient decreased by 18.45% when the value of the magnetic parameter changes from 0.1 to 0.7 in presence of Joule heating and heat generation.

The velocity and temperature are illustrated in Figure 4.4 and the variation of the local skin friction coefficient and local rate of heat transfer are depicted in Figure 4.5 for different values of conjugate conduction parameter χ with Pr=1.0, M=0.1, J=0.01 and Q=0.01. As discussed in earlier chapter, increasing value of conjugate conduction parameter χ resists conduction from the core region to the boundary layer region and consequently, decelerates convection within the boundary layer, as a result both velocity and temperature decrease for increasing values of the

98

conjugate conduction parameters at a particular value of y. Similar situations are observed in presence of Joule heating and heat generation which are presented in Figure 4.4(a) and Figure 4.4(b), respectively. Beside this we can conclude that the maximum velocity increases in presence of Joule heating and heat generation. For example, without Joule heating (J=0.0) and heat generation (Q=0.0) the maximum velocity for conjugate conduction parameter χ=1.0 is 0.284157 where as the maximum velocity is 0.289429 for χ=1.0 with Joule heating (J=0.01) and heat generation (Q=0.01). As the velocity decreases, the skin friction at the surface decreases for increasing value of conjugate conduction parameter χ, as observed in Figure 4.5(a). Since increasing value of the conjugate conduction parameters resists conduction from the core region to the boundary layer as mentioned earlier, it of course resists thermal energy transfer which is observed from Figure 4.5 (b). The maximum values of the velocity and the maximum values of the skin friction coefficient are presented in Table 4.4 and Table 4.9. It can noted that the maximum values of the velocity are 0.289429, 0.272379, 0.258588 and 0.247029 at y=1.509461, 1.545979, 1.583115 and 1.620884 and the maximum values of the skin friction coefficient are 0.749931, 0.686089, 0.635735 and 0.594597 for conjugate conduction parameter χ=1.0, 1.5, 2.0 and 2.5 respectively. Finally, it is observed that the velocity and the skin friction coefficient decreased by 14.65% and 20.71% respectively as the conjugate conduction parameter changes from 1.0 to 2.5.

The velocity profiles and temperature profiles are plotted against y-axis in Figure 4.6 and the skin friction coefficient and heat transfer rate are plotted against x-axis in Figure 4.7 for different values of Prandtl number with M=0.1, χ=1.0, J=0.01 and Q=0.01. As it is known, increasing value of Prandtl number increases viscosity and decreases the thermal action of the fluid. Therefore, the velocity and temperature of fluid are expected to decrease with the increasing Prandtl number which are observed in Figure 4.6(a) and Figure 4.6(b) respectively. Decreasing velocity of the fluid leads to decrease skin friction and the decreasing temperature within in the boundary layer increases the temperature difference between core

99

region to the boundary layer region, which eventually increases heat transfer rate from the core region to the boundary layer region as depicted in Figure 4.7(a) and Figure 4.7(b) respectively. The Tables 4.5 and 4.10 shows the maximum values of the velocities and the maximum values of the skin friction coefficients respectively for different values of Prandtl numbers. It has been observed that the maximum values of the velocities are 0.319714, 0.289429, 0.255821 and 0.244926 at y=1.564468, 1.509461, 1.438224 and 1.420778 for Pr=0.733, 1.000, 1.440 and 1.630 respectively. Again from Table 4.10 it is reported that the maximum values of the skin friction coefficient are 0.801152, 0.749931, 0.691119, 0.671578 at x=1.850049, 1.850049, 1.832596 and 1.832596 for Pr=0.733, 1.000, 1.440 and 1.630 respectively. It is noted that the velocity and the skin friction coefficient decreased by 23.39% and 16.17% respectively as the Prandtl number changes from 0.733 to 1.630.

The effects of the Joule heating parameters on the velocity and temperature are presented in Figure 4.8, and that of on the skin friction coefficient and rate of heat transfer are illustrated in Figure 4.9 respectively with Pr=1.0, M=0.1, χ=1.0 and Q=0.01. The Joule heating parameter having the magnetic-field strength transform electrical energy to the thermal energy due to the electrical resistance of the surrounding fluid and eventually increases temperature within the boundary layer as plotted in Figure 4.8(b). Increasing thermal energy accelerates heat convection, which ultimately increases fluid motion as observed in Figure 4.8(a). Moreover, as the increased thermal energy for increasing Joule heating parameter increases the temperature within the boundary layer which results in the heat transfer rate decrease as illustrated in Figure 4.9(b). The variation of local skin friction coefficient increases for the increasing Joule heating parameter J as depicted in Figure 4.9(a). This is an expected behavior as fluid motion increases for increasing Joule heating parameter. Again it can be noted that the surface temperature is same for all values of Joule heating parameter as seen from Figure 4.8(b). The maximum values of the velocities are obtained as 0.289429, 0.309183, 0.324794 and 0.340690 at y=1.509461 for Joule heating parameters J=0.01, 0.40,

0.70 and 1.00 respectively which are shown in the Table 4.6 and the Table 4.11 shows the maximum values of the skin friction coefficients are 0.749931, 0.800514, 0.846375 and 0.899054 at x=1.850049, 1.937315, 2.007129 and 2.076942 for Joule heating parameters J=0.01, 0.40, 0.70 and 1.00 respectively. That is the maximum value of the skin friction coefficients is shifted along the upper stagnation point for increasing values of the Joule heating parameter. Furthermore, it has been observed that the velocity and the skin friction coefficient increase by 17.71% and 19.88% respectively as the Joule heating parameter changes from 0.01 to 1.0.

Figure 4.10 illustrates the effect of the heat generation parameters on the fluid velocity and temperature profiles, respectively. It is clear that as the heat generation parameter increases both the fluid velocity and temperature of the fluid increase. Figure 4.11 depicts the variation of the heat generation parameters on the skin friction coefficient and the heat transfer rate with Pr=1.0, M=0.1, χ=1.0 and J=0.01. It is observed the local Nusselt number decreases, but the skin friction coefficient increases with increasing heat generation parameter. Table 4.7 and Table 4.12 represent the maximum values of the velocities and the skin friction coefficients respectively for different values of the heat generation parameter with Pr=1.0, M=0.1, χ=1.0 and J=0.01. It is recorded that 0.289429, 0.309677, 0.326156 and 0.349804 are the maximum velocities at y=1.509461 for Heat generation parameter Q=0.01, 0.05, 0.08 and 0.12 respectively. The maximum values of the skin friction coefficient for different values of the heat generation parameter Q=0.01, 0.02, 0.03 and 0.04 are obtained as 0.749931, 0.760938, 0.772185 and 0.783773 respectively. Finally, it is calculated that the velocity increases 20.85% as the heat generation parameter changes from 0.01 to 0.12 and the skin friction coefficient increased by 4.5% as the heat generation parameter changes from 0.01 to 0.04.

101

TABLES

Table 4.1: Comparisons of the present numerical values of $-\theta'(x,0)$ with Merkin (1976) and Molla et al. (2006) for different values of x while Pr=1.0, M =0.0, χ =0.0, J=0.0 and Q=0.0.

$Nu\,Gr^{-1/4} = -\theta'(x,0)$			
x	Merkin (1976)	Molla et al. (2006)	Present
0.0	0.4214	0.4214	0.4216
π/6	0.4161	0.4161	0.4163
π/3	0.4007	0.4005	0.4006
π/2	0.3745	0.3740	0.3742
2π/3	0.3364	0.3355	0.3356
5π/6	0.2825	0.2812	0.2811
π	0.1945	0.1917	0.1912

Table 4.2: Comparisons of the present numerical values of $x f''(x,0)$ with Merkin (1976) and Molla et al. (2006) for different values of x while Pr=1.0, M =0.0, χ =0.0, J=0.0 and Q=0.0.

$C_f\,Gr^{1/4} = x f''(x,0)$			
x	Merkin (1976)	Molla et al. (2006)	Present
0.0	0.0000	0.0000	0.0000
π/6	0.4151	0.4145	0.4139
π/3	0.7558	0.7539	0.7528
π/2	0.9579	0.9541	0.9526
2π/3	0.9756	0.9696	0.9678
5π/6	0.7822	0.7739	0.7718
π	0.3391	0.3264	0.3239

102

Table 4.3: Maximum velocity $f'(x, y)$ against y for different values of magnetic parameter M while Pr=1.0, χ=1.0, J=0.01 and Q=0.01.

Magnetic parameter M	y	Maximum Velocity
0.1	1.509461	0.289429
0.3	1.491429	0.260270
0.5	1.473548	0.236298
0.7	1.455813	0.216355

Table 4.4: Maximum velocity $f'(x, y)$ against y for different values of conjugate conduction parameter χ while Pr=1.0, M=0.1, J=0.01 and Q=0.01.

Conjugate conduction parameter χ	y	Maximum Velocity
1.0	1.509461	0.289429
1.5	1.545979	0.272379
2.0	1.583115	0.258588
2.5	1.620884	0.247029

Table 4.5: Maximum velocity $f'(x, y)$ against y for different values of Prandtl number Pr while M=0.1, χ=1.0, J=0.01 and Q=0.01.

Prandtl number Pr	y	Maximum Velocity
0.733	1.564468	0.319714
1.000	1.509461	0.289429
1.440	1.438224	0.255821
1.630	1.420778	0.244926

103

Table 4.6: Maximum velocity $f'(x, y)$ against y for different values of Joule heating parameter J while Pr=1.0, M=0.1, χ=1.0 and Q=0.01.

Joule heating parameter J	y	Maximum Velocity
0.01	1.509461	0.289429
0.40	1.509461	0.309183
0.70	1.509461	0.324794
1.00	1.509461	0.340690

Table 4.7: Maximum velocity $f'(x, y)$ against y for different values of heat generation parameter Q while Pr=1.0, M=0.1, χ=1.0 and J=0.01.

Heat generation parameter Q	y	Maximum Velocity
0.01	1.509461	0.289429
0.05	1.509461	0.309677
0.08	1.509461	0.326156
0.12	1.509461	0.349804

Table 4.8: Maximum value of the skin friction coefficient $x f''(x,0)$ against x for different values of magnetic parameter M with Pr=1.0, χ=1.0, J=0.01 and Q=0.01.

Magnetic parameter M	x	Maximum Skin friction coefficient
0.1	1.850049	0.749931
0.3	1.797689	0.693555
0.5	1.762783	0.648461
0.7	1.745329	0.611517

104

Table 4.9: Maximum value of the skin friction coefficient $xf''(x,0)$ against x for different values of conjugate conduction parameter χ while Pr=1.0, M=0.1, J=0.01 and Q=0.01.

Conjugate conduction parameter χ	x	Maximum Skin friction coefficient
1.0	1.850049	0.749931
1.5	1.850049	0.686089
2.0	1.850049	0.635735
2.5	1.850049	0.594597

Table 4.10: Maximum value of the skin friction coefficient $xf''(x,0)$ against x for different values of Prandtl number Pr while M=0.1, χ=1.0, J=0.01 and Q=0.01.

Prandtl number Pr	x	Maximum Skin friction coefficient
0.733	1.850049	0.801152
1.000	1.850049	0.749931
1.440	1.832596	0.691119
1.630	1.832596	0.671578

Table 4.11: Maximum value of the skin friction coefficient $xf''(x,0)$ against x for different values of Joule heating parameter J with Pr=1.0, M=0.1, χ=1.0 and Q=0.01.

Joule heating parameter J	x	Maximum Skin friction coefficient
0.01	1.850049	0.749931
0.40	1.937315	0.800514
0.70	2.007129	0.846375
1.00	2.076942	0.899054

105

Table 4.12: Maximum value of the skin friction coefficient $xf''(x,0)$ against x for different values of heat generation parameter Q while Pr=1.0, M=0.1, χ=1.0 and J=0.01.

Heat generation parameter Q	x	Maximum Skin friction coefficient
0.01	1.850049	0.749931
0.02	1.850049	0.760938
0.03	1.850049	0.772185
0.04	1.850049	0.783773

106

FIGURES

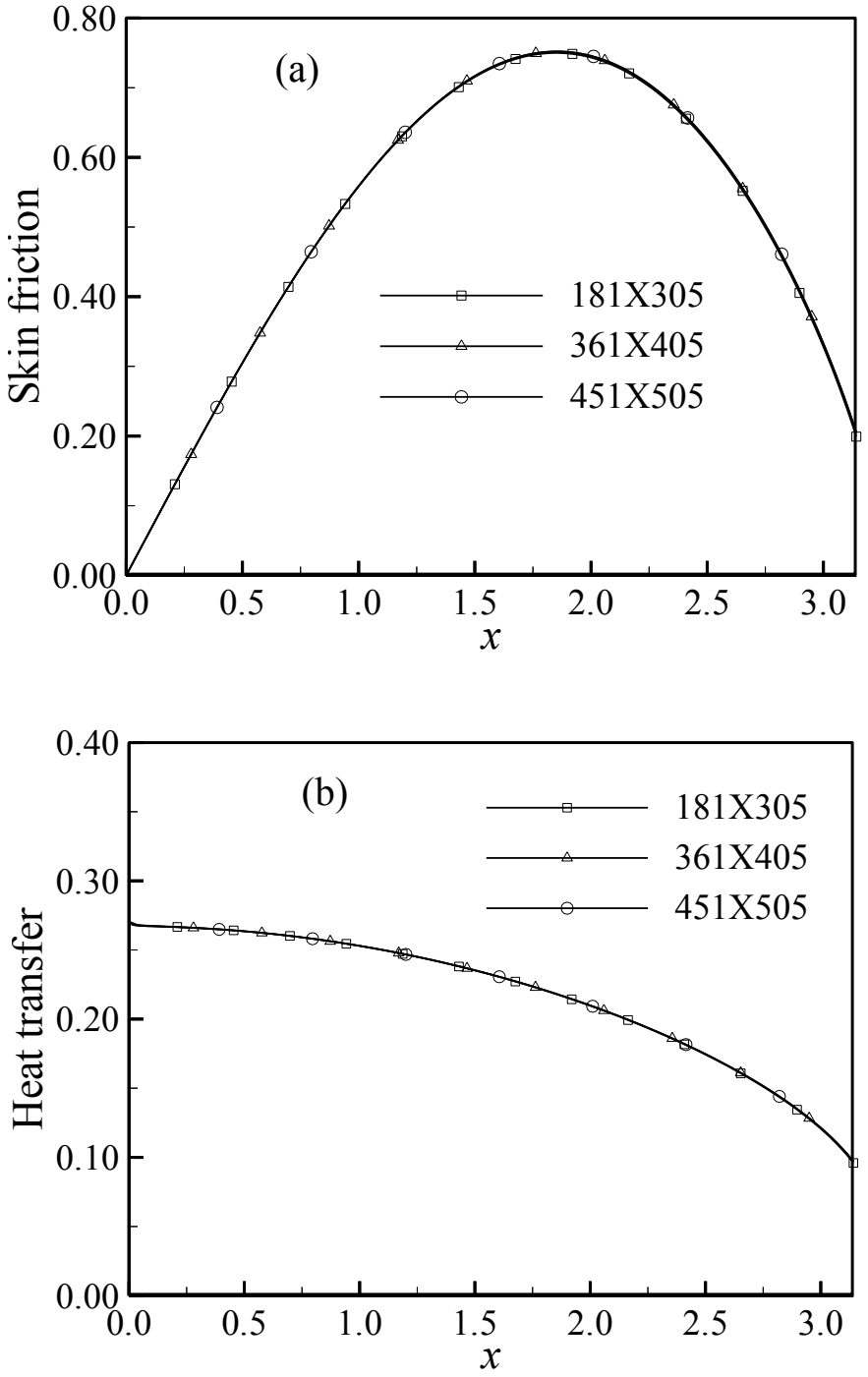

Figure 4.1: (a) The skin friction coefficient and (b) the rate of heat transfer against x for different mesh configurations while Pr = 1.0, M = 0.1, χ = 1.0, J=0.01 and Q=0.01.

107

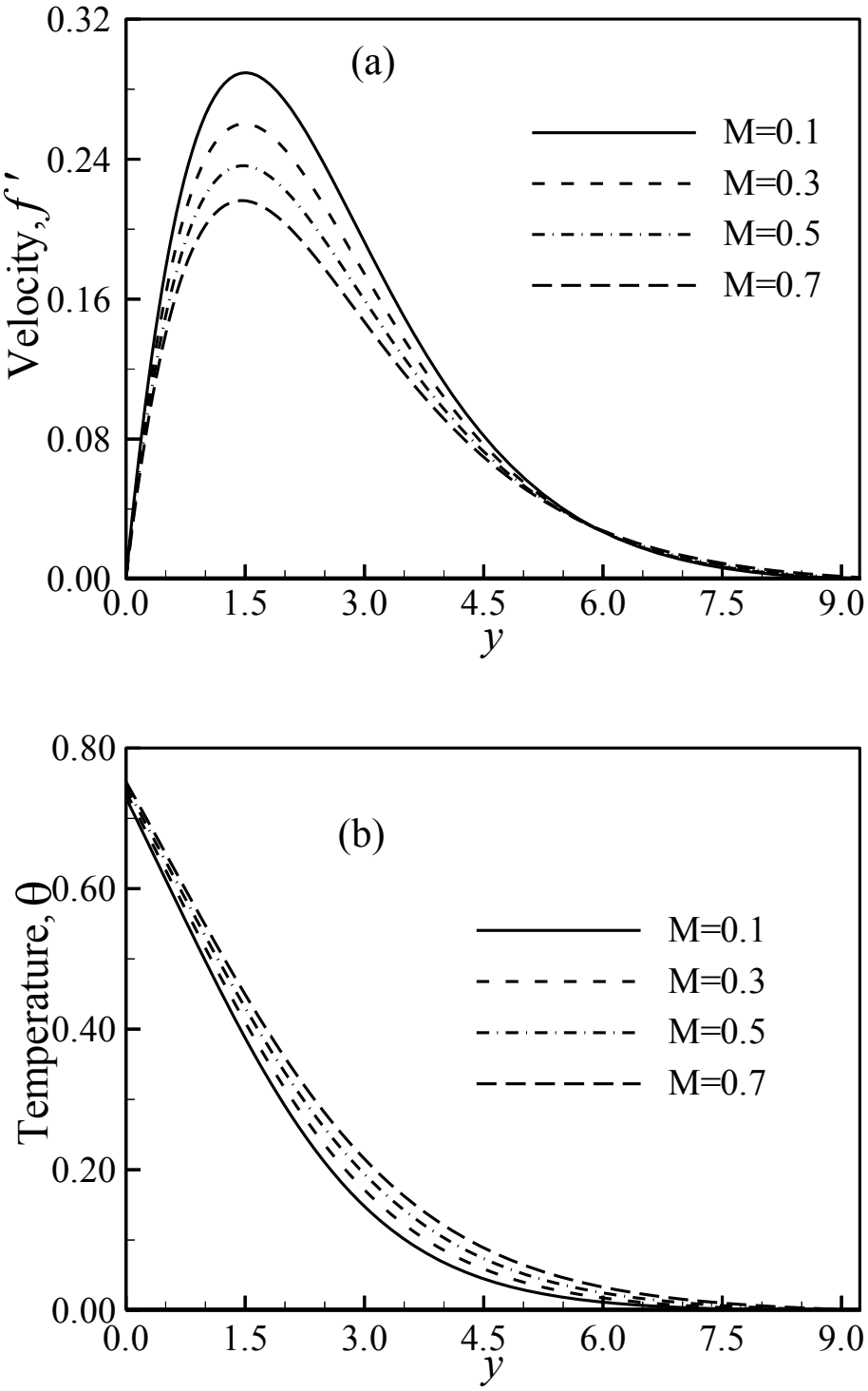

Figure 4.2: (a) Variation of velocity profiles and (b) variation of temperature distributions against y for varying of magnetic parameter M with Pr=1.0, χ=1.0, J=0.01 and Q=0.01.

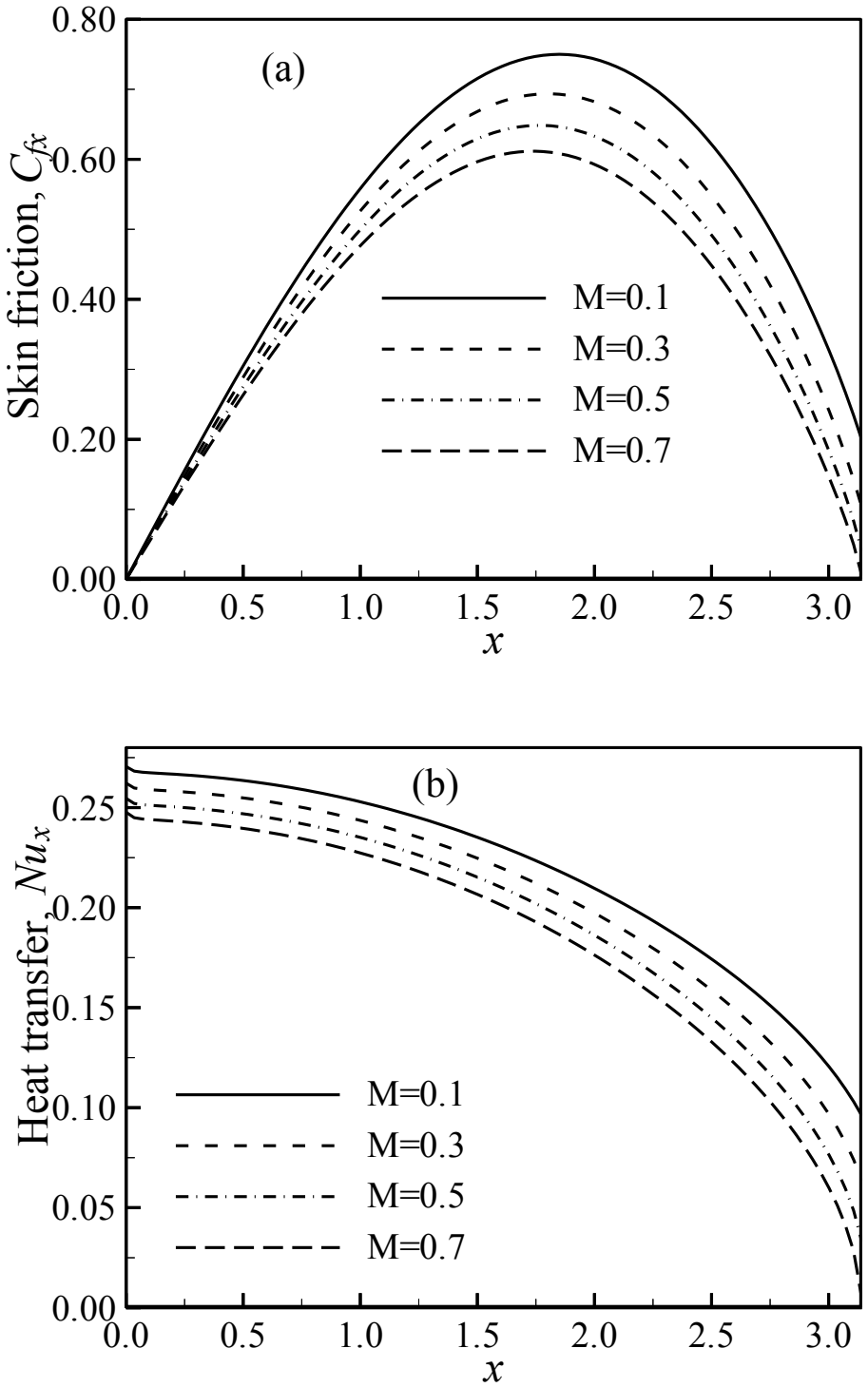

Figure 4.3: (a) Variation of skin friction coefficients and (b) variation of rate of heat transfer against x for varying of magnetic parameter M with Pr=1.0, χ=1.0, J=0.01 and Q=0.01.

109

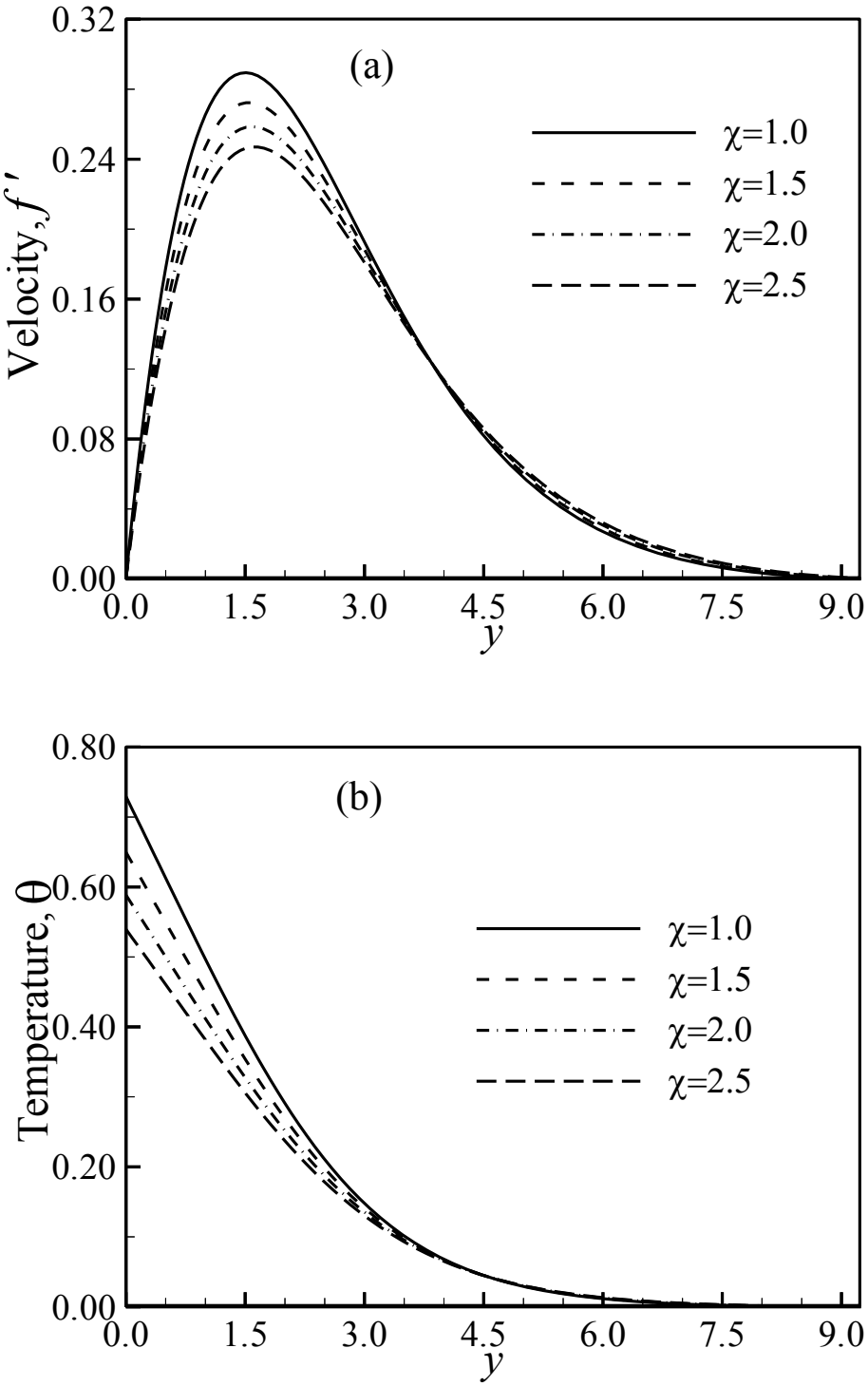

Figure 4.4: (a) Variation of velocity profiles and (b) variation of temperature distributions against y for varying of conjugate conduction parameter χ with Pr=1.0, M=0.1, J=0.01 and Q=0.01.

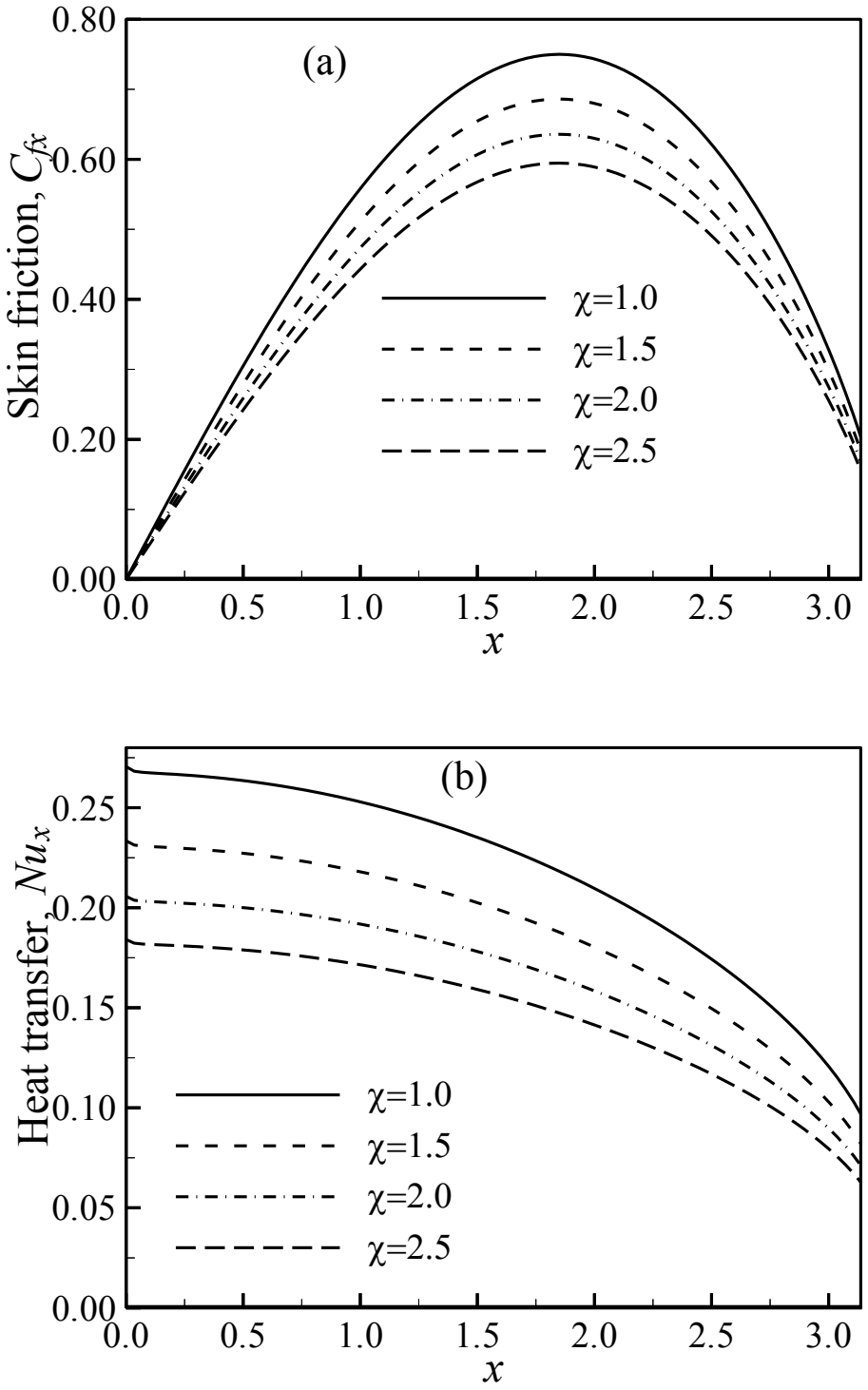

Figure 4.5: (a) Variation of skin friction coefficients and (b) variation of rate of heat transfer against x for varying of conjugate conduction parameter χ with Pr=1.0, M=0.1, J=0.01 and Q=0.01.

111

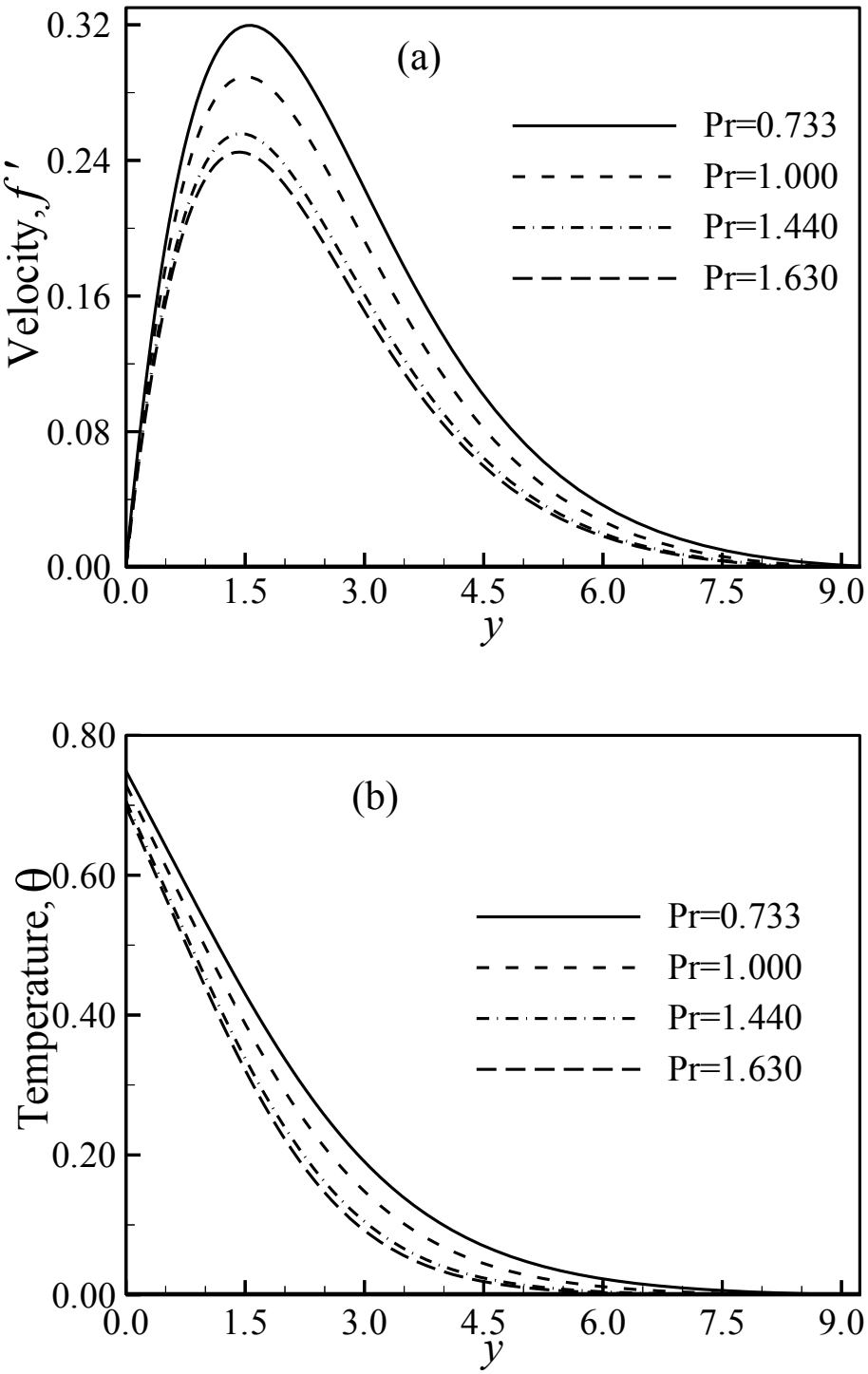

Figure 4.6: (a) Variation of velocity profiles and (b) variation of temperature distributions against y for varying of Pr with M=0.1, χ=1.0, J=0.01 and Q=0.01.

112

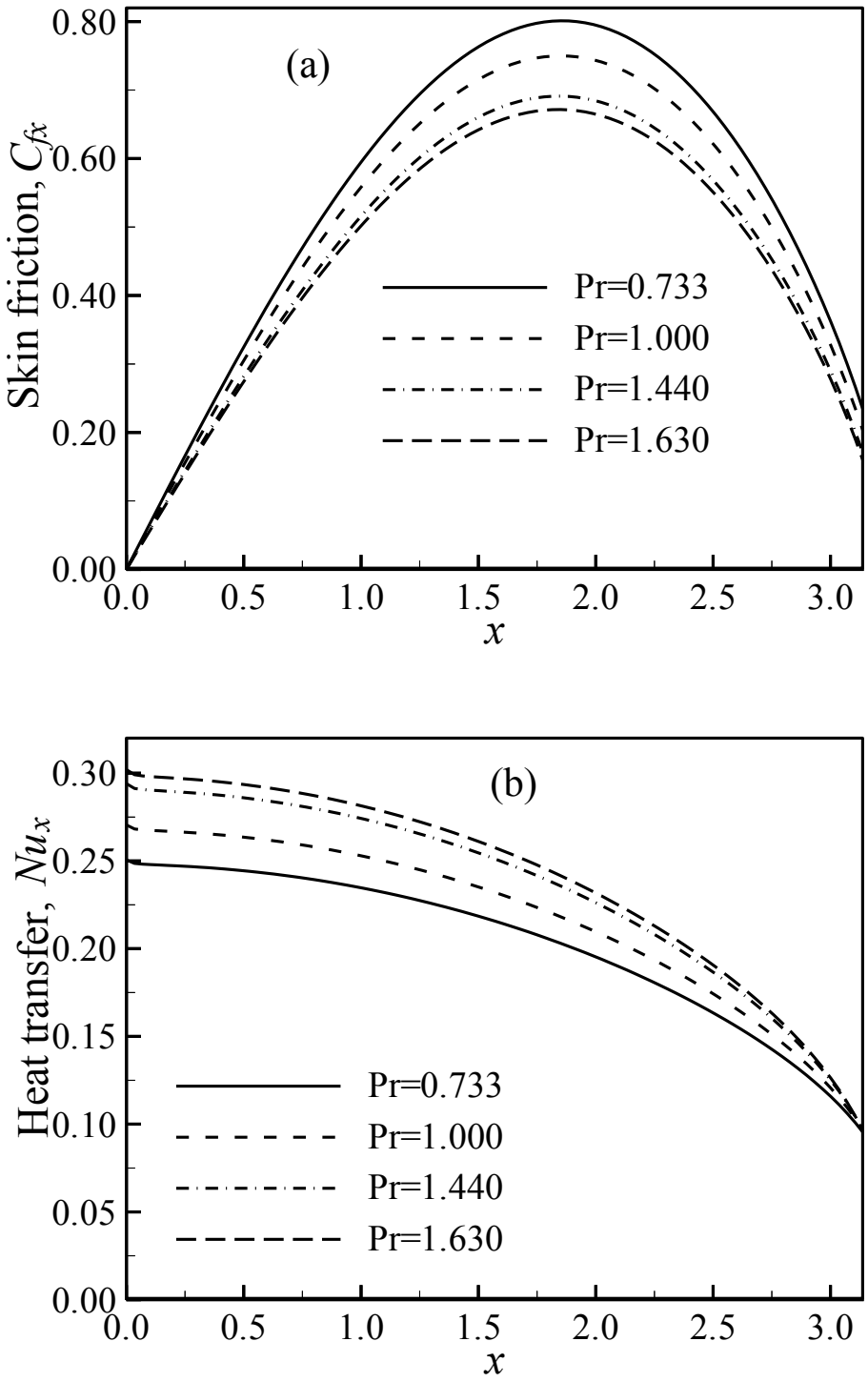

Figure 4.7: (a) Variation of skin friction coefficients and (b) variation of rate of heat transfer against x for varying of Pr with M=0.1, χ=1.0, J=0.01 and Q=0.01.

113

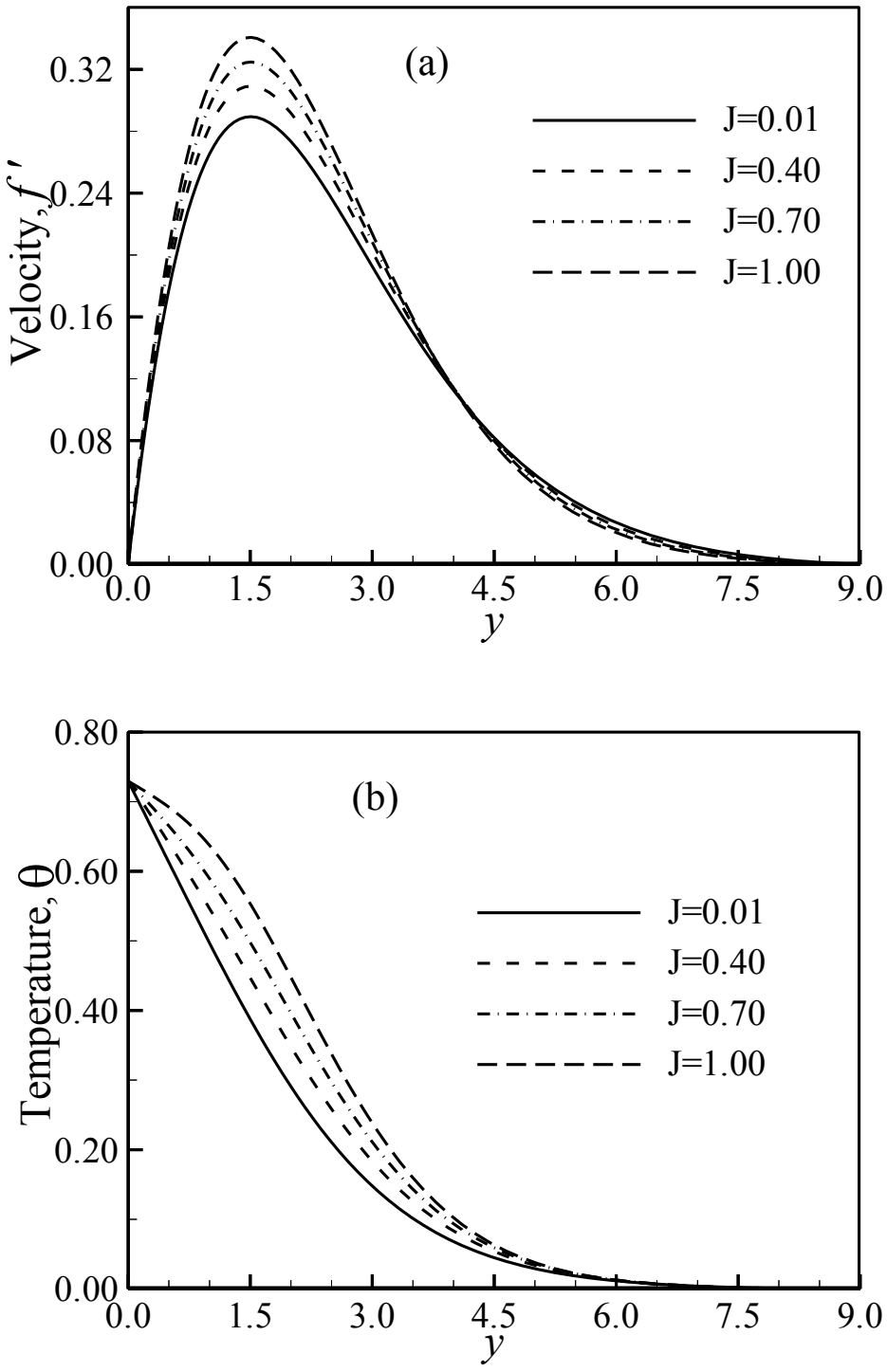

Figure 4.8: (a) Variation of velocity profiles and (b) variation of temperature distributions against y for varying of J with Pr=1.0, M=0.1, χ =1.0 and Q=0.01.

114

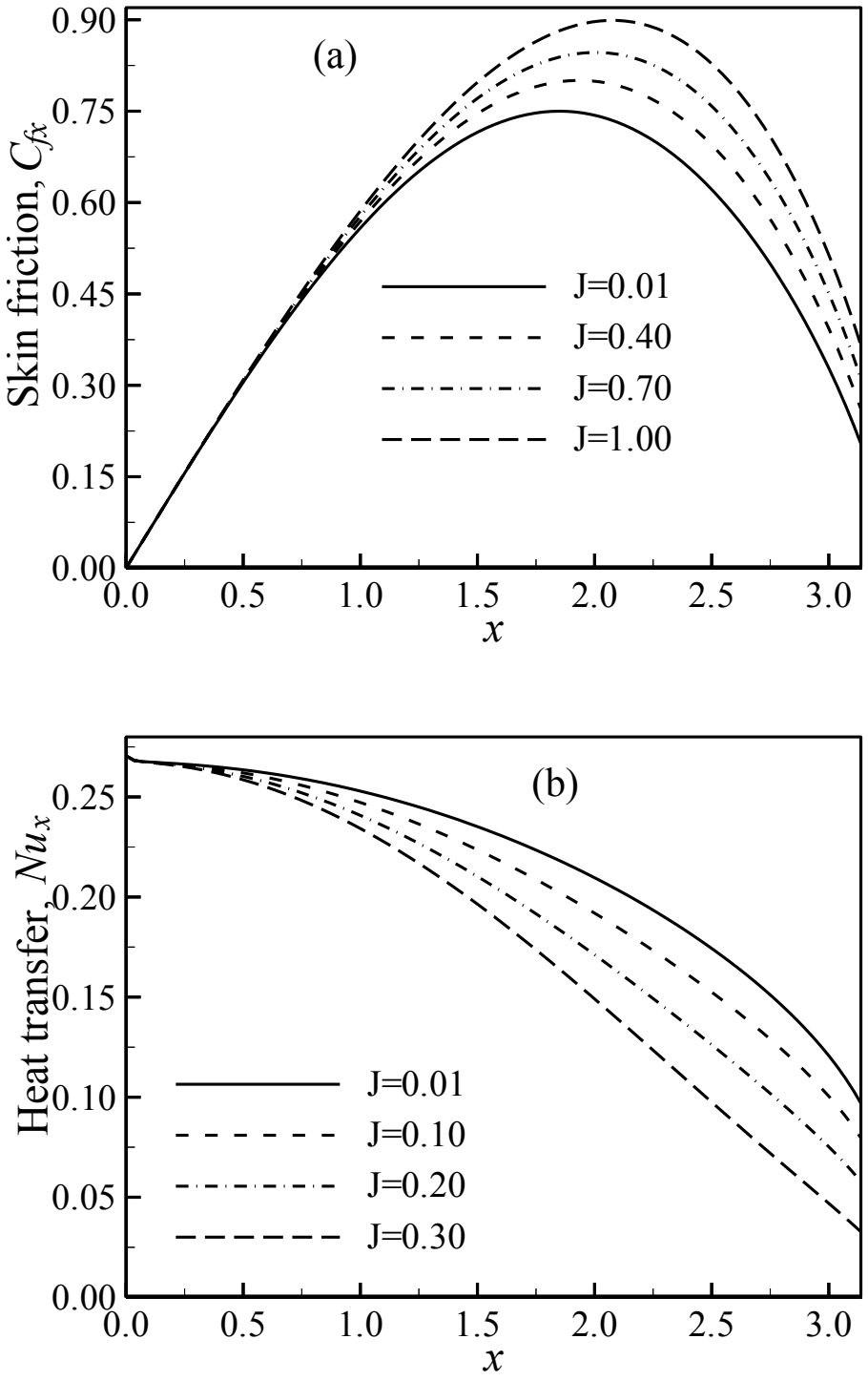

Figure 4.9: (a) Variation of skin friction coefficients and (b) variation of rate of heat transfer against x for varying of J with Pr=1.0, M=0.1, χ =1.0 and Q=0.01.

115

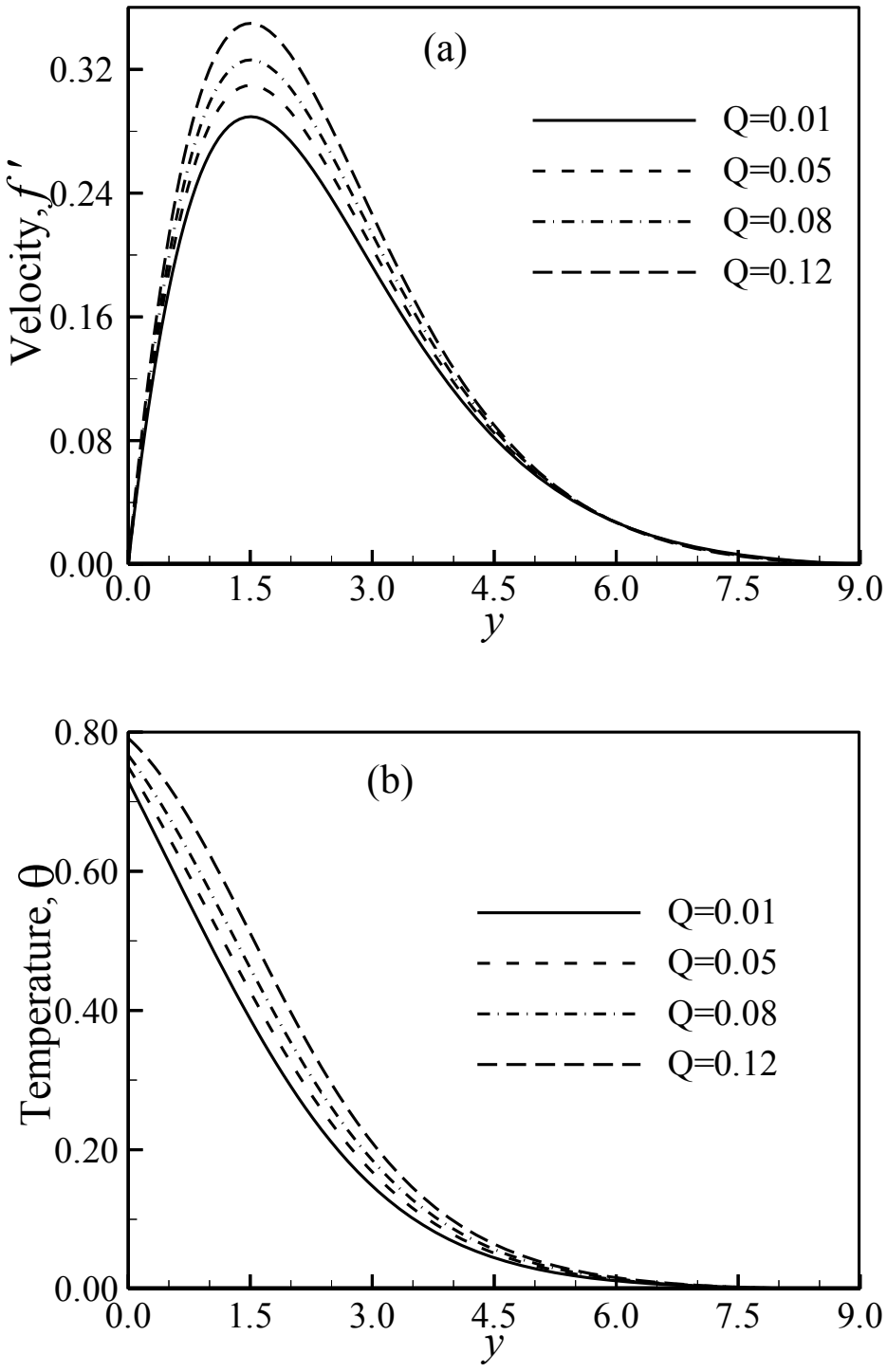

Figure 4.10: (a) Variation of velocity profiles and (b) variation of temperature distributions against y for varying of Q with Pr=1.0, M=0.1, χ =1.0 and J=0.01.

116

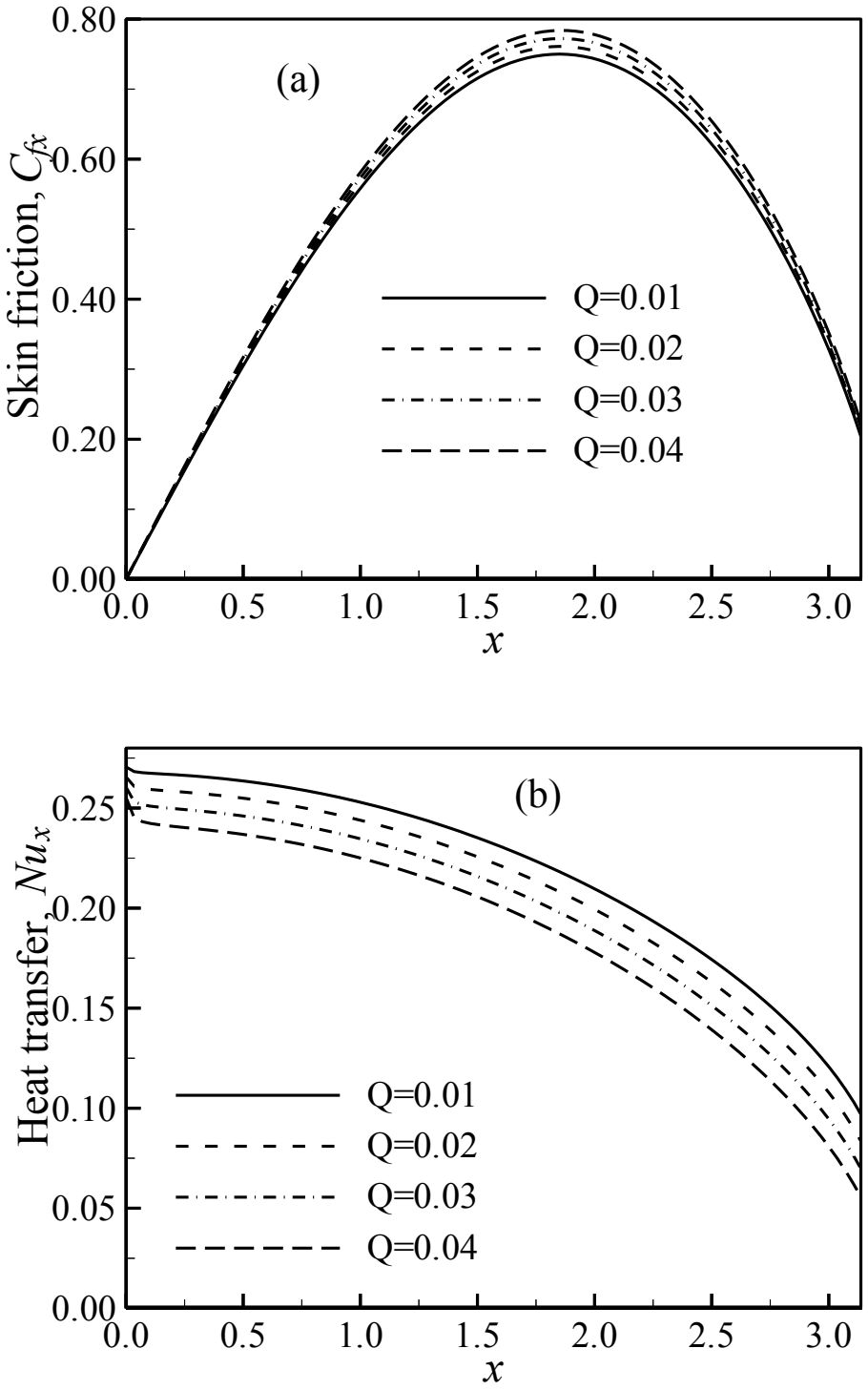

Figure 4.11: (a) Variation of skin friction coefficients and (b) variation of rate of heat transfer against x for varying of Q with Pr=1.0, M=0.1, χ=1.0 and J=0.01.

117

4.3 Conclusion

MHD-conjugate natural convection flow from horizontal cylinder taking into account Joule heating in presence of heat generation is studied. Numerical results are obtained for the physical parameters and discussed. From the results, it is established that the velocity of the fluid within the boundary layer decreases with increasing magnetic parameter, conjugate conduction parameter and Prandtl number while it increases for increasing Joule heating parameter, and heat generation parameter. The temperature within the boundary-layer increases for increasing magnetic parameter, Joule heating parameter and heat generation parameter whereas it decreases for increasing conjugate conduction parameter and Prandtl number. Moreover, the skin friction along the surface of the cylinder decreases for increasing magnetic parameter, conjugate conduction parameter and Prandtl number, and it increases for increasing Joule heating parameter and heat generation parameter. Furthermore, the rate of heat transfer along the surface increases for increasing Prandtl number while it decreases for remaining parameters.

118

Chapter V

Stress Work and Viscous Dissipation on MHD-Conjugate Free Convection Flow from an Isothermal Horizontal Circular Cylinder

5.1 Introduction

Convective heat transfer involves flows with large temperature differences, and thus the equations are coupled through an equation of state. That is the momentum equation is dependent on the energy equation simultaneously the energy equation is dependent on the momentum equation. The coupling arises because of kinetic heating in high speed flows or because of large temperature difference in flows. In the governing equations of these flows two extra coupling terms appear in the enthalpy equation, one being the enthalpy equivalent of the work done by the pressure gradients, which is known as pressure stress work and the other is the rate of dissipation of kinetic energy into thermal internal energy by viscous stresses which is well known as viscous dissipation. For two-dimensional boundary layer equation the terms $\mu\left(\frac{\partial \bar{u}}{\partial y}\right)^2$ and $T\,\bar{u}\beta\frac{\partial p}{\partial x}$ are included in the energy equation which are accounts for viscous dissipation and the stress work respectively. Where T, β are the temperature and volumetric of thermal expansion respectively.

In the previous chapters effects of viscous dissipation and pressure stress work has been neglected in the energy equation. However, Ostrach (1952, 1958) showed that viscous dissipation plays an important role in natural convection in vertical channels. Gebhart (1962) was the first who studied the problem of laminar natural convection along a vertical heated plate taking into account the viscous dissipation. Ackroyd (1974) treated the problem of natural convection along a heated vertical plate taking into account both the viscous dissipation and the pressure work in the energy equation. He proved that, for this problem, the

119

pressure work effect is more important than that of viscous dissipation. Joshi and Gebhart (1981) studied, with the perturbation method, the problem of natural convection over a vertical isothermal plate taking into account both the viscous dissipation and the pressure work in the energy equation using two non-dimensional numbers. Mahajan and Gebhart (1989), after conducting an order of magnitude analysis, had shown that the viscous dissipation effect is smaller than the pressure effect for all values of Pr number. The numerical solution of the effect of viscous dissipation and pressure stress work in natural convection along a vertical isothermal plate is studied by Pantokratoras (2003) without any approximation. Barletta and Nield (2009) studied mixed convection with viscous dissipation and pressure work in a lid-driven square enclosure.

In this chapter, the numerical results of stress work and viscous dissipation on MHD-conjugate free convection flow from an isothermal horizontal circular cylinder has been discussed.

5.2 Governing equations

Formulation of the governing equations has been discussed in section 2.4.3 as case III of chapter II. The equations (2.50), (2.51) and (2.80) are the dimensionless form of the continuity equation, momentum equation and energy equation. Further we have the equations (2.66) and (2.81) as the momentum equation and energy equation using stream function defined in equation (2.54) and (2.55) which satisfies dimensionless continuity equation (2.50). The final form of the momentum and energy equations (2.66) and (2.81) are solved using implicit finite difference method based on the boundary condition defined in equation (2.68).

$$f''' + ff'' - f'^2 - Mf' + \theta\frac{\sin x}{x} = x\left(f'\frac{\partial f'}{\partial x} - f''\frac{\partial f}{\partial x}\right)$$

$$\frac{1}{\Pr}\theta'' + f\theta' + Nx^2 f''^2 - \varepsilon\left(T_r x f' - xf'\theta\right) = x\left(f'\frac{\partial \theta}{\partial x} - \theta'\frac{\partial f}{\partial x}\right)$$

$$f = f' = 0,\ \theta - 1 = \chi \frac{\partial \theta}{\partial y}\ at\ y = 0,\ x > 0$$

$$f' \to 0,\ \theta \to 0\ as\ y \to \infty,\ x > 0$$

where $N = \dfrac{\nu^2 Gr}{a^2 c_p (T_b - T_\infty)}$ is the viscous dissipation parameter, $\varepsilon = \dfrac{g\beta a}{c_p}$ is the stress work parameter and $T_r = \dfrac{T_\infty}{T_b - T_\infty}$ is the temperature ratio parameter.

Present governing equations and boundary conditions completely match with the problem of Merkin (1976) if the values of the parameters considered as: M=0.0 in equation (2.66); N=0.0 and ε=0.0 in equation (2.81) and χ= 0.0 in equation (2.68). Accordingly, a comparison has been given in section 5.3.

The governing momentum equation (2.66) and energy equation (2.81) are solved numerically using the implicit finite difference method together with the Keller box technique. The shearing stress and the rate of heat transfer in terms of skin friction coefficient and Nusselt number respectively and the velocity and temperature distributions within the boundary-layer can be calculated by the relations (2.70) and (2.71) respectively.

5.3 Findings and analysis

The conjugate heat transfer analysis from an isothermal horizontal circular cylinder considering stress work and viscous dissipation effects is the main purpose of the present study. The Prandtl numbers are considered to be 1.63, 1.44, 1.0 and 0.733 for the simulation that correspond to glycerin, water, steam and hydrogen, respectively. The remaining parameters are taken as follows: magnetic parameter M=0.10-0.70 and the conjugate conduction parameter χ=1.00-2.00, viscous dissipation parameter N=0.01-0.90, temperature ratio parameter T_r=0.1-1.5 and stress work parameter ε = 0.01-0.30.

121 Table 5.1 and Table 5.2 show the comparisons of the present numerical values of heat transfer rate in terms of Nusselt number $-\theta'(x,0)$ and the shear stress skin

friction coefficient $x f''(x,0)$ respectively with Merkin (1976) and Nazar et al. (2002) for different values of x while Pr=1.0, M=0.0, χ=0.0, N=0.0, ε =0.0 and T_r=0.0. It can be concluded that the present result absolutely agree with the previous results.

The velocity profiles and temperature distributions for different values of stress work parameter, viscous dissipation parameter, temperature ratio parameter, magnetic parameter, Prandtl number and conjugate conduction parameter are illustrated in Figures 5.1, 5.3, 5.5, 5.7, 5.9 and 5.11 respectively at $x=\pi/2$. The skin friction coefficient and the local rate of heat transfer in terms of Nusselt number for different values of stress work parameter, viscous dissipation parameter, temperature ratio parameter, magnetic parameter, Prandtl number and conjugate conduction parameter are depicted in Figures 5.2, 5.4, 5.6, 5.8, 5.10 and 5.12 respectively.

The velocity profiles, temperature distributions, local skin friction coefficients and the heat transfer rate for different values of stress work parameter ε are presented in Figures 5.1(a), 5.1(b), 5.2(a) and 5.2(b), respectively with Pr=1.0, M=0.1, χ=1.0, N=0.01 and T_r=1.0. Increasing value of the stress work parameter containing gravitational force $\boldsymbol{g}$ work against the buoyancy force as a result the motion of the fluid is decreased as plotted in Figure 5.1(a). The reduced velocity decelerates fluid flow which ultimately decreases the shear stress at the wall which is observed from Figure 5.2(a). On the other hand from Figure 5.1(b), it could be concluded that the temperature within the boundary layer decreases for increasing stress work parameter. The decreased temperature for increasing stress work parameter within the boundary layer reduces the temperature difference between the boundary layer region and the core region eventually increases heat transfer rate as illustrated in Figure 5.2(b). Besides this the maximum velocities occur as 0.281548, 0.270846, 0.257874 and 0.233610 at y=1.491429, 1.491429, 1.473548 and 1.420778 for stress work parameter ε=0.01, 0.05, 0.1 and 0.20 respectively. Further it is found from Table 5.4 that the maximum values of the

122

skin friction coefficient are 0.733141, 0.712763, 0.688879 and 0.646364 for stress work parameter ε=0.01, 0.05, 0.1 and 0.20 at x=1.832596, 1.815142, 1.780235837 and 1.745329 respectively. Moreover it can be concluded that the maximum velocities is decreased by 17.03% and the maximum values of the skin friction coefficient is decreased by 11.84% as the stress work parameter changes from 0.01 to 0.20.

Figure 5.3(a) and 5.3(b) illustrate the variation of the velocity and temperature profiles against y for selected values of viscous dissipation parameter N while Pr=1.0, M=0.1, χ=1.0, ε =0.1 and T_r=1.0. It can be noted from Figure 5.3(a) that an increase in the viscous dissipation parameter N is associated with a slight increase in the velocity. This behavior is similar to that of temperature profile as shown in Figure 5.3(b). It implies that the viscous dissipation enhances the temperature and therefore increases the velocity. Figure 5.4(a) and Figure 5.4(b) illustrate the effect of viscous dissipation parameter on the local skin friction coefficient and the local heat transfer rate, respectively while Pr=1.0, M=0.1, χ=1.0, ε =0.1 and Tr=1.0. It can be seen that the skin friction factor increases with an increase in the viscous parameter. This is to be expected since the fluid motion within the boundary layer increases for increasing N (fig. 5.3(a)) and eventually increases the skin friction factor. Figure 5.4(b) shows that the effect of the viscous parameter leads to a decrease of the local heat transfer rate. The maximum values of the velocities are obtained as 0.257874, 0.261995, 0.265203 and 0.268444 at y=1.473548 for viscous dissipation parameter N=0.01, 0.40, 0.70 and 1.00 respectively which are shown in the Table 5.11 and the Table 5.12 shows the maximum values of the skin friction coefficients are 0.688879, 0.701550, 0.711799 and 0.722494 at x=1.780236, 1.797689, 1.815142 and 1.832596 for viscous dissipation parameter N=0.01, 0.40, 0.70 and 1.00 respectively. That is the maximum value of the skin friction coefficients is shifted along the upper stagnation point for increasing values of the viscous dissipation parameter. Furthermore, it has been observed that the velocity and the skin friction coefficient increased by 4.1% and 4.88% respectively as the viscous dissipation

123

parameter changes from 0.01 to 1.0.

Figures 5.5(a) and 5.5(b) illustrate the velocity and temperature distribution against y for different values of the temperature ratio parameter T_r, where as the skin friction coefficient and the heat transfer rate against x for different values of the temperature ratio parameter T_r, with Pr=1.0, M=0.1, χ=1.0, ε =0.1 and N=0.01 are depicted in Figures 5.6(a) and 5.6(b) respectively. Increasing value of the temperature ratio parameter T_r increases the effect of the stress work, which is observed in the fourth term of the energy equation (2.81). Therefore the velocity of the fluid decreases with increasing value of the temperature ratio parameter T_r as illustrated in Figure 5.5(a). The skin friction coefficient decreases with the increasing value of the temperature ratio parameter T_r which is observed from Figure 5.6(a). From Figure 5.5(b), it is found that the temperature within the boundary layer decreases for increasing value of the temperature ratio parameter T_r. The decreased temperature for increasing value of the temperature ratio parameter T_r within the boundary layer increases heat transfer rate as illustrated in Figure 5.6(b). Table 5.13 and Table 5.14 present the maximum values of the velocities and the skin friction coefficients respectively for different values of the temperature ratio parameter T_r with Pr=1.0, M=0.1, χ=1.0, ε =0.1 and N=0.01. It is recorded that 0.277047, 0.257874, 0.247555 and 0.237559 are the maximum velocities at y=1.509461, 1.473548, 1.438224 and 1.420778 for temperature ratio parameter T_r=0.1, 0.5, 1.0 and 1.5 respectively. The maximum values of the skin friction coefficient for different values of the temperature ratio parameter T_r=0.1, 0.5, 1.0 and 1.5 are obtained as 0.723061, 0.688879, 0.671079 and 0.654174 at x=1.832596, 1.780236, 1.762783 and 1.745329 respectively. Finally, it is calculated that the velocity decreased by 14.25% and the skin friction coefficient decreased by 9.5% as the temperature ratio parameter changes from 0.1 to 1.5.

Figures 5.7(a) and 5.7(b) illustrate the velocity and temperature distribution against y for different values of the magnetic parameter, and the skin friction coefficient and the heat transfer rate against x for varying magnetic parameter

124

with Pr=1.0, χ=1.0, ε =0.1, N=0.01 and T_r=1.0 are depicted in figures 5.8(a) and 5.8(b) respectively. Peak velocities and skin friction coefficients are presented in Table 5.5 and Table 5.6 respectively while Pr=1.0, χ=1.0, ε =0.1, N=0.01 and T_r=1.0. It is observed that the maximum velocities are 0.257874, 0.231585, 0.210228 and 0.192598 for magnetic parameter M=0.1, 0.3, 0.5 and 0.7 at y=1.473548, 1.438224, 1.420778 and 1.403475 respectively. That is maximum velocities decreases with the increasing M as shown in Figure 5.7(a). From Figure 5.7(b) it can be observed that the increasing value magnetic parameter increases temperature within the boundary in presence of stress work and viscous dissipation. The maximum values of the skin friction coefficient are 0.688879, 0.640579, 0.601799 and 0.569888 at x=1.780236, 1.745329, 1.727876 and 1.692969 for magnetic parameter M=0.1, 0.3, 0.5 and 0.7 respectively. Therefore, it is clear that the shear stress at the wall decreases with increasing values of magnetic parameter M as illustrated in Figure 5.8(a). The heat transfer rate also decreases with increasing value of magnetic parameter in presence of pressure stress work and viscous dissipation as figured in Figure 5.8(b). Lastly, it is revealed that the maximum velocity decreased by 25.31% and the maximum value of the skin friction coefficient decreased by 17.27% as magnetic parameter changes from 0.1 to 0.7.

The velocity and temperature are illustrated in Figure 5.9 and the variation of the local skin friction coefficient and local rate of heat transfer are depicted in Figure 5.10 for different values of Prandtl number Pr with M=0.1, χ=1.0, ε =0.1, N=0.01 and T_r=1.0. It is found that the velocity and temperature decreases with increasing values of Pr in presence of stress work and viscous dissipation. Although the skin friction at the surface decreases for increasing value of Prandtl number Pr as observed in Figure 5.10(a), however the heat transfer rate increases with increasing value of Prandtl number in presence of the pressure stress work and viscous dissipation as shown in Figure 5.10(b). It has been observed from Table 5.9 that the maximum values of the velocities are 0.289226, 0.257874, 0.223029 and 0.211734 at y=1.527644, 1.473548, 1.403475 and 1.369287 for Pr=0.733,

125

1.000, 1.440 and 1.630 respectively. Further Table 5.10 presents the maximum values of the skin friction coefficient for the Prandtl numbers 0.733, 1.000, 1.440 and 1.630 at x=1.850049, 1.850049, 1.832596 and 1.832596 and the maximum values of the skin friction coefficients are 0.801152, 0.749931, 0.691119 and 0.671578 respectively. It is noted that the velocity and the skin friction coefficient decreased by 26.79% and 18.51% respectively as the Prandtl number changes from 0.733 to 1.630.

The maximum values of the velocity and the maximum values of the skin friction coefficient are presented in Table 5.7 and Table 5.8 respectively for different values of the conjugate conduction parameter χ while Pr=1.0, M=0.1, ε=0.1, N=0.01 and T_r=1.0. It is reported that the maximum values of the velocity are 0.257874, 0.239762, 0.224979 and 0.212582 at y=1.473548, 1.509461, 1.527643 and 1.564468 and the maximum values of the skin friction coefficient are 0.688879, 0.624758, 0.574174 and 0.532949 for conjugate conduction parameter χ=1.0, 1.5, 2.0 and 2.5 respectively. It has been revealed that the velocity and the skin friction coefficient decreased by 17.56% and 22.64% respectively as the conjugate conduction parameter changes from 1.0 to 2.5. Moreover, the velocity profiles and temperature profiles are plotted against y-axis in Figure 5.11 and the skin friction coefficient and heat transfer rate are plotted against x-axis in Figure 5.12 for different values of conjugate conduction parameter χ with Pr=1.0, M=0.1, ε =0.1, N=0.01 and T_r=1.0. From Figures 5.11(a) and 5.11(b) it is clear that both the velocity profiles and temperature distributions decrease for increasing conjugate conduction parameter χ as we consider the presence of stress work and viscous dissipation. It can be noted from Figure 5.12(a) and Figure 5.12(b) that, both the skin friction coefficient and heat transfer rate decrease as the values of conduction parameter increase.

126

TABLES

Table 5.1: Comparisons of the present numerical values of $-\theta'(x,0)$ with Merkin (1976) and Nazar et al. (2002) for different values of x while Pr=1.0, M=0.0, χ=0.0, N=0.0, ε =0.0 and T_r=0.0.

$Nu\,Gr^{-1/4} = -\theta'(x,0)$			
x	Merkin (1976)	Nazar et al. (2002)	Present
0.0	0.4214	0.4214	0.421446
$\pi/6$	0.4161	0.4161	0.416158
$\pi/3$	0.4007	0.4005	0.400519
$\pi/2$	0.3745	0.3741	0.374071
$2\pi/3$	0.3364	0.3355	0.335553
$5\pi/6$	0.2825	0.2811	0.281152
π	0.1945	0.1916	0.191565

Table 5.2: Comparisons of the present numerical values of $x f''(x,0)$ with Merkin (1976) and Nazar et al. (2002) for different values of x while Pr=1.0, M=0.0, χ=0.0, N=0.0, ε =0.0 and T_r =0.0.

$C_f\,Gr^{1/4} = x f''(x,0)$			
x	Merkin (1976)	Nazar et al. (2002)	Present
0.0	0.0000	0.0000	0.000000
$\pi/6$	0.4151	0.4148	0.414380
$\pi/3$	0.7558	0.7542	0.753549
$\pi/2$	0.9579	0.9545	0.953656
$2\pi/3$	0.9756	0.9698	0.969071
$5\pi/6$	0.7822	0.7740	0.773223
π	0.3391	0.3265	0.325651

127

Table 5.3: Maximum velocity $f'(x, y)$ against y for different values of stress work parameter ε while Pr=1.0, M=0.1, χ=1.0, N=0.01 and T_r =1.0.

Stress work parameter ε	y	Maximum Velocity
0.01	1.491429	0.281548
0.05	1.491429	0.270846
0.10	1.473548	0.257874
0.20	1.420778	0.233610

Table 5.4: Maximum value of the skin friction coefficient $x f''(x,0)$ against x for different values of stress work parameter ε while Pr=1.0, M=0.1, χ=1.0, N=0.01 and T_r =1.0.

Stress work parameter ε	x	Maximum Skin friction coefficient
0.01	1.832596	0.733141
0.05	1.815142	0.712763
0.10	1.780236	0.688879
0.20	1.745329	0.646364

Table 5.5: Maximum velocity $f'(x, y)$ against y for different values of magnetic parameter M with Pr=1.0, χ=1.0, ε =0.1, N=0.01 and T_r =1.0.

Magnetic Parameter M	y	Maximum Velocity
0.1	1.473548	0.257874
0.3	1.438224	0.231585
0.5	1.420778	0.210228
0.7	1.403475	0.192598

128

Table 5.6: Maximum value of the skin friction coefficient $x f''(x,0)$ against x for different values of magnetic parameter M with Pr=1.0, χ=1.0, ε =0.1, N=0.01 and T_r =1.0.

Magnetic parameter M	x	Maximum Skin friction coefficient
0.1	1.780236	0.688879
0.3	1.745329	0.640579
0.5	1.727876	0.601799
0.7	1.692969	0.569888

Table 5.7: Maximum velocity $f'(x, y)$ against y for different values of conjugate conduction parameter χ with Pr=1.0, M=0.1, ε =0.1, N=0.01 and T_r=1.0.

Conjugate conduction parameter χ	y	Maximum Velocity
1.0	1.473548	0.257874
1.5	1.509461	0.239762
2.0	1.527644	0.224979
2.5	1.564468	0.212582

Table 5.8: Maximum value of the skin friction coefficient $x f''(x,0)$ against x for different values of conjugate conduction parameter χ with Pr=1.0, M=0.1, ε =0.1, N=0.01 and T_r =1.0.

Conjugate conduction parameter χ	x	Maximum Skin friction coefficient
1.0	1.780236	0.688879
1.5	1.780236	0.624758
2.0	1.780236	0.574174
2.5	1.762783	0.532949

129

Table 5.9: Maximum velocity $f'(x, y)$ against y for different values of Prandtl number Pr while M=0.1, χ =1.0, ε =0.1, N=0.01 and T_r =1.0.

Prandtl number Pr	y	Maximum Velocity
0.733	1.527644	0.289226
1.000	1.473548	0.257874
1.440	1.403475	0.223029
1.630	1.369287	0.211734

Table 5.10: Maximum value of the skin friction coefficient $x f''(x,0)$ against x for different values of Prandtl number Pr while M=0.1, χ =1.0, ε =0.1, N=0.01 and T_r =1.0.

Prandtl number Pr	x	Maximum Skin friction coefficient
0.733	1.797689	0.743259
1.000	1.780236	0.688879
1.440	1.780236	0.626429
1.630	1.762783	0.605665

Table 5.11: Maximum velocity $f'(x, y)$ against y for different values of viscous dissipation parameter N while Pr=1.0, M=0.1, χ =1.0, ε =0.1 and T_r=1.0.

Viscous dissipation parameter N	y	Maximum Velocity
0.01	1.473548	0.257874
0.40	1.455813	0.261995
0.70	1.455813	0.265203
1.00	1.455813	0.268444

Table 5.12: Maximum value of the skin friction coefficient $x f''(x,0)$ against x for different values of viscous dissipation parameter N while Pr=1.0, M=0.1, χ=1.0, ε =0.1 and T_r =1.0.

Viscous dissipation parameter N	x	Maximum Skin friction coefficient
0.01	1.780236	0.688879
0.40	1.797689	0.701550
0.70	1.815142	0.711799
1.00	1.832596	0.722494

Table 5.13: Maximum velocity $f'(x, y)$ against y for different values of temperature ratio parameter T_r while Pr=1.0, M=0.1, χ =1.0, ε =0.1 and N=0.01.

Temperature ratio parameter T_r	y	Maximum Velocity
0.1	1.509461	0.277047
0.5	1.473548	0.257874
1.0	1.438224	0.247555
1.5	1.420778	0.237559

Table 5.14: Maximum value of the skin friction coefficient $x f''(x,0)$ against x for different values of temperature ratio parameter T_r while Pr=1.0, M=0.1, χ =1.0, ε=0.1 and N=0.01.

Temperature ratio parameter T_r	x	Maximum Skin friction coefficient
0.1	1.832596	0.723061
0.5	1.780236	0.688879
1.0	1.762783	0.671079
1.5	1.745329	0.654174

FIGURES

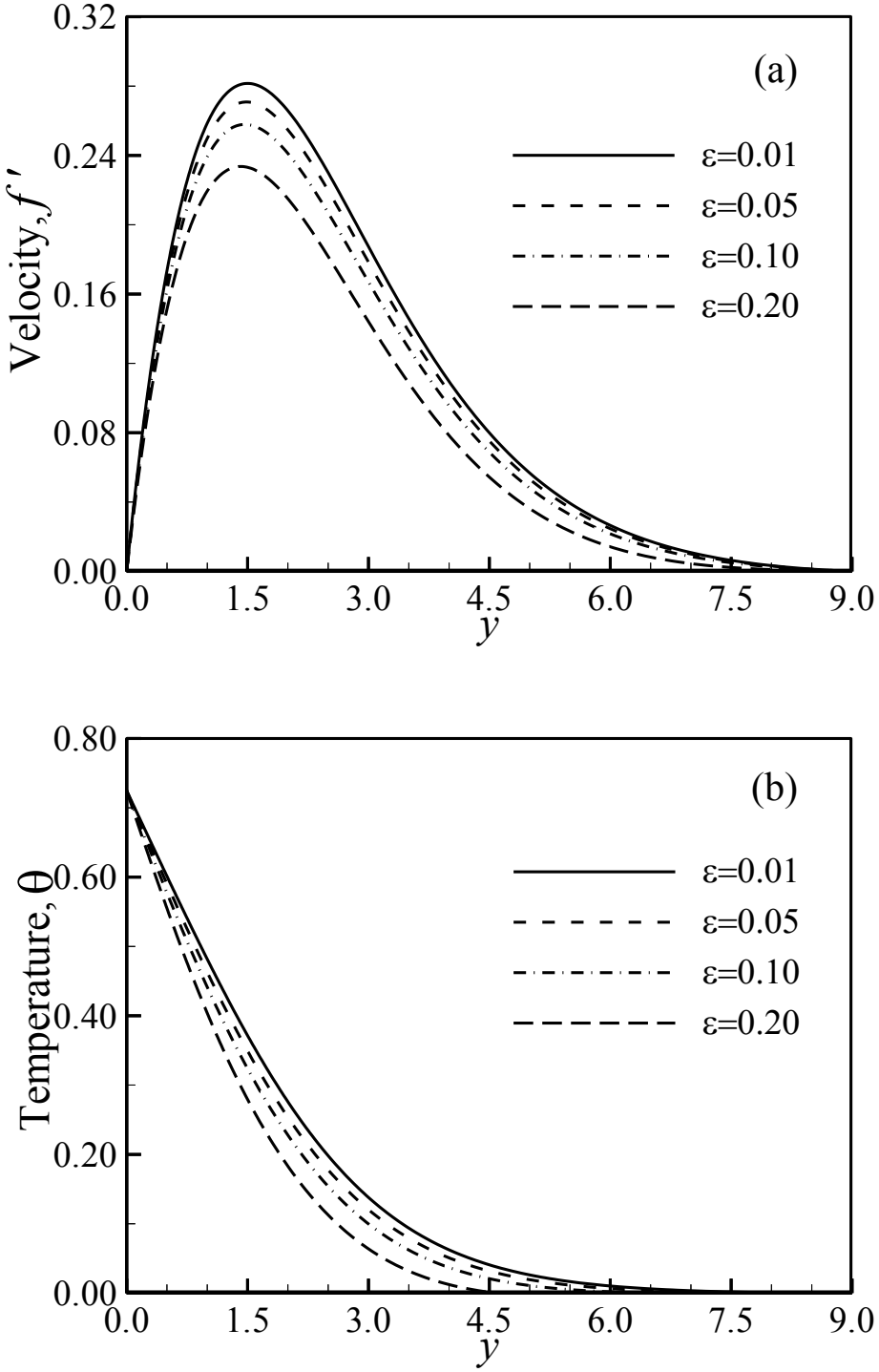

Figure 5.1: (a) Variation of velocity profiles and (b) variation of temperature profiles against y for varying of stress work parameter ε with Pr=1.0, M=0.1, χ=1.0, N=0.01 and T_r=1.0.

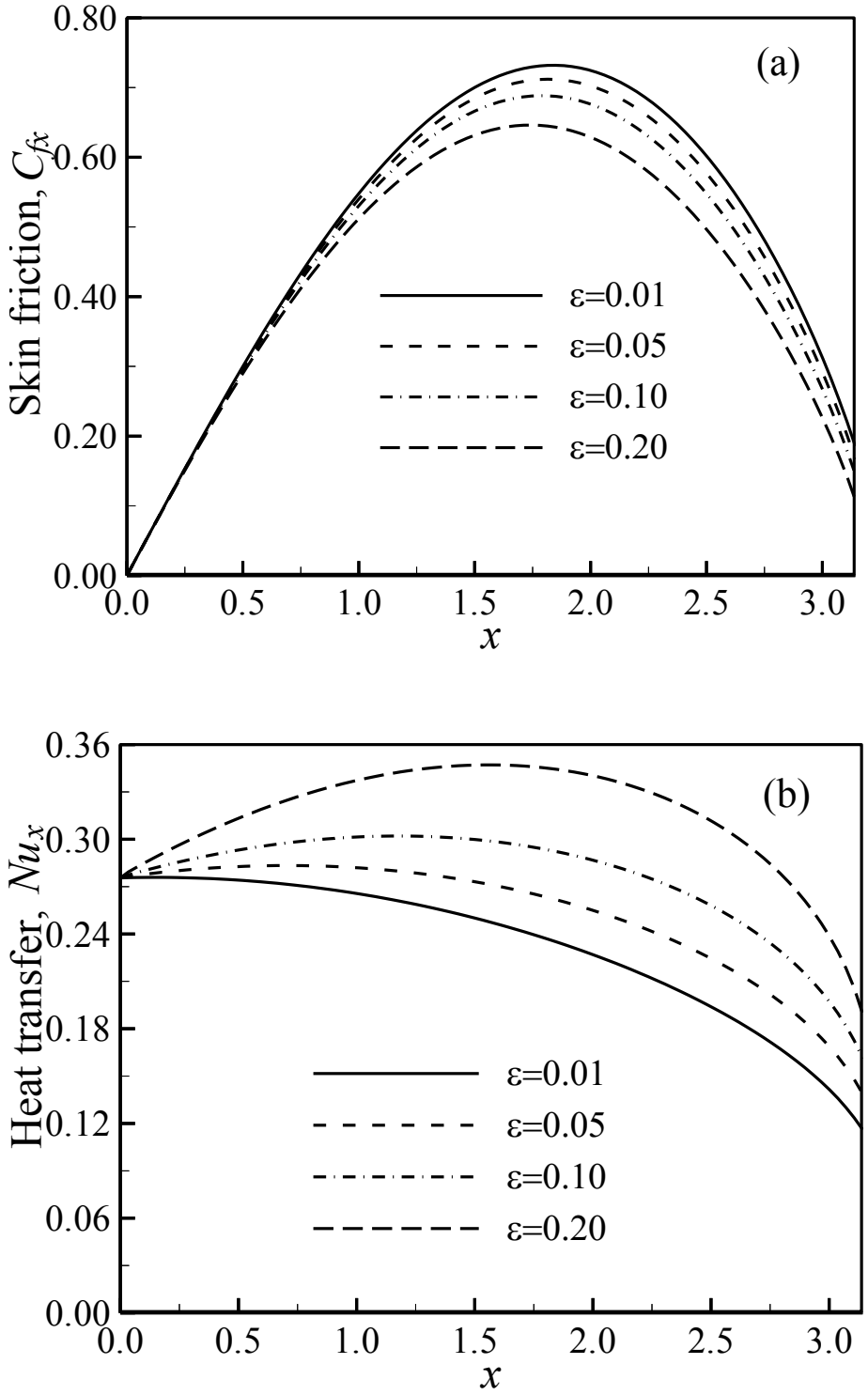

Figure 5.2: (a) Variation of the local skin friction coefficients and (b) variation of local Nusselt number against x for varying of stress work parameter ε with with Pr=1.0, M=0.1, χ =1.0, N=0.01 and T_r=1.0.

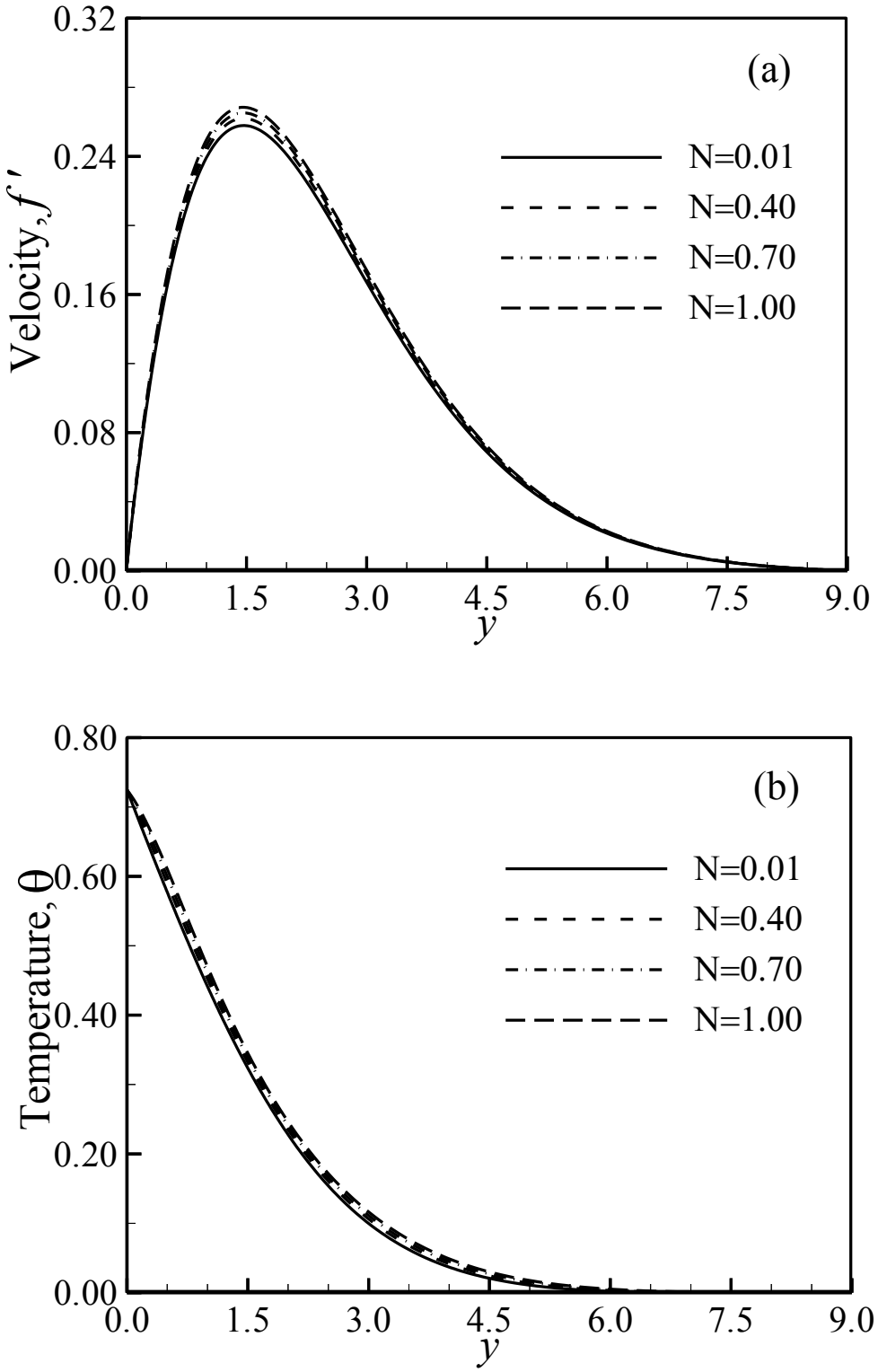

Figure 5.3: (a) Variation of velocity profiles and (b) variation of temperature profiles against y for varying of viscous dissipation parameter N with Pr=1.0, M=0.1, χ =1.0, ε=0.1 and T_r=1.0.

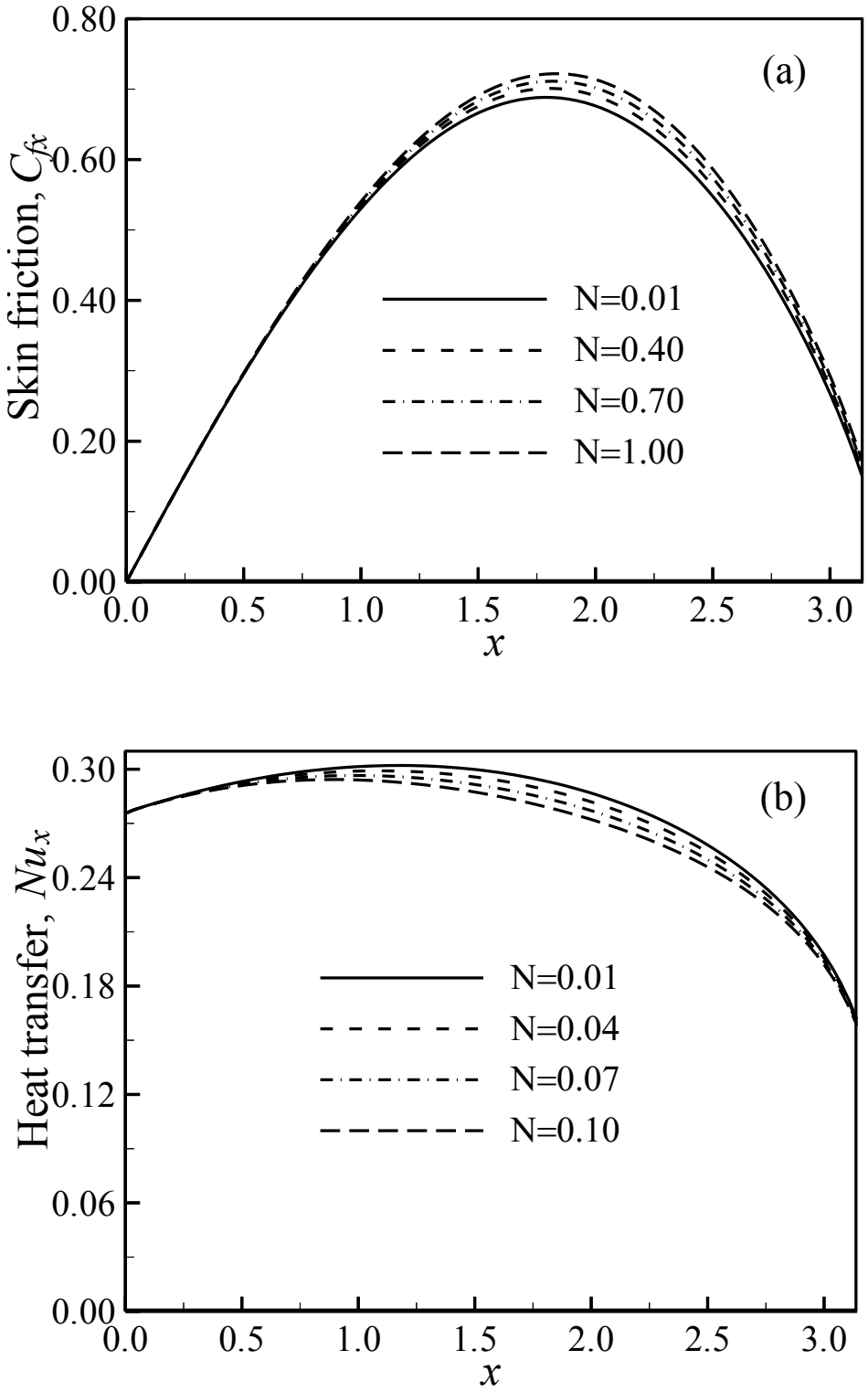

Figure 5.4: (a) Variation of the local skin friction coefficients and (b) variation of local Nusselt number against x for varying of viscous dissipation parameter N with Pr=1.0, M=0.1, χ =1.0, ε =0.1 and T_r=1.0.

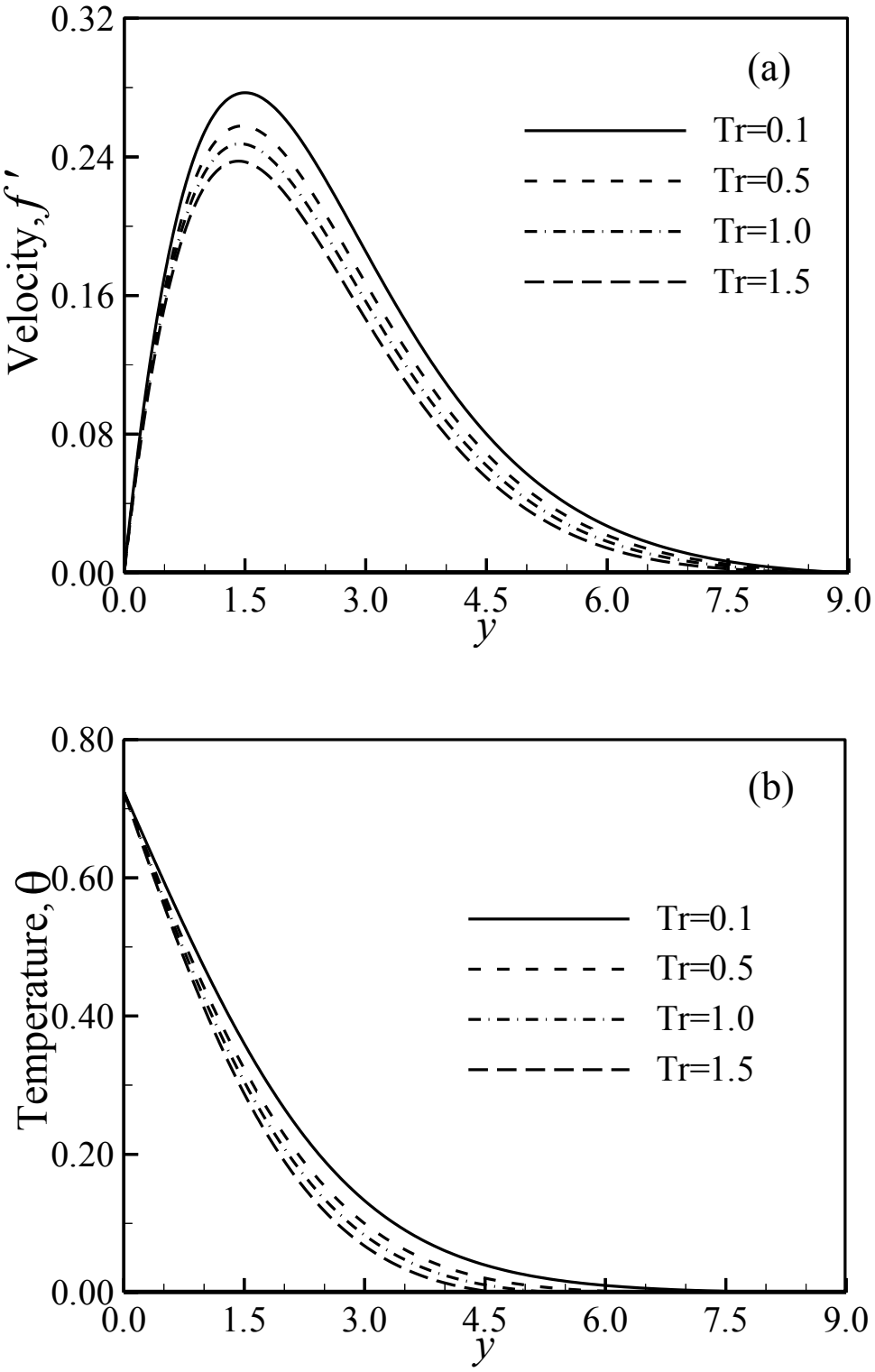

Figure 5.5: (a) Variation of velocity profiles and (b) variation of temperature profiles against y for varying of temperature ratio parameter T_r with Pr=1.0, M=0.1, χ =1.0, ε=0.1 and N=0.01.

136

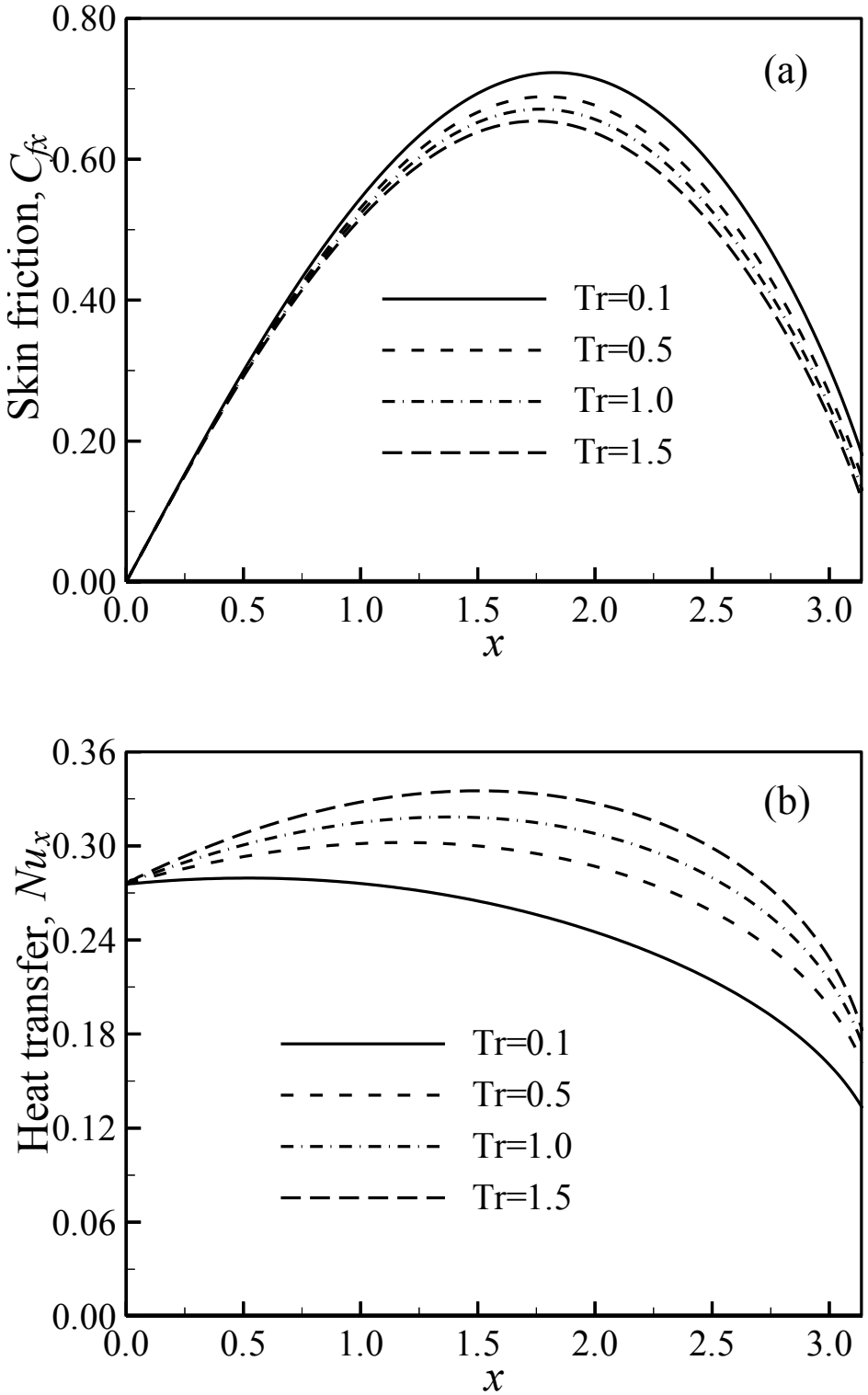

Figure 5.6: (a) Variation of the local skin friction coefficients and (b) variation of local Nusselt number against x for varying of temperature ratio parameter T_r with Pr=1.0, M=0.1, χ =1.0, ε =0.1 and N=0.01.

137

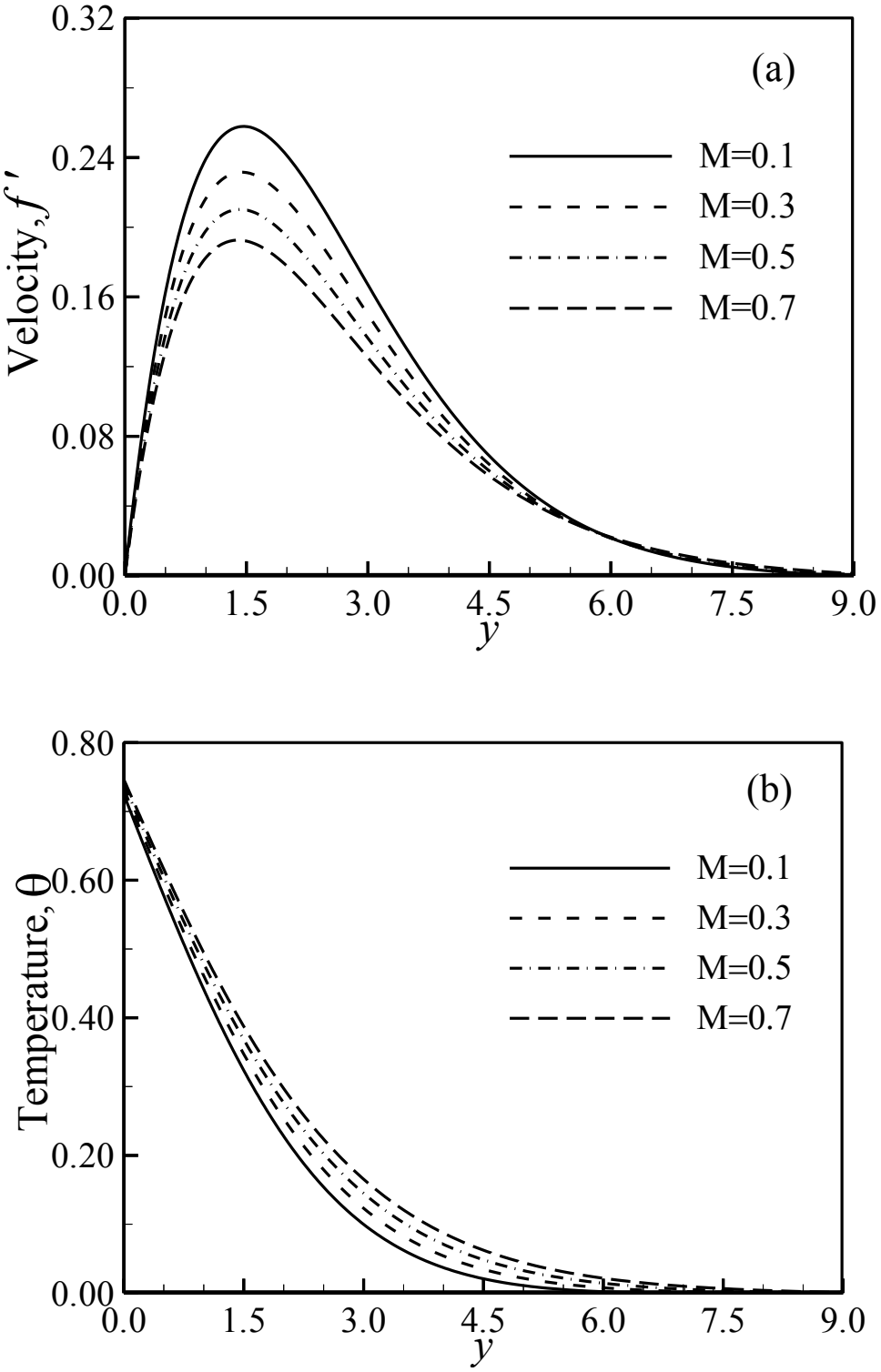

Figure 5.7: (a) Variation of velocity profiles and (b) variation of temperature profiles against y for varying of magnetic parameter M with Pr=1.0, χ =1.0, ε=0.1, N=0.01 and T_r=1.0.

138

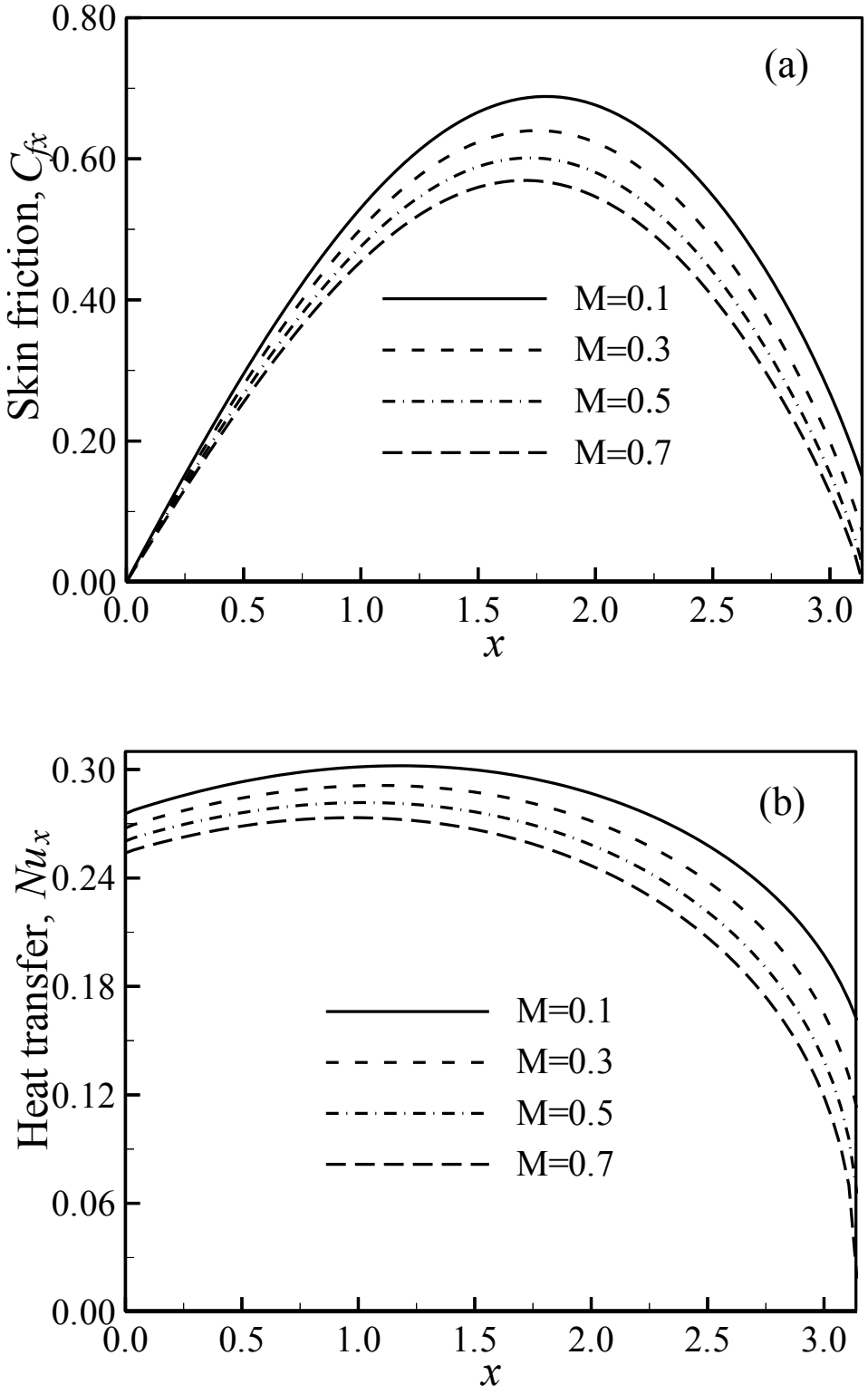

Figure 5.8: (a) Variation of the local skin friction coefficients and (b) variation of local Nusselt number against x for varying of magnetic parameter M with Pr=1.0, χ =1.0, ε=0.1, N=0.01 and T_r=1.0.

139

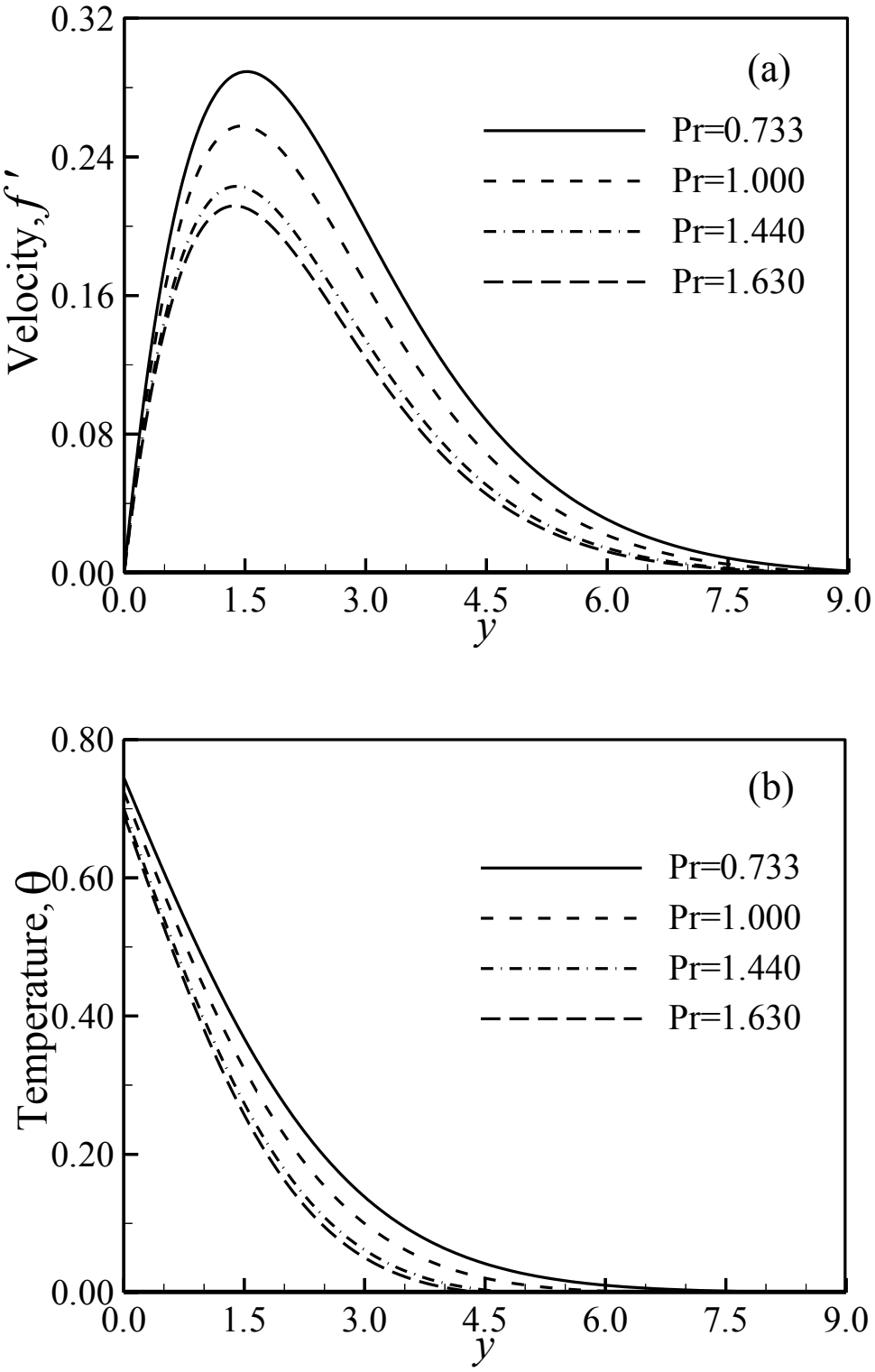

Figure 5.9: (a) Variation of velocity profiles and (b) variation of temperature profiles against y for varying of Prandtl number Pr with M=0.1, χ =1.0, ε=0.1, N=0.01 and T_r=1.0.

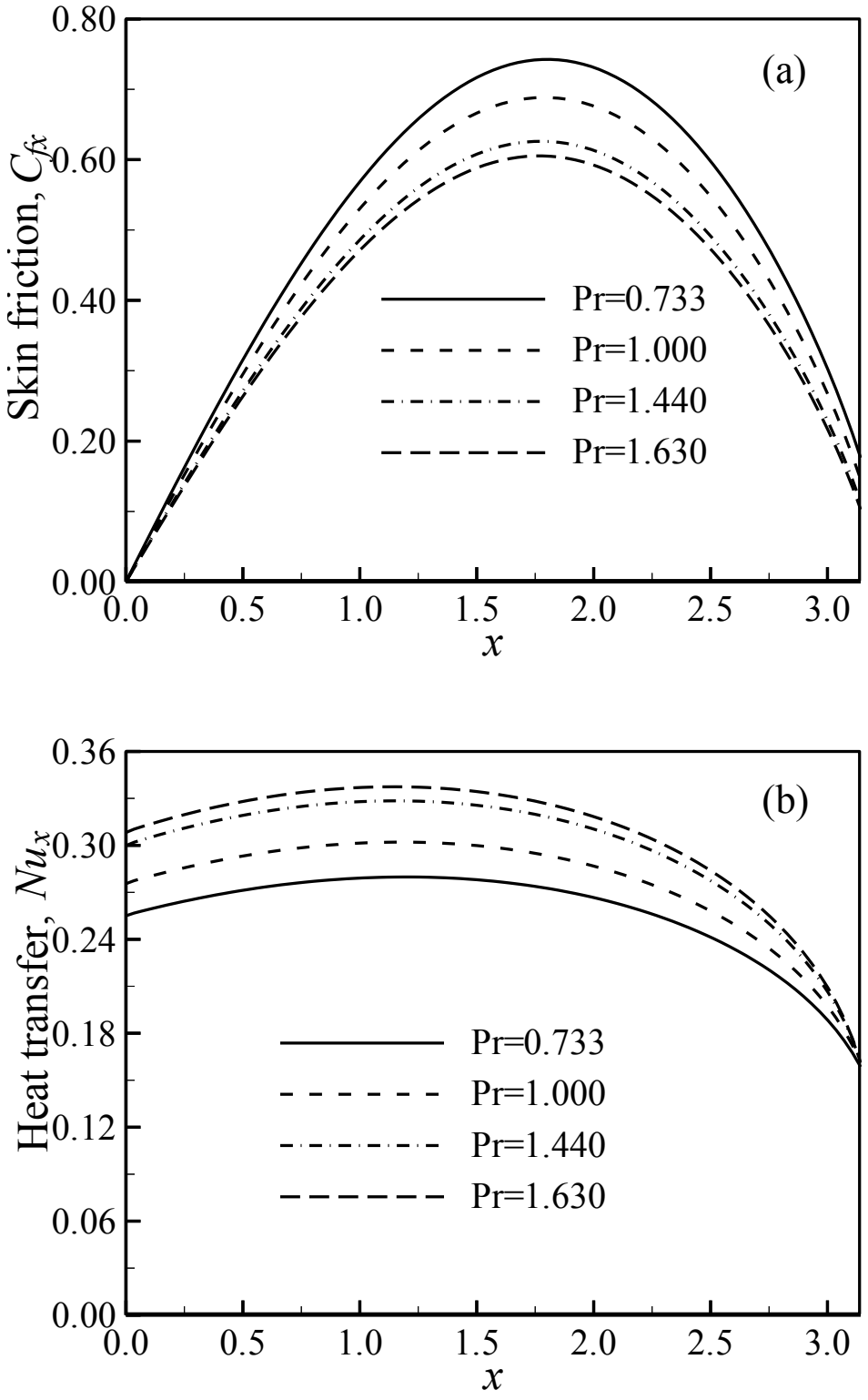

Figure 5.10: (a) Variation of the local skin friction coefficients and (b) variation of local Nusselt number against x varying of Prandtl number Pr with M=0.1, χ=1.0, ε=0.1, N=0.01 and T_r=1.0.

141

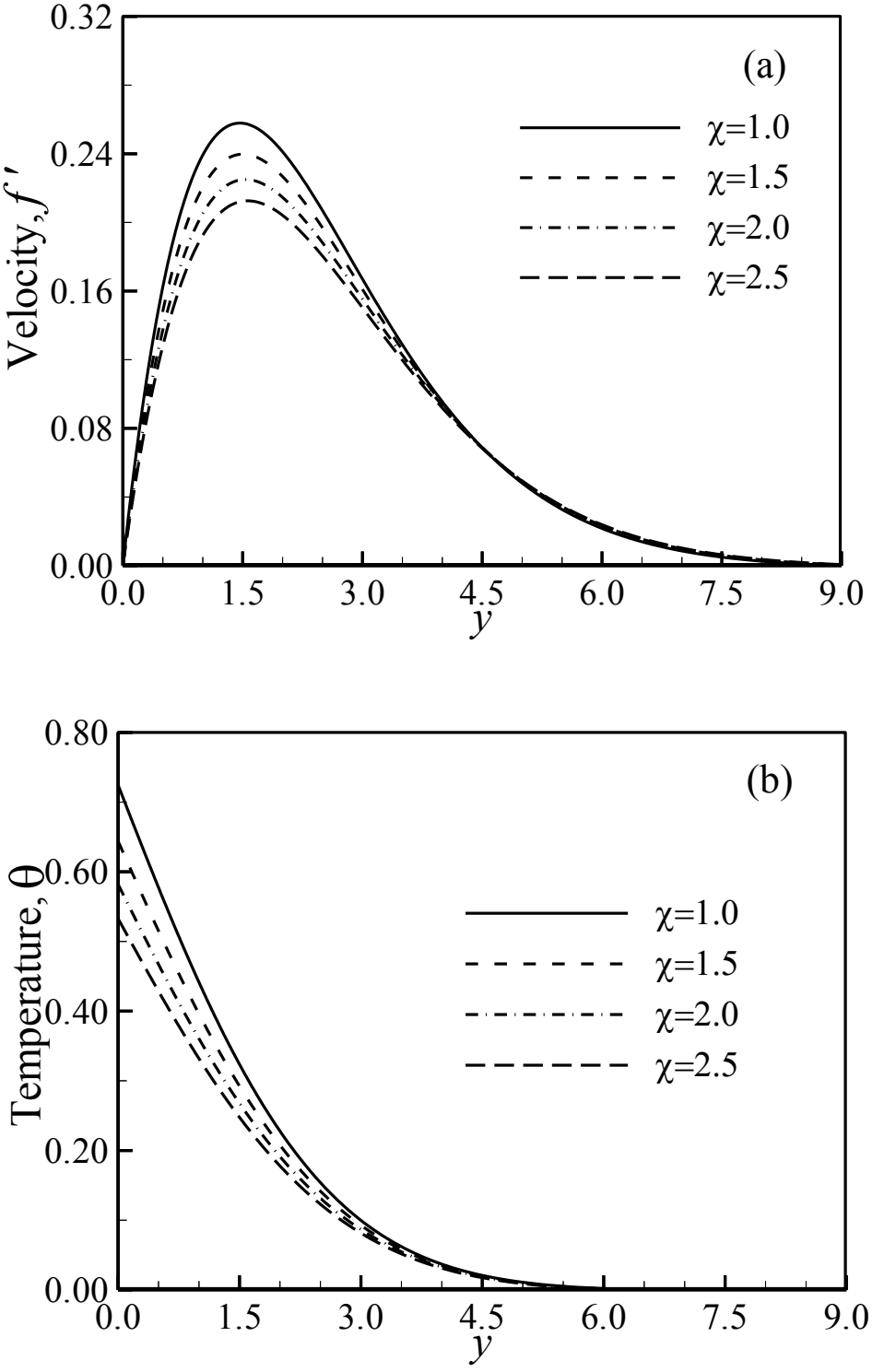

Figure 5.11: (a) Variation of velocity profiles and (b) variation of temperature profiles against y for varying of conjugate conduction parameter χ with Pr=1.0, M=0.1, ε =0.1, N=0.01 and T_r=1.0.

142

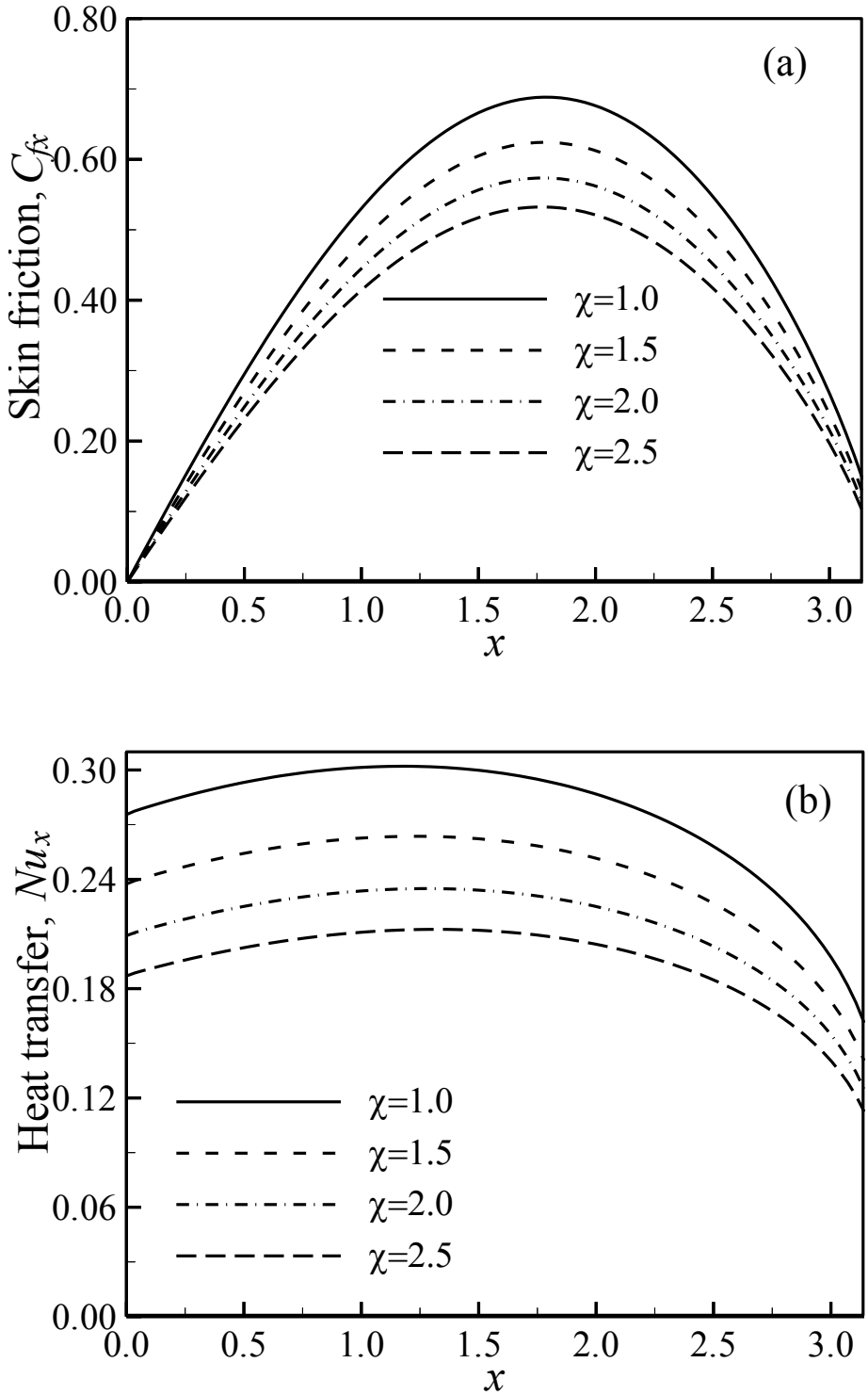

Figure 5.12: (a) Variation of the local skin friction coefficients and (b) variation of local Nusselt number against x for varying of conjugate conduction parameter χ with Pr=1.0, M=0.1, ε =0.1, N=0.01 and T_r=1.0.

143

5.4 Conclusion

Stress work and viscous dissipation on MHD-conjugate free convection flow from a horizontal circular cylinder is studied. The effects of the Stress work parameter, viscous dissipation parameter, temperature ratio parameter, Magnetic parameter, Prandtl number and Conjugate conduction parameter are analysed on the fluid flow and heat transfer. The velocity of the fluid within the boundary layer decreases with increasing Prandtl number, magnetic parameter, stress work parameter, temperature ratio parameter and conjugate conduction parameter where as it increases slightly for increasing viscous dissipation parameter. The temperature in the boundary layer region increases for increasing magnetic parameter and viscous dissipation parameter while it decreases with increasing Prandtl number, stress work parameter, temperature ratio parameter and conjugate conduction parameter. The skin friction coefficient along the surface decreases for all parameters except viscous dissipation parameter. However the rate of heat transfer increases for increasing Prandtl number, stress work parameter and temperature ratio parameter while it decreases for increasing magnetic parameter, viscous dissipation parameter and conjugate conduction parameter.

144

Chapter VI

MHD-Conjugate Free Convective Heat Transfer Analysis of an Isothermal Horizontal Circular Cylinder with Temperature Dependent Viscosity

6.1 Introduction

In some heat-transfer problems, temperature differences are small compared with the absolute temperature and pressure difference are small compared with absolute pressure. Therefore, the changes in density, viscosity, and conductivity produced by the temperature differences are small enough to be neglected in the momentum and energy equation. However, in heat transfer problems with large temperature differences, the temperature-field equations become nonlinear and are coupled to the velocity-field equations, as the viscosity depends on the temperature. Viscosity may change significantly with temperature, for instance, the viscosity of water decreases by about 240% when the temperature increases from 10^0C (μ= 0.00131 kg $m^{-1}s^{-1}$) to 50^0C (μ = 0.000548 kg $m^{-1}s^{-1}$). To predict the flow behavior accurately, temperature dependent variation of viscosity is necessary to take into account. Several authors studied flow and heat transfer analysis considering temperature dependent variation of viscosity which have been discussed in section 1.2 of chapter I. From Figure 1.3 one may realizes that the viscosity of some of the fluids like engine oil, mercury and water etc. are inversely proportional to linear function of temperature where as the viscosity of some of the fluids like hydrogen and air are directly proportional to linear function of temperature. Out of many forms of viscosity variation, which are available in the literature, we have considered the following form proposed by Lings and Dybbs (1987) and described in equation (2.83).

$$\mu = \frac{\mu_\infty}{1+\gamma\left(T_f - T_\infty\right)}$$

The problem, MHD-conjugate free convective heat transfer analysis from an isothermal horizontal circular cylinder with temperature dependent viscosity has been considered in this chapter.

145

6.2 Governing Equations

Mathematical formulation of the present problem has been discussed in section 2.4.4 as case IV of chapter II. The dimensionless continuity equation, energy equation and the boundary conditions are same as equations (2.50), (2.52) and (2.53) however there are some modifications in the momentum equation due to variable viscosity. The modified dimensionless momentum equation is given in equation (2.86). Finally, we have the equations (2.87) and (2.67) as the momentum equation and energy equation using stream function defined in equation (2.54) and (2.55) which satisfies dimensionless continuity equation (2.50). The final form of the momentum equation, energy equation and respective boundary conditions are given in equations (2.87), (2.67) and (2.68). Thus the equations governing present problem and the boundary condition are:

Momentum equation:

$$\frac{1}{1+\lambda\theta} f''' + ff'' - f'^2 - \frac{\lambda}{(1+\lambda\theta)^2}\theta' f'' - Mf' + \frac{\sin x}{x}\theta = x\left(f' \frac{\partial f'}{\partial x} - f'' \frac{\partial f}{\partial x} \right)$$

Energy equation:

$$\frac{1}{\Pr}\theta'' + f\theta' = x\left(f' \frac{\partial \theta}{\partial x} - \theta' \frac{\partial f}{\partial x} \right)$$

Boundary condition:

$$f = f' = 0,\ \theta - 1 = \chi \frac{\partial \theta}{\partial y} \ at\ y = 0,\ x > 0$$

$$f' \to 0,\ \theta \to 0\ as\ y \to \infty,\ x > 0$$

where, $M = \left(\sigma a^2 {B_0}^2\right)/\left(\nu_\infty \rho_\infty Gr^{1/2}\right)$ is the magnetic parameter, $\lambda = \gamma\left(T_b - T_\infty\right)$ is the temperature dependent viscosity variation parameter, $Pr = \frac{\mu_\infty (c_p)_\infty}{\kappa_f}$ is the

146

Prandtl number and $\chi = \left(b\kappa_f Gr^{1/4}\right)/\left(a\kappa_s\right)$ is the conjugate conduction parameter. Certainly, the present problem is governed by the above parameters. The shearing stress in terms of skin friction coefficient C_f has been modified as equation (2.91) due to variable viscosity.

$$C_f Gr^{\frac{1}{4}} = \frac{x}{1+\lambda\theta} f''(x,0)$$

Numerical results of the skin friction coefficient are determined from equation (2.91) where as the rate of heat transfer in terms of Nusselt number can be determined by equation (2.70) and the equation (2.71) is accountable for the velocity and temperature distributions.

6.3 Numerical results and explanation

There are four parameters in the governing equations which are very important to analyse the flow and heat transfer behaviour for the current problem. Two parameters in momentum equation and they are magnetic parameter M and temperature dependent viscosity variation parameter λ, one parameter in the energy equation namely Prandtl number Pr and one in the boundary condition which is conjugate conduction parameter χ. The governing momentum equation (2.87) and energy equation (2.67) has been solved numerically based on the boundary condition (2.68) for different values of the above parameters using the implicit finite difference method together with the Keller box technique which is elaborately discussed in chapter II.

The Prandtl numbers are considered to be 3.50 2.97, 1.63 and 1.00 that correspond to Dichlorodifluoromethane (Freon) at 50^0C, Methyl chloride at 50^0C, Glycerin at 50^0C and Steam at 700^0K respectively. The remaining parameters are taken as follows: magnetic parameter M=0.0-0.5; conjugate conduction parameter χ=0.0-2.0 and temperature dependent viscosity variation parameter λ=0.01–1.20.

147

Table 6.1 shows the comparison of the local Nusselt number obtained in the present work with M=0.0, χ= 0.0, λ=0.0 and Pr = 1.0 and the results obtained by Merkin (1976) and Nazar et al. (2002) where as a comparison of the local skin friction factor is presented in Table 6.2 with the present solution while M=0.0, χ=0.0, λ=0.0 and Pr=1.0 and the results obtained by Merkin (1976) and Nazar et al. (2002). It has been observed that there is an excellent agreement among these results.

The maximum values of the velocities are shown in Tables 6.3, 6.5, 6.7 and 6.9 for different values of viscosity variation parameter, magnetic parameter, Prandtl number and conjugate conduction parameter respectively. On the other hand the maximum values of the skin friction coefficients are presented in Tables 6.4, 6.6, 6.8 and 6.10 for different values of viscosity variation parameter, magnetic parameter, Prandtl number and conjugate conduction parameter respectively.

Figures 6.1, 6.3, 6.5 and 6.7 illustrate the velocity and temperature distributions at $x = \pi/2$ against y, the direction along the normal to the surface of the cylinder, and Figures 6.2, 6.4, 6.6 and 6.8 depict the skin friction coefficients and heat transfer rates against x at y=0 (along the surface of the cylinder) for different values of the viscosity variation parameter, magnetic parameter, Prandtl number and conjugate conduction parameter, respectively.

The effects of the temperature dependent viscosity variation parameter λ on the velocity and temperature distribution are illustrated in Figures 6.1(a) and 6.1(b) respectively while Prandtl number Pr=1.0, magnetic parameter M=0.1 and conjugate conduction parameter χ=1.0. Then again, Figures 6.2(a) and 6.2(b) show the influence of the temperature dependent viscosity variation parameter λ on the skin friction coefficient and the rate of heat transfer respectively. It has been observed from equation (2.84) that the viscosity of the fluid within the boundary layer decreases with increasing value of viscosity variation parameter λ. As the viscosity of the fluid within the boundary layer decreases with increasing viscosity variation parameter accordingly the velocity increases and the skin

148

friction coefficient decreases with increasing viscosity variation parameter as observed in Figures 6.1(a) and 6.2(a) respectively. From Figure 6.1(b) it is seen that the temperature within the boundary layer slightly decreases with increasing value of the viscosity variation parameter λ which leads to an increase in heat transfer rate as found in Figure 6.2(b). Moreover it is found from Figure 6.1(a) and from Table 6.3 that the maximum velocity become closer to the surface as we consider higher value of viscosity variation parameter λ. The maximum values of the velocities are reported as 0.308463, 0.322075, 0.333891 and 0.344185 at y=1.438224, 1.302542, 1.237881 and 1.114402 for viscosity variation parameter λ=0.01, 0.40, 0.80 and 1.20 respectively. Alternatively, It is also reported that the maximum values of the skin friction coefficient are 0.821498, 0.744191, 0.685632 and 0.640179 at x=1.884956 for viscosity variation parameter λ=0.01, 0.40, 0.80 and 1.20 respectively. Therefore it is concluded that the maximum velocity increases by 11.58% and maximum value of the skin friction coefficient decreases by 22.07% as the viscosity variation parameter λ increased from 0.01 to 1.20.

It is observed from Figure 6.3(a) that the motion of the fluid decreases within the boundary layer for increasing value of the magnetic parameter *M,* if temperature dependent viscosity is taken into account. Therefore, the skin friction coefficient at the surface to the cylinder is decreased, which is shown from Figure 6.4(a). Temperature within the thermal boundary-layer increases for increasing value of the magnetic parameters as revealed from Figure 6.3(b) and the heat transfer rate decreases with increasing magnetic parameter as illustrated in Figure 6.4(b). The maximum values of the velocity are recorded to be 0.317195, 0.308463, 0.292272 and 0.277603 for magnetic parameter M=0.0, 0.1, 0.3 and 0.5 respectively with viscosity variation parameter λ=0.01, which are presented in Table 6.5. It is also observed from Table 6.6 that the maximum values of the skin friction coefficient are 0.839187, 0.821498, 0.788942 and 0.759936 for magnetic parameter M=0.0, 0.1, 0.3 and 0.5 with viscosity variation parameter λ=0.01 at x=1.919862, 1.884956, 1.850049 and 1.850049 respectively. Here it is observed that the velocity decreases by 12.48% and the skin friction coefficient decreases by 9.44%

when the value of the magnetic parameter changes from 0.0 to 0.5 in presence of viscosity variation parameter.

The velocity profiles and temperature profiles are plotted against y-axis in Figure 6.5 and the skin friction coefficient and heat transfer rate are plotted against x-axis in Figure 6.6 for different values of Prandtl number with M=0.1, χ=1.0 and λ=0.01. The velocity and temperature of fluid are expected to decrease with the increasing Prandtl number which are observed in Figure 6.5(a) and Figure 6.5(b) respectively. Thus the skin friction decreases and the heat transfer rate from the core region to the boundary layer region increases for increasing value of Prandtl number as depicted in Figure 6.6(a) and Figure 6.6(b) respectively. The Tables 6.7 and 6.8 show the maximum values of the velocities and the maximum values of the skin friction coefficients respectively for different values of Prandtl numbers. It has been observed that the maximum values of the velocities are 0.308463, 0.260281, 0.207878 and 0.194862 for Prandtl number Pr=1.00, 1.63, 2.97 and 3.50 respectively. It is also found that the maximum values of the skin friction coefficient are 0.821498, 0.733352, 0.631341and 0.604892 for Prandtl number Pr=1.00, 1.63, 2.97 and 3.50 respectively. It is noted that the velocity and the skin friction coefficient decrease by 36.83% and 26.37% respectively as the Prandtl number changes from 1.0 to 3.5.

Figures 6.7(a) and 6.7(b) illustrate the effects of the conjugate conduction parameter χ on the fluid velocity and temperature distributions, respectively. It is clear from these Figures that the fluid velocity and temperature within the boundary layer decrease with the increasing value of the conjugate conduction parameter χ as temperature dependent viscosity is considered. Figures 6.8(a) and 6.8(b) depict the variation of the conjugate conduction parameter χ on the skin friction coefficient and the heat transfer rate with Pr=1.0, M=0.1 and λ=0.01. It is observed the local Nusselt number and the skin friction coefficient both decreases with increasing value of the conjugate conduction parameter χ. The maximum values of the velocity and the maximum values of the skin friction coefficient are presented in Table 6.9 and Table 6.10 respectively. It can noted that the maximum

values of the velocity are 0.346776, 0.324516, 0.308463 and 0.286700 at y=1.369287, 1.438224, 1.438224 and 1.509461 and the maximum values of the skin friction coefficient are 0.963528, 0.880927, 0.821498 and 0.741197 for conjugate conduction parameter χ=0.0, 1.0, 1.5 and 2.0 respectively. At the end of this section, it is found that the velocity and the skin friction coefficient decreased by 17.32% and 23.07% respectively as the conjugate conduction parameter changes from 0.0 to 2.0.

151

TABLES

Table 6.1: Comparisons of the present numerical values of $-\theta'(x,0)$ with Merkin (1976) and Nazar et al. (2002) for different values of x while Prandtl number Pr=1.0, magnetic parameter M=0.0, conjugate conduction parameter χ=0.0 and temperature dependent viscosity variation parameter λ=0.0.

$Nu\,Gr^{-1/4} = -\theta'(x,0)$			
x	Merkin (1976)	Nazar et al. (2002)	Present
0.0	0.4214	0.4214	0.421414
π/6	0.4161	0.4161	0.416130
π/3	0.4007	0.4005	0.400500
π/2	0.3745	0.3741	0.374069
2π/3	0.3364	0.3355	0.335582
5π/6	0.2825	0.2811	0.281234
π	0.1945	0.1916	0.191783

Table 6.2: Comparisons of the present numerical values of $xf''(x,0)$ with Merkin (1976) and Nazar et al. (2002) for different values of x while Prandtl number Pr=1.0,magnetic parameter M=0.0, conjugate conduction parameter χ=0.0 and temperature dependent viscosity variation parameter λ=0.0.

$C_f\,Gr^{1/4} = xf''(x,0)$			
x	Merkin (1976)	Nazar et al. (2002)	Present
0.0	0.0000	0.0000	0.000000
π/6	0.4151	0.4148	0.414564
π/3	0.7558	0.7542	0.753901
π/2	0.9579	0.9545	0.954147
2π/3	0.9756	0.9698	0.969669
5π/6	0.7822	0.7740	0.773898
π	0.3391	0.3265	0.326476

Table 6.3: The maximum value of the velocities $f'(x, y)$ against y for different values of temperature dependent viscosity variation parameter λ while Pr=1.0, M=0.1 and χ=1.0.

Viscosity variation parameter λ	y	Maximum Velocity
0.01	1.438224	0.308463
0.40	1.302542	0.322075
0.80	1.237881	0.333891
1.20	1.114402	0.344185

Table 6.4: Maximum value of the skin friction coefficient $x f''(x,0)$ against x for different values of temperature dependent viscosity variation parameter λ while Pr=1.0, M=0.1 and χ=1.0.

Viscosity variation parameter λ	x	Maximum Skin friction coefficient
0.01	1.884956	0.821498
0.40	1.884956	0.744191
0.80	1.884956	0.685632
1.20	1.884956	0.640179

Table 6.5: The maximum value of the velocities $f'(x, y)$ against y for different values of magnetic parameter M with Pr=1.0, χ =1.0, and λ=0.01.

Magnetic parameter M	y	Maximum Velocity
0.0	1.438224	0.317195
0.1	1.438224	0.308463
0.3	1.438224	0.292272
0.5	1.438224	0.277603

153

Table 6.6: Maximum value of the skin friction coefficient $x f''(x,0)$ against x for different values of magnetic parameter M with Pr=1.0, χ =1.0, and λ=0.01.

Magnetic parameter M	x	Maximum Skin friction coefficient
0.0	1.919862	0.839187
0.1	1.884956	0.821498
0.3	1.850049	0.788942
0.5	1.850049	0.759936

Table 6.7: The maximum value of the velocities $f'(x, y)$ against y for different values of Prandtl number Pr while M=0.1, χ =1.0, and λ=0.01.

Prandtl number Pr	y	Maximum Velocity
1.00	1.438224	0.308463
1.63	1.369287	0.260281
2.97	1.302542	0.207878
3.50	1.302542	0.194862

Table 6.8: Maximum value of the skin friction coefficient $x f''(x,0)$ against x for different values of Prandtl number Pr while M=0.1, χ =1.0, and λ=0.01.

Prandtl number Pr	x	Maximum Skin friction coefficient
1.00	1.884956	0.821498
1.63	1.884956	0.733352
2.97	1.884956	0.631341
3.50	1.884956	0.604892

154

Table 6.9: The maximum value of the velocities $f'(x, y)$ against y for different values of conjugate conduction parameter χ with Pr=1.0, M=0.1 and λ=0.01.

Conjugate conduction parameter χ	y	Maximum Velocity
0.0	1.369287	0.346776
1.0	1.438224	0.324516
1.5	1.438224	0.308463
2.0	1.509461	0.286700

Table 6.10: Maximum value of the skin friction coefficient $x f''(x,0)$ against x for different values of conjugate conduction parameter χ with Pr=1.0, M=0.1 and λ=0.01.

Conjugate conduction parameter χ	x	Maximum Skin friction coefficient
0.0	1.850049	0.963528
1.0	1.884956	0.880927
1.5	1.884956	0.821498
2.0	1.884956	0.741197

155

FIGURES

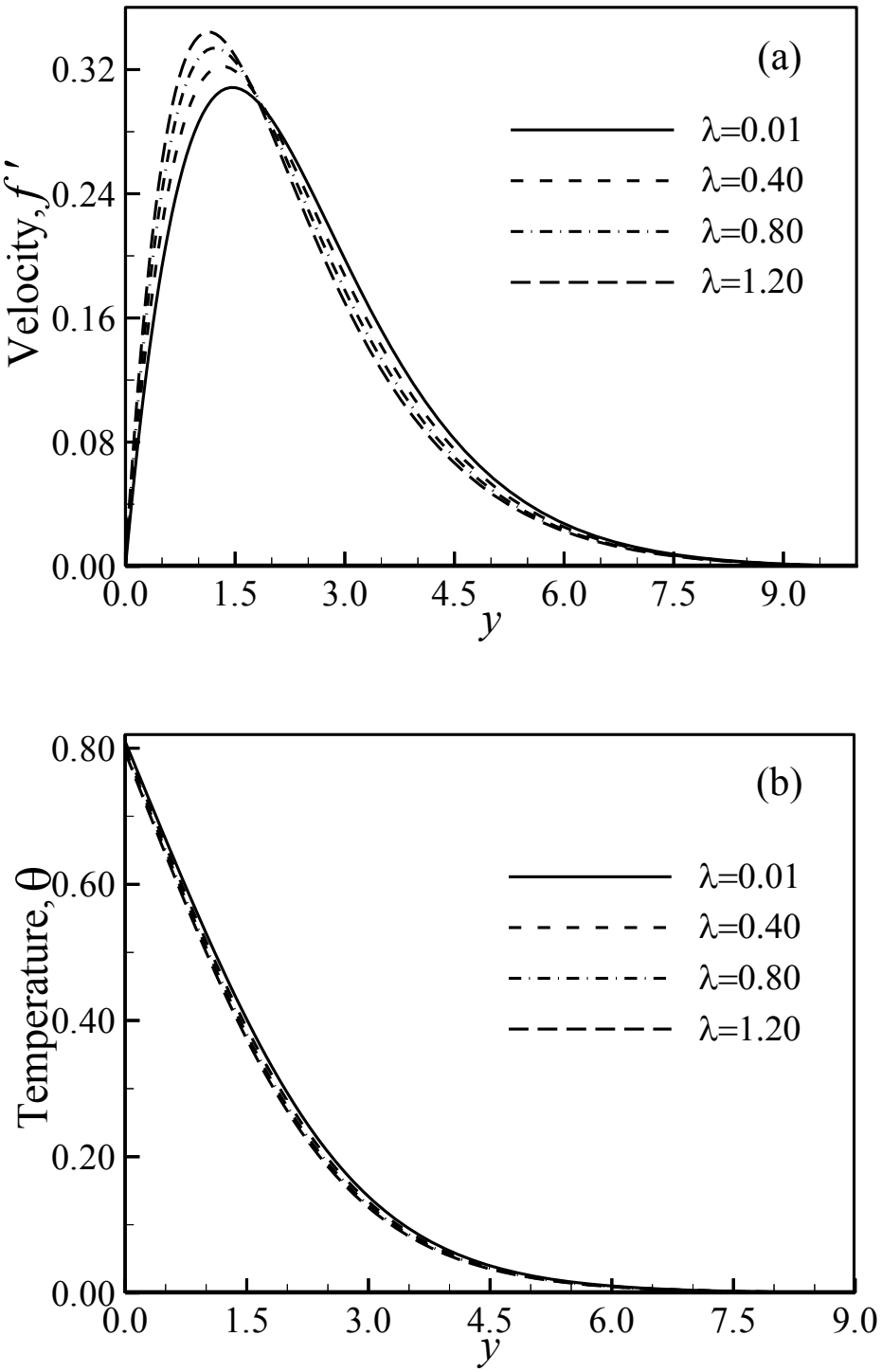

Figure 6.1: (a) Variation of velocity profiles and (b) variation of temperature profiles against y for varying of viscosity variation parameter λ with Pr=1.0, M=0.1, χ=1.0 and λ=0.01.

156

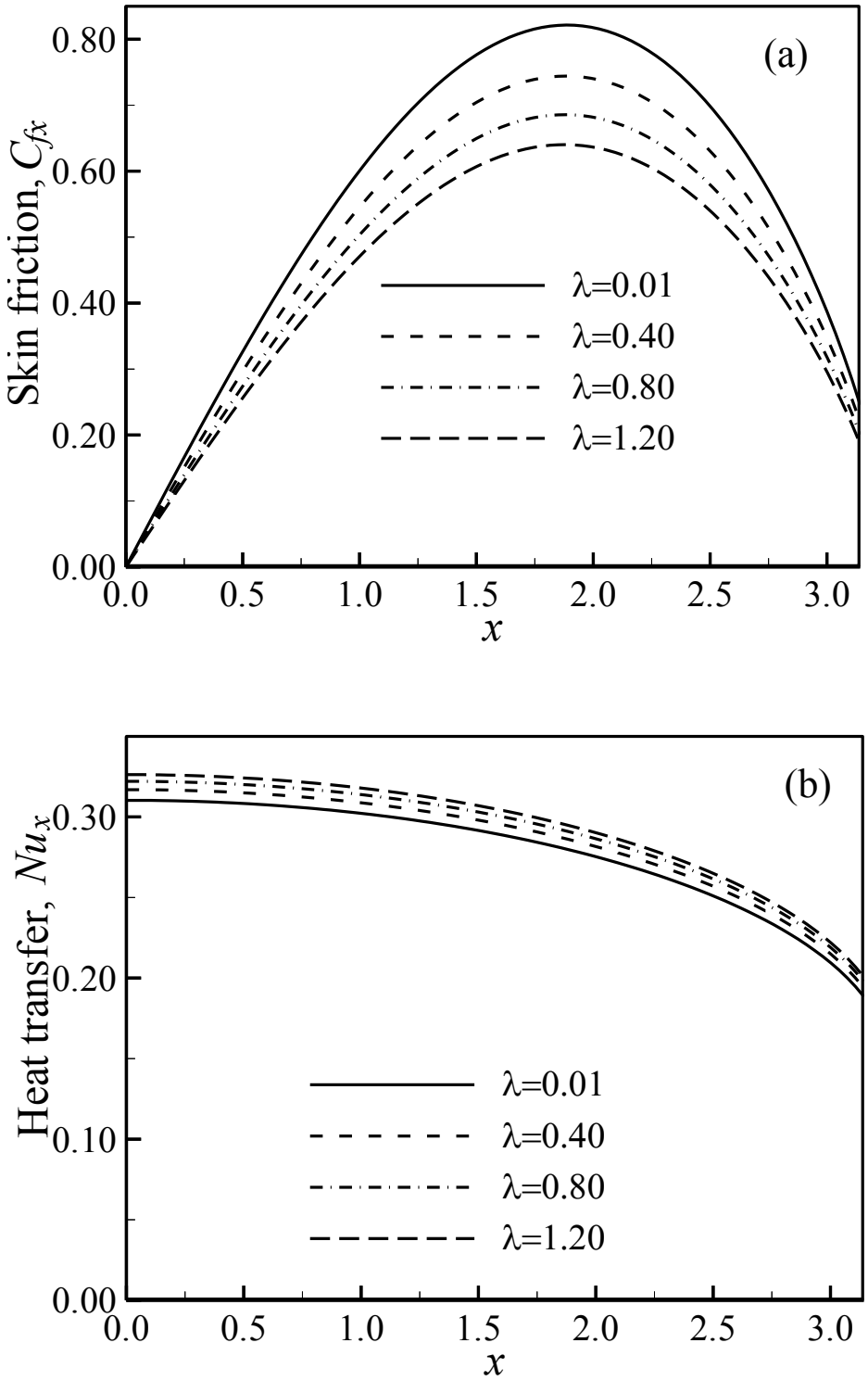

Figure 6.2: (a) Variation of the local skin friction coefficients and (b) variation of local Nusselt number against x for varying of viscosity variation parameter λ with Pr=1.0, M=0.1, χ=1.0 and λ=0.01.

157

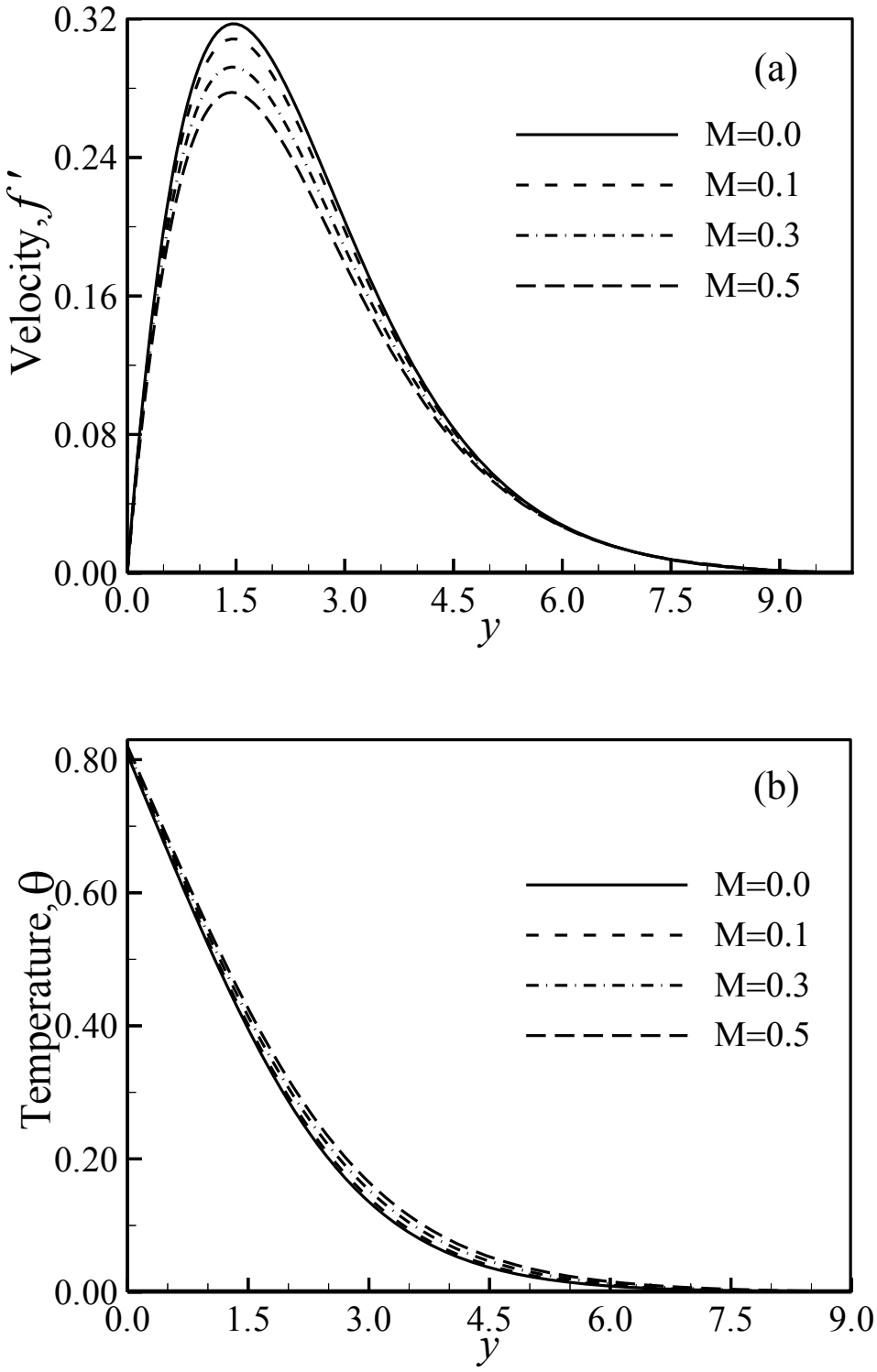

Figure 6.3: (a) Variation of velocity profiles and (b) variation of temperature profiles against y for varying of magnetic parameter M with Pr=1.0, χ=1.0 and λ=0.01.

158

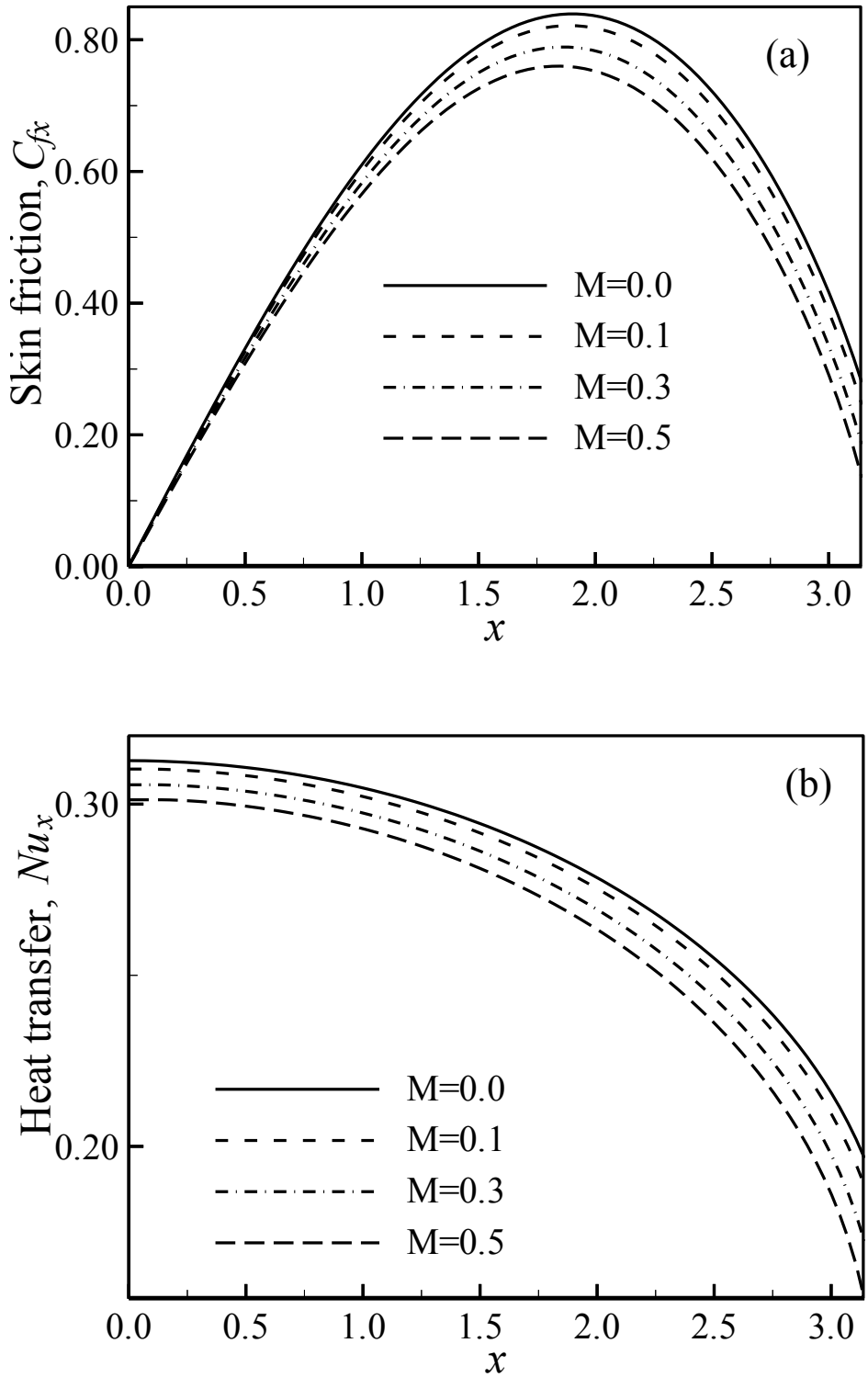

Figure 6.4: (a) Variation of the local skin friction coefficients and (b) variation of local Nusselt number against x for varying of magnetic parameter M with Pr=1.0, χ=1.0 and λ=0.01.

159

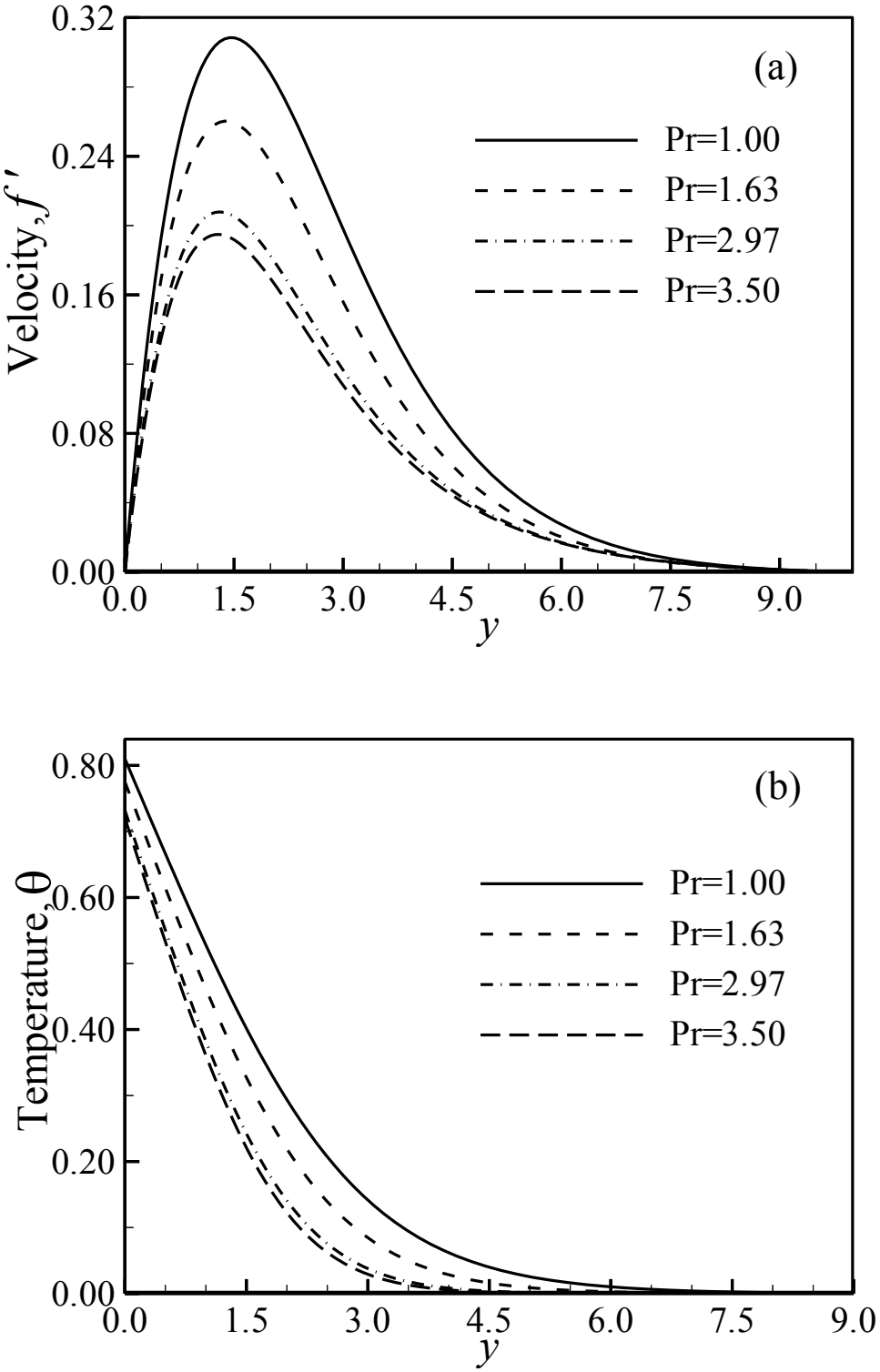

Figure 6.5: (a) Variation of velocity profiles and (b) variation of temperature profiles against y for varying of Prandtl number Pr with M=0.1, χ=1.0 and λ=0.01.

160

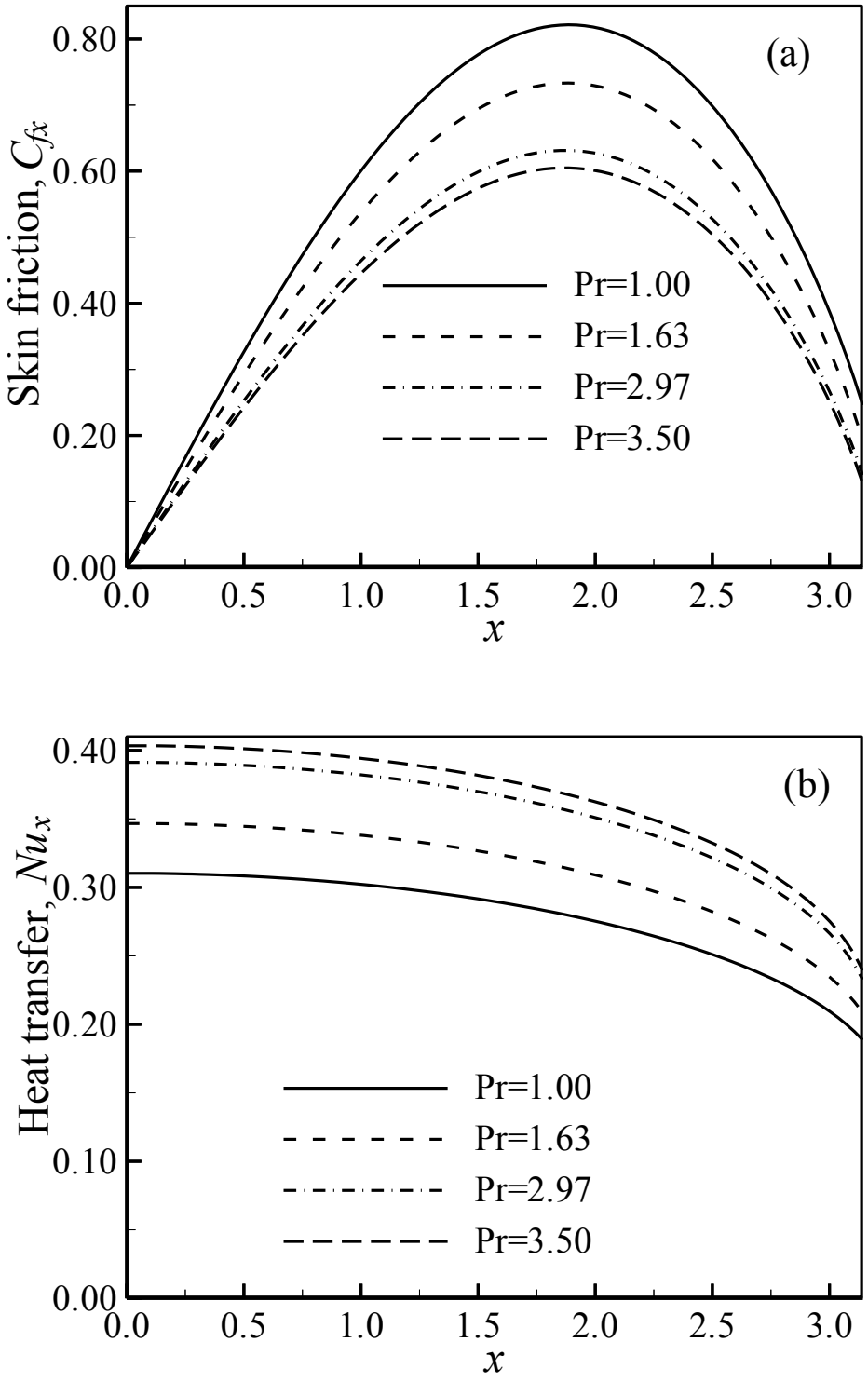

Figure 6.6: (a) Variation of the local skin friction coefficients and (b) variation of local Nusselt number against x varying of Prandtl number Pr with M=0.1, χ=1.0 and λ=0.01.

161

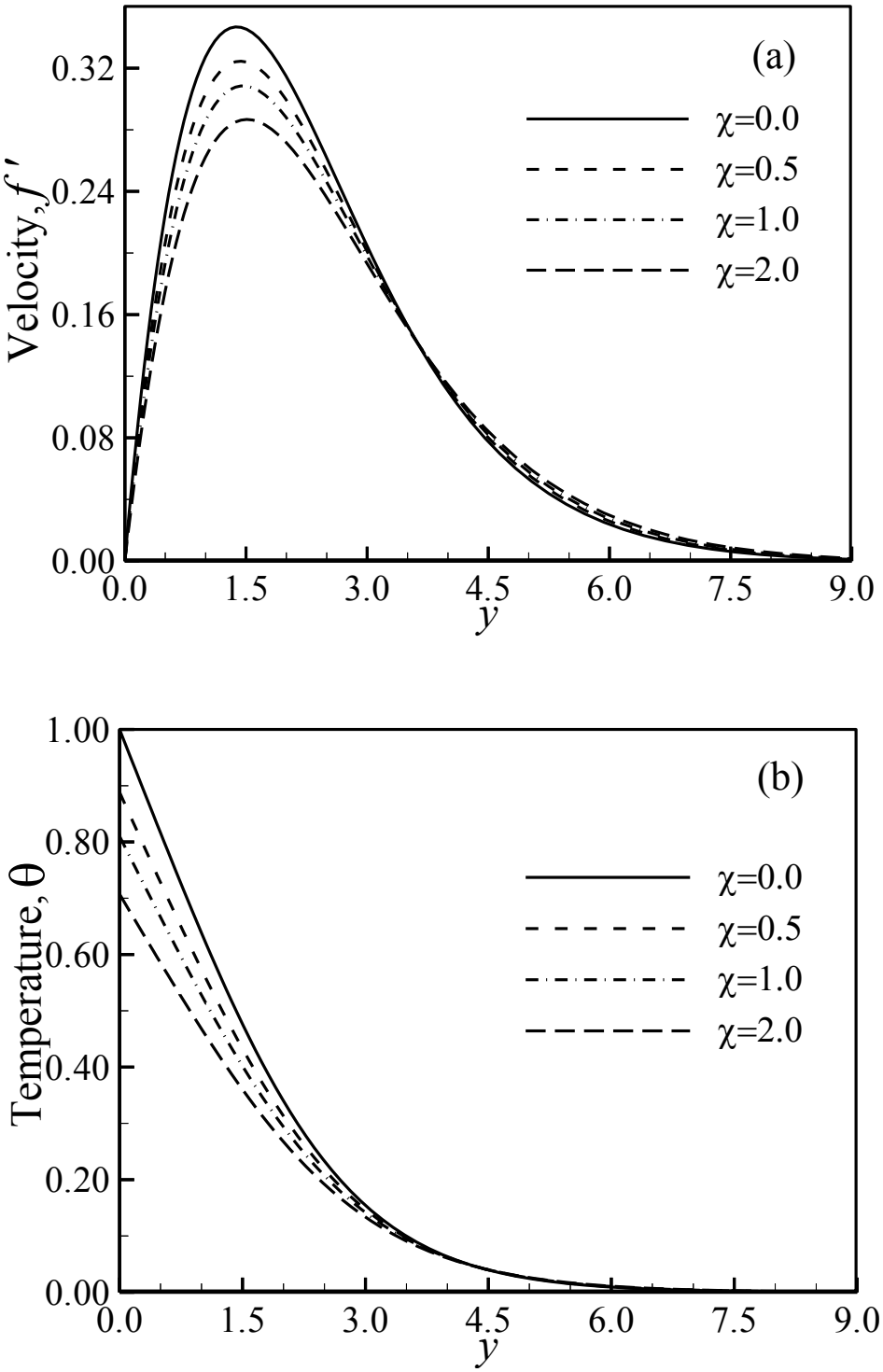

Figure 6.7: (a) Variation of velocity profiles and (b) variation of temperature profiles against y for varying of conjugate conduction parameter χ with Pr=1.0, M=0.1 and λ=0.01.

162

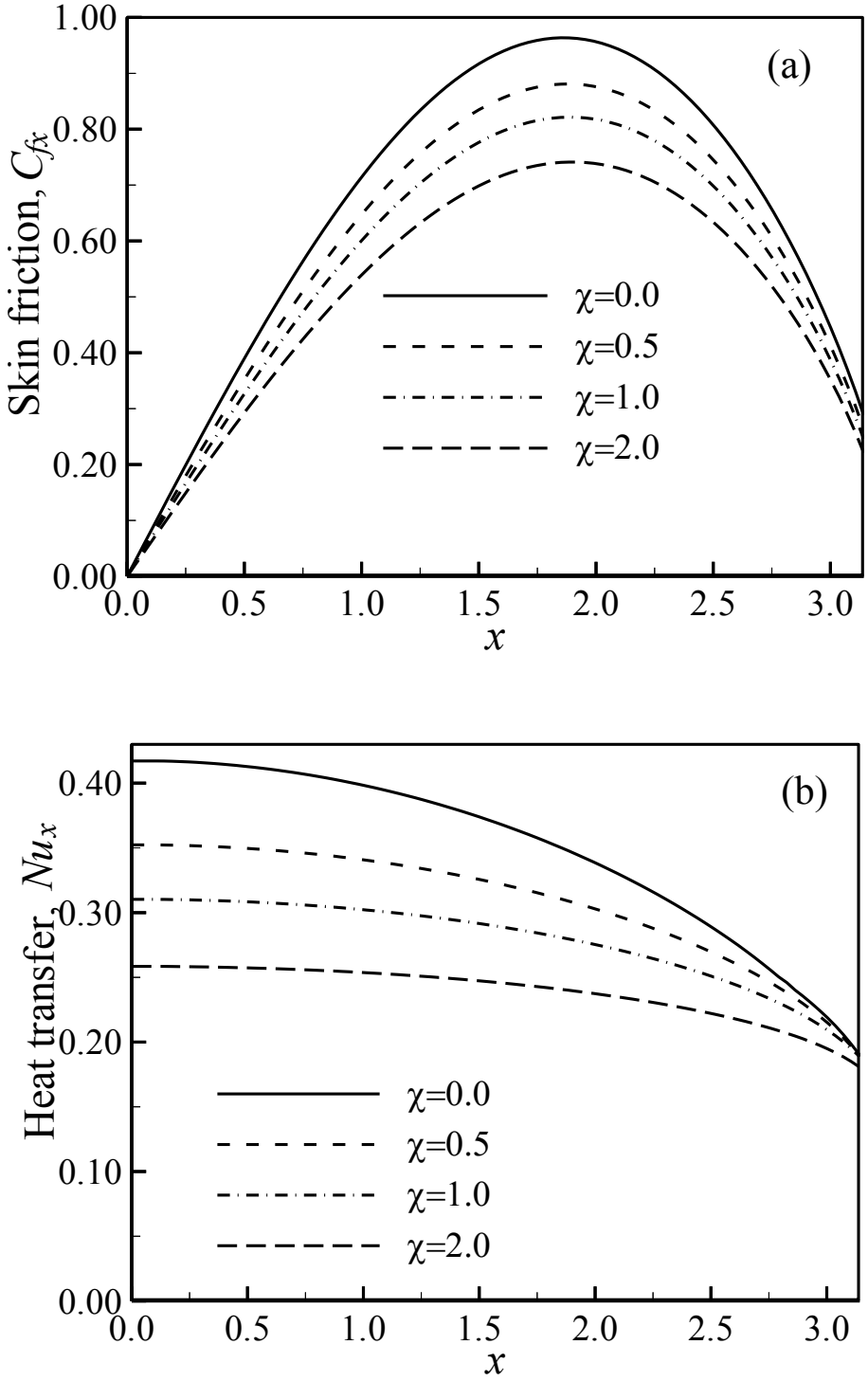

Figure 6.8: (a) Variation of the local skin friction coefficients and (b) variation of local Nusselt number against x for varying of conjugate conduction parameter χ with Pr=1.0, M=0.1 and λ=0.01.

163

6.4 Conclusion

The effect of temperature dependent viscosity on MHD-conjugate free convection flow from an isothermal horizontal circular cylinder is studied. The flow and heat transfer are governed by viscosity variation parameter, Magnetic parameter, Prandtl number and conjugate conduction parameter. It is found that the velocity increases and the temperature decreases within the boundary layer for increasing values of the viscosity variation parameter where as the skin friction decreases and heat transfer increases with increasing viscosity variation parameter. The effect of the magnetic parameter, Prandtl number and conjugate conduction parameter on the velocity and temperature within the boundary layer region and on the skin friction coefficient and heat transfer rate along the surface are similar as found in chapter III, if we consider temperature dependent viscosity.

164

Chapter VII
Concluding Remarks and Future Works

7.1 General conclusion

Regions of high heat transfer in a fluid flow are usually shear layers, associated with the regions of high momentum transfer. Undoubtedly the most common kind of shear layer in heat transfer problems is the boundary layer. In this thesis, the author has developed a physical model of magnetohydrodynamic conjugate free convection flow from an isothermal horizontal circular cylinder along with a coordinate system considering boundary layer approximation. The governing boundary layer equations are then derived according to the physical model and the boundary conditions are taken on the base of conjugate heat transfer process. The governing equations and boundary conditions are made dimensionless form using a set of non-dimensional variables. The ultimate resulting equations obtained by introducing the stream function have been solved numerically using the implicit finite difference method for the said boundary conditions. There are nine parameters obtained throughout the thesis, three parameters in chapter III and those are magnetic parameter, Prandtl number and conjugate conduction parameter; two new parameters in chapter IV and those are Joule heating parameter and heat generation parameter; three new parameters in chapter V and those are stress work parameter, viscous dissipation parameter and temperature ratio parameter and one new parameter in chapter VI and that is viscosity variation parameter. A representative set of numerical results for the velocity and temperature profiles, the skin friction coefficients as well as the rate of heat transfer are presented graphically and discussed in the respective chapters for the above parameters. However, a general conclusion on the works is presented below in brief:

165

The velocity becomes thinner where as the thermal boundary layer becomes thicker with increasing values of the magnetic parameter. The skin friction coefficient decreases however the rate of heat transfer increases with increasing value of the magnetic parameter which are found in chapter III, chapter IV, chapter V and chapter VI.

The skin friction coefficient decreases and the rate of heat transfer increases on the surface where as the velocity and temperature decreases in the boundary layer region with the increasing value of the Prandtl number. The effects of the Prandtl number on the velocity and temperature distribution and on the skin friction coefficient as well as heat transfer rate are similar in presence of the other parameters as discussed in chapter IV, chapter V and chapter VI.

Increasing value of the conjugate conduction parameter (more accurately conjugate conduction resistance parameter) decreases temperature as well as velocity within boundary layer region and it also decreases the skin friction coefficient on the surface and the heat transfer rate from the surface. These effects are true in presence of the other parameters as found in chapter IV, chapter V and chapter VI.

The effects of the Joule heating parameter, heat generation parameter and viscous dissipation parameter are similar that is the velocity and temperature increases in the boundary layer region, the skin friction increases on the surface and the heat transfer rate decreases from the surface with the increasing values of the parameters. However it is found that the temperature on the surface for a particular value of x and the heat transfer rate from the surface at the lower stagnation point are same for all values of the Joule heating parameter and viscous dissipation parameter, alternatively different values of the temperature and heat transfer rate has been occurred for different values of the heat generation parameters. These phenomenons are supported by the definition of these physical parameters and the outcome is received from the discussion of chapter IV.

166

From chapter V it is revealed that the velocity and temperature in the boundary layer region and the skin friction on the surface of the cylinder decreases however the rate of heat transfer increases with increasing value of the stress work parameter and temperature ratio parameter.

Lastly, the effect of the temperature dependent variable viscosity has been discussed in chapter VI. It is found that the velocity within the boundary layer increases conversely the skin friction coefficient decreases with increasing value of the viscosity variation parameter although this phenomenon is completely supported. On the other hand, it is observed that there is a small decrease in the temperature within the boundary layer accordingly an increase in the heat transfer rate with increasing value of the viscosity variation parameter.

7.2 Possible future works based on the thesis

The study on this thesis may be extended considering following cases:

- The effect of radiation has not been considered throughout the thesis; this mode of heat transfer may be considered with the present model.
- The study can be extended considering porous medium.
- The author has considered a steady two-dimensional laminar flow in this thesis. One can consider steady three dimensional flows, unsteady two-dimensional flow and unsteady three-dimensional flow.
- Natural convection is taken into account in this study. It can be extended by considering mixed convection and forced convection.
- The effect of temperature dependent viscosity may be extended considering Joule heating, heat generation, stress work and viscous dissipation.
- Temperature dependent thermal conductivity and Prandtl number has not been considered in the study. This study may be extended with considering these fluid properties with different physics.

167

References

Ackroyd, J. A. D., (1974): "Stress work effects in laminar flat-plate natural convection", J. Fluid Mech., Vol.62, pp.677-695.

Ackroyd, J. A. D., (1976): "Laminar natural convection boundary layers on near-horizontal plates" Proc. Roy. Soc., A 352, pp.249-274.

Ahmad, S., Arifin, N. M., Nazar, R., and Pop, I., (2009): "Mixed convection boundary layer flow past an isothermal horizontal circular cylinder with temperature-dependent viscosity", International journal of thermal sciences, Vol.48, pp.1943-1948.

Alam, Md. M., Alim, M. A., and Chowdhury, M. A.,(2007): "Stress work effect on natural convection flow along a vertical flat plate with joule heating and heat conduction", Journal of mechanical engineering, ME38, pp.18-24.

Aldoss, T. K., Ali, Y. D. and Al-Nimr, M. A., (1996): "MHD mixed convection from a horizontal circular cylinder", Numerical Heat Transfer, Part A, Vol.30, pp.379-396.

Alfven, H., (1942): "On the existence of electromagnetic Hydrodynamics waves", Arkiv F. mat. Astro. O. Fysik, Bd., 295, No.2.

Alim, M.A., Alam, Md. M., Abdullah-Al-Mamun and Belal Hossain, (2008): "Combined effect of viscous dissipation and joule heating on the coupling of conduction and free convection along a vertical flat plate", International communications in heat and mass transfer, Vol.35, pp.338-346.

Azim, NHM. A., Mamun, A. A. and Chowdhury, M. K., (2007a): Magnetohydrodynamic (MHD) laminar free convective flow across a horizontal circular cylinder, Proceedings of the 7th International Conference on Mechanical Engineering, ICME2007-FL-15, December 29-31, 2007, Dhaka, Bangladesh.

Azim, NHM. A., Mamun, A. A. and Chowdhury, M. K., (2007b): Conduction and Joule heating effects on magnetohydrodynamic (MHD) natural convection flow along a vertical flat plate, Fifteenth mathematics conference, December 29-31, 2007, Department of Mathematics, University of Dhaka, Bangladesh.

Azim, NHM. A., Mamun, A. A. and Chowdhury, M. K., (2008): Natural convection flow along a vertical flat plate in presence of conduction, 12th Annual Paper Meet, Paper ID: 132-NM03, 8-9 February, 2008, IEB Headquarter, Dhaka, Bangladesh.

168 Azim, NHM. A., Rahman, ATM. M. and Chowdhury, M. K., (2009a): "Magnetohydrodynic (MHD) conjugate free convection flow from an isothermal

horizontal circular cylinder in presence of heat generation", Proceedings of the 16th Mathematics Conference of Bangladesh Mathematical Society, 16MC09-053, 17-19 December, 2009 Dhaka, Bangladesh.

Azim, NHM. A., Mahtab, S. B. and Chowdhury, M. K., (2009b): "Magnetohydrodynamic(MHD)-conjugate free convection flow from an isothermal horizontal circular cylinder with joule heating effect", Proceedings of the International Conference on Mechanical Engineering 2009, ICME09-TH-11, 26- 28 December 2009, Dhaka, Bangladesh.

Azim, NHM. A., Rahman, ATM. M. and Chowdhury, M. K., (2010a): MHD-conjugate free convection flow from an isothermal horizontal cylinder with stress work, Proceedings of the International conference on Marine Technology, 11-12 December 2010, Dhaka, Bangladesh.

Azim, NHM. A. and Chowdhury, M. K., (2010b): "Natural convection flow from an isothermal horizontal circular cylinder in presence of conduction and heat generation", Proceedings of the 13th Asian Congress of Fluid Mechanics, 17-21 December, Dhaka, Bangladesh, pp.855-859.

Azim, NHM. A., Mamun, A.A., and Rahman, M.M., (2010c): "Viscous Joule heating MHD–conjugate heat transfer for a vertical flat plate in the presence of heat generation", International communications in heat and mass transfer, Vol.37, pp.666-674.

Azim, NHM. A. and Chowdhury M. K., (2012a): "Effect of Conduction on Magnetohydrodynamic (MHD) Natural Convection Flow from an Isothermal Horizontal Circular Cylinder", Journal of Energy, Heat and Mass Transfer, vol.34, pp.233-244.

Azim, NHM. A., (2012b): "Effect of viscous dissipation on Magnetohydrodynamic (MHD) conjugate free convection flow from a horizontal cylinder", Journal of Dhaka International University, Vol.4, No.1, pp.40-49.

Azim, NHM. A. and Chowdhury, M. K., (2013a): "Hydromagnetic conjugate free convection flow from an isothermal horizontal circular cylinder with stress work and heat generation", International Journal of Energy & Technology, vol. 5 (17) pp.1-9.

Azim, NHM. A. and Chowdhury, M. K., (2013b): "MHD-conjugate free convection from an isothermal horizontal circular cylinder with joule heating and heat generation", Journal of Computational Methods in Physics, Hindawi Publishing Corporation, http://dx.doi.org/10.1155/2013/180516.

169

Barletta, A., and Nield, D. A., (2009): "Mixed convection with viscous dissipation and pressure work in a lid-driven square enclosure", International Journal of Heat and Mass Transfer, Vol.52, pp.4244-4253.

Cebeci, T. and Bradshaw, P., (1984): "Physical and computational aspects of convective heat transfer", Springer, Berlin Heidelberg, New York.

Chamkha, A. J., (1997): "Hydromagnetic natural convection from an isothermal inclined surface adjacent to a thermally stratified porous medium", International Journal of Engineering Science, Vol.35, pp.975-986.

Chamkha, A.J., and Camille, I., (2000): "Effects of heat generation/absorption and the thermophoresis on hydromagnetic flow with heat and mass transfer over a flat plate", International Journal of Numerical Methods Heat Fluid Flow, Vol.10, pp.432–448.

Chapman, D. R., (1979): "Computational Aerodynamics Development and Outlook", AIAA J., Vol.17, pp.1293-1313.

Charraudeau, J., (1975) : "Influence de gradients de properties physiques en convection force application au cas du tube"", International Journal of Heat and Mass Transfer, Vol.18, pp.87–95.

Ching-Yang Cheng, (2006): "The effect of temperature-dependent viscosity on the natural convection heat transfer from a horizontal isothermal cylinder of elliptic cross section", International Communications in Heat and Mass Transfer, Vol.33, pp.1021–1028.

Ching-Yang Cheng, (2006): "Natural convection heat transfer from a horizontal isothermal elliptical cylinder with internal heat generation", International Communications in Heat and Mass Transfer, Vol.36, pp.346–350.

Cramer, K. R. and Pai, S. I., (1974): "Magnetofluid dynamics for engineering and applied physicists", McGraw-Hill, New York, pp.164-172.

El-Amin, M. F., (2003): "Combined effect of viscous dissipation and Joule heating on MHD forced convection over a non-isothermal horizontal cylinder embedded in a fluid saturated porous medium", Journal of Magnetism and Magnetic materials, Vol.263, pp.337-343.

Farouk B. and Guceri S.I., (1981): "Natural convection from horizontal circular cylinder-laminar regime", ASME, J. Heat transfer vol.103, pp.522-526.

Gdalevich, L.B., and Fertman, V.E., (1977): "Conjugate problems of natural convection", INZHENERNO-FIZICHESKII ZHURNAL, Vol.33, pp.539–547.

Gebhart B., (1962): "Effect of dissipation in natural convection", Journal of Fluid Mechanics, Vol.14, pp.225-232.

Gray, J., Kassory, D. R., Tadjeran, H. and Zebib A., (1982): "The effect of significant viscosity variation on convective heat transport in water-saturated porous media", Journal of Fluid Mechanics, Vol.117, pp.233-249.

Hossain, M. A., (1992): "Viscous and Joule heating effects on MHD-free convection flow with variable plate temperature", International Journal of Heat and Mass Transfer, Vol.35, pp.3485-3487.

Hossain, M. A., Munir, M. S. and Rees, D. A. S., (2000): "Flow of viscous incompressible fluid with temperature dependent viscosity and thermal conductivity past a permeable wedge with variable heat flux", International journal of thermal science, Vol.39, pp.635-644.

Joshi, Y. and Gebhart, B., (1981): "Effect of pressure stress work and viscous dissipation in some natural convection flows", International Journal of Heat and Mass Transfer, Vol.24, No.10, pp.1577-1588.

Keller, H. B., (1978): "Numerical methods in the boundary layer theory", Annual Reviews of Fluid Mechanics, Vol.10, pp.417–433.

Kimura, S. and Pop, I., (1992): "Conjugate free convection from a circular cylinder in a porous medium", International Journal of Heat and Mass Transfer, Vol.35, No.11, pp.3105-3113.

Kimura, S. and Pop, I., (1994): "Conjugate natural convection from a horizontal circular cylinder", Numerical heat transfer, Part A, Vol.25, pp.347-361.

Kuehn, T. H. and Goldstein, R. J., (1980): "Numerical solution to the Navier-Stokes equations for laminar natural convection about a horizontal isothermal circular cylinder", International Journal of Heat and Mass Transfer, Vol.23, pp-971-979.

Lings, J. X. and Dybbs, A., (1987): "Forced convection over a flat plate submersed in a porous medium: variable viscosity case", Paper 87-WA/HT-23, ASME, New York.

Luciano M. De Socio, (1983): "Laminar free convection around horizontal circular cylinders", International Journal of Heat and Mass Transfer, Vol.26, No.11, pp.1669-1677.

Luikov, A.K., Aleksashenko, V. A. and Aleksashenko, A. A. (1971): "Analytic methods of solution on conjugated problems in convective heat transfer", International Journal of Heat and Mass Transfer, Vol.14, pp.1047–1056.

171

Luikov, A.K., (1974): "Conjugate convective heat transfer problems", International Journal of Heat and Mass Transfer, Vol.17, pp.257–265.

Mahajan, R.L., and Gebhart, B., (1989): "Viscous dissipation effects in buoyancy induced flows", International Journal of Heat and Mass Transfer, Vol.32, pp.1380–1382.

Mamun, A.A., Chowdhury, Z.R., Azim, M.A., Molla, M.M., (2008): "MHD-conjugate heat transfer analysis for a vertical flat plate in presence of viscous dissipation and heat generation", International Communications in Heat and Mass Transfer, Vol.35, pp.1275–1280.

Mehta, K. N. and Sood, S., (1992): "Transient free convection flow with temperature dependent viscosity in a fluid saturated porous media", International Journal of Engineering Science, Vol.30, pp.1083-1087.

Mendez, F., Trevino, C., (2000): "The conjugate conduction-natural convection heat transfer along a thin vertical plate with non-uniform internal heat generation, International Journal of Heat Mass Transfer , Vol.43, pp.2739–2748.

Merkin, J. H., (1976): "Free convection boundary layer on an isothermal horizontal cylinder", ASME, paper no.76-HT-16.

Merkin, J.H., (1977): "Free convection boundary layers on cylinders of elliptic cross section", ASME Journal of Heat Transfer, 99, 453–457.

Merkin, J. H. and Pop, I., (1988): "A note on the free convection boundary layer on a horizontal circular cylinder with constant heat flux", Wärme und Stoffübertragung, Vol. 22, pp-79-81.

Michiyoshi, I., Takahashi, I. and Serizawa, A., (1976): "Natural convection heat transfer from a horizontal cylinder to mercury under magnetic field", International Journal of Heat and Mass Transfer, Vol.19, pp.1021-1029.

Miyamoto, M., Sumikawa, J., Akiyoshi, T., and Nakamura, T., (1980): "Effects of axial heat conduction in a vertical flat plate on free convection heat transfer", International Journal of Heat and Mass Transfer, Vol.23, pp.1545-1553.

Molla, M. M., Hossain, M. A. and Gorla, R. S. R., (2001): "Natural convection flow from an isothermal horizontal circular cylinder with temperature dependent viscosity", Heat mass transfer, Part A, Vol.44, pp.827-836.

Mansour, M. A., El-Hakiem and El-Kabir, S. M., (2000): "Heat and mass transfer in magnetohydrodynamic flow of micropolar fluid on a circular cylinder with uniform heat and mass flux", Journal of magnetism and magnetic materials, vol.220, pp.259-270.

172

Molla, M. M., Hossain, M. A., Paul, M. C., (2006): "Natural convection flow from an isothermal horizontal circular cylinder in presence of heat generation", International Journal of Engineering Science, Vol.44, pp.949-958.

Molla, M. M. and Hossain, M. A., (2006): "Effects of chemical reaction heat and mass diffusion in natural convection flow from an isothermal sphere with temperature dependent viscosity", International Journal for computer-aided engineering and software, Vol.23, No.7, pp.840-857.

Nazar, R., Amin, N., and Pop, I., (2002): "Free convection boundary layer on an isothernal horizontal circular cylinder in a micropolar fluid", Heat transfer, proceeding of the 12th international conference.

Ostrach, S., (1952): "Laminar natural convection flow and heat transfer of fluids with and without heat sources in channels with constant wall temperatures", National Advisory Committee for Aeronautics, United States, pp.1-55.

Ostrach, S., (1958): "Internal viscous flows with body forces", in: H. Gortler (Ed.), Grenzschichtforschung, Springer Verlag.

Ostrach, S., and Albers, L.U., (1958): "On pairs of solution of a class of internal viscous flow problems with body force", NACATN 4273.

Pantokratoras, A., (2003): "Effect of viscous dissipation and pressure stress work in natural convection along a vertical isothermal plate. New results", International Journal of Heat and Mass Transfer, Vol.46, pp.4979-4983.

Perelman, T. L., (1961): "On conjugated problems of heat transfer", International Journal of Heat and Mass Transfer, Vol.3, pp.293-303.

Pop, I., Ingham, D. B., (2001): "Convective heat transfer", First edition, Pergamon, Oxford, pp.179-189.

Pozzi, A., and Lupo, M., (1988): "The coupling of conduction with laminar natural convection along a flat plate", International Journal of Heat and Mass Transfer, Vol.31, pp.1807–1814.

Saville, D.A., and Churchill, S.W., (1967): "Laminar free convection in boundary layers near horizontal cylinders and vertical axisymmetric bodies", Journal of Fluid Mechanics Vol.29, pp.391–399.

Schlichting, H. and Gersten, K., (2000): "Boundary-Layer Theory", Springer-Verlag Berlin/Heidelberg.

173

Sparrow E. M. and Cess R.D., (1961): "Effect of magnetic field on free convection heat transfer", International Journal of Heat and Mass Transfer Vol.3, pp.267-274.

Takhar, H. S. and Soundalgekar, V. M., (1980): "Dissipation effects on MHD free convection flow past a semi-infinite vertical plate", Applied Science Research, Vol.36, pp.163-171.

Terrill, R. M., (1960): "Laminar boundary-layer flow near separation with and without suction ", Phil. Trans. R. Soc. A 253, pp.59-100.

Vajravelu, K., Hadjinicolaou, A., (1993): "Heat transfer in a viscous fluid over a stretching sheet with viscous dissipation and internal heat generation", International Communication Heat Mass Transfer, Vol.20, pp.417–430.

Wang, P., Kahawita, R. and Nguyen, T. H., (1990): "Numerical computation of natural convection flow about a horizontal cylinder Using Splines", Numerical Heat Transfer, Part-A, Vol.17, pp.191-215.

Wilks, G., (1976): "Magnetohydrodynamics free convection about a semi-infinite vertical plate in a strong cross field", ZAMP, Vol.27, pp.621-631.

Yih, K. A., (1999): "MHD Forced convection flow adjacent to a non-isothermal wedge", International Communications of Heat and Mass Transfer, Vol.26, pp.819-827.99.

174

Appendix

Table A1: Percentage increase/decrease of the maximum values of the velocity with a referred increase of the Prandtl number Pr, magnetic parameter M and conjugate conduction parameter χ (chapter III).

Parameters		**Maximum velocity**	**Percentage Change**	**Remarks**
Pr	0.733	0.314559	23.87	Decrease
	1.630	0.239484		
M	0.1	0.284157	25.73	Decrease
	0.7	0.211052		
χ	0.75	0.294869	14.26	Decrease
	2.00	0.252827		

Table A2: Percentage increase/decrease of the maximum values of the skin friction coefficient with a referred increase of the Prandtl number Pr, magnetic parameter M and conjugate conduction parameter χ (chapter III).

Parameters		**Maximum value of the skin friction coefficient**	**Percentage Change**	**Remarks**
Pr	0.733	0.790054	16.66	Decrease
	1.630	0.658416		
M	0.1	0.738048	18.63	Decrease
	0.7	0.600514		
χ	0.75	0.778009	19.95	Decrease
	2.00	0.622761		

175

Table A3: Percentage increase/decrease of the maximum values of the velocity for a referred increase of the Prandtl number Pr, magnetic parameter M conjugate conduction parameter χ, Joule heating parameter J and heat generation Q (chapter IV).

Parameters		**Maximum velocity**	**Percentage Change**	**Remarks**
Pr	0.733	0.319714	23.39	Decrease
	1.63	0.244926		
M	0.1	0.289429	25.25	Decrease
	0.7	0.216355		
χ	1.0	0.289429	14.65	Decrease
	2.5	0.247029		
J	0.01	0.289429	17.71	Increase
	1.00	0.340690		
Q	0.01	0.289429	20.86	Increase
	0.12	0.349804		

Table A4: Percentage increase/decrease of the maximum values of the skin friction coefficient for a referred increase of the Prandtl number Pr, magnetic parameter M conjugate conduction parameter χ, Joule heating parameter J and heat generation Q (chapter IV).

Parameters		**Maximum value of the skin friction coefficient**	**Percentage Change**	**Remarks**
Pr	0.733	0.801152	16.17	Decrease
	1.630	0.671578		
M	0.1	0.749931	18.46	Decrease
	0.7	0.611517		
χ	1.0	0.749931	20.71	Decrease
	2.5	0.594597		
J	0.01	0.749931	19.88	Increase
	1.00	0.899054		
Q	0.01	0.749931	4.51	Increase
	0.04	0.783773		

176

Table A5: Percentage increase/decrease of the maximum values of the velocity for a referred increase of the Prandtl number Pr, magnetic parameter M, conjugate conduction parameter χ, stress work parameter ε, viscous dissipation parameter N and temperature ratio parameter T_r (chapter V).

Parameters		Maximum velocity	Percentage Change	Remarks
Pr	0.733	0.289226	26.79	Decrease
	1.630	0.211734		
M	0.1	0.257874	25.31	Decrease
	0.7	0.192598		
χ	1.0	0.257874	17.56	Decrease
	2.5	0.212582		
ε	0.01	0.281548	17.03	Decrease
	0.20	0.233610		
N	0.01	0.257874	4.09	Increase
	1.0	0.268444		
T_r	0.1	0.277047	14.25	Decrease
	1.5	0.237559		

Table A6: Percentage increase/decrease of the maximum values of the skin friction coefficient with a referred increase of the Prandtl number Pr, magnetic parameter M, conjugate conduction parameter χ, stress work parameter ε, viscous dissipation parameter N and temperature ratio parameter T_r (chapter V).

Parameters		Maximum value of the skin friction coefficient	Percentage Change	Remarks
Pr	0.733	0.743259	18.51	Decrease
	1.630	0.605665		
M	0.1	0.688879	17.27	Decrease
	0.7	0.569888		
χ	1.0	0.688879	22.64	Decrease
	2.5	0.532949		
ε	0.01	0.733141	11.84	Decrease
	0.20	0.646364		
N	0.01	0.688879	4.88	Increase
	1.0	0.722494		
T_r	0.1	0.723061	9.53	Decrease
	1.5	0.654174		

177

Table A7: Percentage increase/decrease of the maximum values of the velocity with a referred increase of the Prandtl number Pr, magnetic parameter *M,* conjugate conduction parameter χ and viscosity variation parameter λ (chapter VI).

Parameters		Maximum velocity	Percentage Change	Remarks
Pr	1.0	0.341307	23.74	Decrease
	3.5	0.260281		
M	0.0	0.317195	12.48	Decrease
	0.5	0.277603		
χ	0.0	0.346776	17.32	Decrease
	2.0	0.2867		
λ	0.01	0.308463	11.58	Increase
	1.20	0.344185		

Table A8: Percentage increase/decrease of the maximum values of the skin friction coefficient with a referred increase of the Prandtl number Pr, magnetic parameter *M,* conjugate conduction parameter χ and viscosity variation parameter λ (chapter VI).

Parameters		Maximum velocity	Percentage Change	Remarks
Pr	1.0	0.878961	16.57	Decrease
	3.5	0.733352		
M	0.0	0.839187	9.44	Decrease
	0.5	0.759936		
χ	0.0	0.963528	23.07	Decrease
	2.0	0.741197		
λ	0.01	0.821498	22.07	Decrease
	1.20	0.640179		

178